76-15,822

RITCHIE, Adrian Augustus, Jr., 1941-
A VARIATIONAL OPTIMIZATION ANALYSIS APPROACH
TO CONTINUOUS DATA ASSIMILATION.

The University of Oklahoma, Ph.D., 1975
Physics, atmospheric science

Xerox University Microfilms, Ann Arbor, Michigan 48106

THE UNIVERSITY OF OKLAHOMA

GRADUATE COLLEGE

A VARIATIONAL OPTIMIZATION ANALYSIS APPROACH TO CONTINUOUS DATA ASSIMILATION

A DISSERTATION

SUBMITTED TO THE GRADUATE FACULTY

in partial fulfillment of the requirements for the

degree of

DOCTOR OF PHILOSOPHY

By

ADRIAN A. RITCHIE JR.

Norman, Oklahoma

1975

A VARIATIONAL OPTIMIZATION ANALYSIS

APPROACH TO CONTINUOUS DATA ASSIMILATION

APPROVED BY

Dissertation Committee

ABSTRACT

The assimilation or dynamic matching of asynoptic meteorological data with existing forecast fields, in space and time, is necessary to obtain the maximum benefit from the "new" data and to preclude the excitation of large-amplitude inertial-gravity waves. Prognostic fields of wind and geopotential, produced by the nonlinear longwave equations, plus simulated asynoptic geopotential observations are matched by the numerical variational analysis method. The linearized balance equation, integrated continuity equation, and observations weakly constrain the analysis. The three coupled assimilation equations are solved as boundary value problems by a cyclic relaxation technique.

The response function is investigated for a simpler system of analysis equations which result when horizontal non-divergence is used as a constraint instead of the integrated continuity equation. The response functions show that amplification, phase shifting, and anisotropic filtering occurs in the dynamic matching process.

The variational assimilation model is tested using simulated data. When the "observed" geopotential deviates significantly from the pre-existing forecast, the model adjusts the variables, wind and geopotential, such that the amplitude of the inertial-gravity waves is reduced by 60-82% of its original value depending on the specific choice of the weak constraint weights. The expected amplification of the shorter wavelength components of the wind field in response to the geopotential is observed.

ACKNOWLEDGMENTS

I wish to express my sincere gratitude to Dr. Yoshi K. Sasaki who was both my scientific and personal counselor. His encouragement, understanding of meteorology, and most of all, his knowledge of the research process helped me immeasurably during the difficult periods of this research.

I am deeply thankful of the interest and suggestions given by the other members of my Doctoral Committee—Drs. Stanley Barnes, Rex Inman, Martin Jischke, David Pitts and Jay Fein. These gentlemen are truly scientists.

This dissertation would not have been completed without the help of my fellow graduate students. They were always willing to discuss my research and help with many of the special problems associated with programming. Special thanks are given to Joe McFarland, Bob Stucky, Wally Chaplin, Main Hutcheson, Alvina Wei, and Wen Jey Liang. A hearty thanks is extended to Ms. Anita Cameron for her patience during the typing of this manuscript.

The opportunity to pursue this degree was provided by the United States Air Force. The research was sponsored by the National Science Foundation under Grant #30976.

All of this was possible because of the love and understanding of my wife, Margaret. To Margaret and my children—Love.

TABLE OF CONTENTS

LIST OF TABLES

LIST OF FIGURES

Figure		Page

LIST OF SYMBOLS

C_g	phase speed of gravity waves
d	horizontal distance between grid points
F	characteristic Coriolis parameter
f	Coriolis parameter
$\underset{\sim}{G}$	amplification matrix
g	gravity
h	total mass
$\tilde{h}_o$	initial value of total mass
$\underset{\sim}{I}$	identity matrix
J	adjustment functional
J_E	energy adjustment functional
k	normalized wave number in the x direction
L	Lagrangian density, characteristic length
L_x, L_y	wavelength in the x and y directions, respectively
m	normalized wave number in the y direction, image scale factor
P	cycle number
R	spatial region
R_1	inverse Rossby number
TE	total energy
T^o	initial value of total energy
t	time
U	non-dimensional analyzed u component wave amplitude, non-dimensional basic state u component

$\tilde{U}$	non-dimensional observed u component wave amplitude
u	non-dimensional scaled x component of velocity (horizontal velocity, earth distance per unit time, divided by the image scale factor), velocity scaling factor
u'	non-dimensional u component perturbation
$\tilde{u}$	non-dimensional observed u component
V	non-dimensional analyzed v component wave amplitude, wind scaling factor, non-dimensional basic state v component, spatial domain
$\tilde{V}$	non-dimensional observed v component wave amplitude
v	non-dimensional scaled y component of velocity
v'	non-dimensional v component perturbation
$\tilde{v}$	non-dimensional observed v component
x,y	horizontal cartesian coordinates on a polar stereographic projection
α	any dependent variable
$\tilde{\alpha},\tilde{\beta}$	observational weak constraint weights
Γ_{vi}	second derivative filter weight
γ	weak constraint weight
γ_{vi}	first derivative filter weight
Δ	weak constraint weight, horizontal grid spacing or time increment
$\Delta x, \Delta y, \Delta s$	spatial separation between grid points
Δt	temporal grid interval
δ	variational operator
θ	latitude
λ	eigenvalue of the amplification matrix, Rossby radius of deformation
λ_E	Lagrange multiplier
ν	iteration level
Φ	non-dimensional geopotential, non-dimensional geopotential perturbation

Φ'	non-dimensional geopotential perturbation
Φ_s	non-dimensional basic state geopotential
$\tilde{\Phi}$	observed non-dimensional geopotential
$\bar{\Phi}$	characteristic geopotential
$\underline{\Phi}$	analyzed geopotential wave amplitude
$\underline{\tilde{\Phi}}$	observed geopotential wave amplitude
τ	characteristic time

A VARIATIONAL OPTIMIZATION ANALYSIS APPROACH TO CONTINUOUS DATA ASSIMILATION

CHAPTER I

INTRODUCTION

The increasing abundance of satellite sensed meteorological data has generated considerable interest in the assimilation of these asynoptic data into the forecast model in order to update the model and improve the accuracy of the forecasts. But, in actuality, the assimilation problem has existed since the advent of numerical weather prediction. The operational technique has been to restart the time evolution of the atmosphere at specified times. Prior to restarting, the conventional radiosonde observations have been blended with the forecast by an objective analysis technique (Shumbera, 1970). The resulting fields can be matched by dynamic relationships, such as, the balance equation (Charney, 1955), or they may be dynamically adjusted through a variational approach (Lewis, 1972). These analyses are then used to initiate the forecast cycle. This analysis-forecast procedure is repeated every six or twelve hours.

From a forecast model perspective, assuming a judicious time interval, there are no asynoptic data. At certain times, clusters of data exist with varying distributions and spatial extent. Examples are the conventional radiosonde network in North America, Africa, or temperature profiles in cloud-free areas derived from polar orbiting satellite data. The problem now is how to extract from these data useful information to force the subsequent forecast to better describe the actual atmosphere. Once the forecast is beyond the time that the observations are available, it still may be necessary to adjust or modify the forecast variables due to the numerics of the forecast scheme. An illustration of this is the existence of the computational mode when using centered-time differences (Haltiner, 1971). To suppress this mode, Kurihara (1965) suggests that at regular intervals the forecast scheme be changed, for a few time steps, to one that selectively damps the high-frequency oscillations of the computational mode. Thus, an assimilation scheme should have multiple capabilities: forecast modification during the observational incorporation phase (phase I), and forecast adjustment or filtering during the pure forecast phase (phase II). This implies that the assimilation and forecast models could be separate, but intimately related, or combined such that the forecast model itself has multiple capabilities. The dual phase approach would be repeated as frequently as data availability and operational requirements permit. In no case would the time evolution of the atmosphere be restarted. Instead, forecasts from the previous cycle which have a valid time prior to the earliest valid time of the current observational data set would be used to initiate the process. The phase I portion of the process has succinctly been called continuous four-dimensional assimilation of observational data (Bengtsson, 1975).

Due to the rotational and gravitational effects of the earth, the primary balance between the mass and wind fields for large-scale horizontal motions is quasi-geostrophic in nature. Superimposed on this flow are acoustic, gravitational, and inertial motions, hereafter referred to as gravity motions. The very high-frequency portion of the superimposed motion is suppressed by dissipative forces in the atmosphere. The low-frequency modes are relatively insensitive to these viscous forces and may be long lived. The primitive equations (P.E.), which are used to model the atmosphere, allow the above types of wave motion except vertically propagating sound waves (Haltiner, 1971). When these models are used to forecast large-scale flow, the gravity motion is commonly referred to as "noise" and the energy it contains is kept small by filtering the fields. Energy is input into the higher frequencies by both physical and fictitious phenomena. Nonlinear wave interaction (Kaplin and Paine, 1973) is an example of a physical effect while lateral boundary conditions, and round-off and truncation are fictitious effects. If the amplitudes of these waves are not continually suppressed the large-scale patterns can be distorted, destroying the validity of the forecast of large-scale flow. The high-frequency control mechanism is built into the forecast scheme so that there is a continual quasi-geostrophic balance between the mass and motion field although it is extremely complicated (Økland, 1972). The subtle balance can be destroyed if observational data are introduced directly into the forecast. This is commonly called the "shock" effect in meteorology. The energy in the high frequencies is increased dramatically and because of the large phase speeds, the entire forecast is contaminated quite rapidly. The process of restoring the state of balance in the model, not necessarily identical to the original state, can take a considerable amount of time depending on the degree and nature of the imbalance between the forecast and observations (Nitta, 1971). The observations themselves or the objectively analyzed values also are not necessarily in a state of balance. Thus, both of these effects contribute to the excitation of the high-frequency, gravity motion.

The mechanism for maintaining or restoring the low-frequency, quasi-geostrophic balance between pressure and velocity is model dependent and lies at the heart of data assimilation. The process is called geostrophic adjustment and has been studied theoretically by many authors (Rossby, 1938; Bolin, 1953; Washington, 1964; Williamson and Dickinson, 1973). It describes the dependence of the final balanced state on the initial state and the speed at which this balance is achieved. Økland (1970) investigated the adjustment process for a linearized P.E. model taking into account the limited forecast region, the specific finite-differencing scheme for horizontal derivatives, and a time-differencing scheme which selectively damps high frequencies. He found that the frequency of gravity waves was a function of the Coriolis parameter, horizontal and vertical wavelengths of the perturbations, and the static stability of the atmosphere. The influence of the initial fields, mass or motion, on the balanced state was dependent on the ratio of this frequency to the Coriolis parameter. In general, the heights tended to adjust to the winds for small horizontal scales and large vertical scales and more so for small values of Coriolis parameter. For mid-latitudes and large horizontal scales, the winds adjusted to the initial mass field, while for the tropics the adjustment direction is reversed. The dependence on static stability was more complicated, but the phase speeds tended to increase as the stability increased, indicating that for high static stability the mass field adjusted to the wind field. In transforming to the finite-difference representation, the short wavelengths tended to behave like the longer wavelengths. This changed the direction of the adjustment in that the winds tended to adjust to the mass field. The speed of adjustment depended on the dispersion of wave energy away from the source—the group velocity. For large phase speeds, the group velocity was large and the adjustment was rapid.

Euler-backward time differencing has been used by many authors (Nitta and Hovermale, 1969; Nitta, 1971; Hayden, 1973) to achieve the dynamic balance. This scheme requires the continued reinsertion of the mass or motion field and can force an unnatural adjustment to take place. It damps the amplitude of high-frequency waves quite rapidly but affects the group velocity very little. The low-frequency waves are also significantly damped through repeated applications of the backward-difference technique.

Charney, et al. (1969) first demonstrated the update concept whereby there is a systematic replacement of the predicted temperatures by the observed temperatures. The observed temperatures are generated by a long-term integration of the forecast model. Different initial conditions are used for the second integration. The observed temperatures, which contain varying amounts of random or systematic error, are directly inserted into the second forecast where appropriate; the created gravity waves are damped or controlled, and the integration continued. The resulting forecast is then compared to a control forecast. The frequency of insertion can be varied, but it must be greater than the model dependent damping period for the gravity waves or else their amplitude will grow too much and they become too difficult to eliminate (Talagrand, 1972). Charney observed a rapid decrease in errors the first day or two for a 12-hour insertion frequency. The error then leveled off but was greater when larger random error was added to the observed temperatures. The adjustment was better in high latitudes than near the equator where the wind error did not fall below an acceptable level if the temperature error was large.

The update technique is not confined to temperature alone but may be applied for any or all of the forecast variables. Jastrow and Halem (1970), Williamson and Kasahara (1971), Gordon, et al. (1972) have used the update concept with long-term model integration. The principal differences among the preceeding authors involved (a) model characteristics, (b) variables to be updated, and the domain and frequency of insertion, and (c) the actual method used to assimilate the data and damp the gravity waves. The specific results are generally in agreement with simple adjustment theory and show the need for wind data in the tropics to reduce the errors. This error in the tropics does influence the wind error in the extra-tropics but only after a few days.

The source of the assimilation data can significantly alter the results. Jastrow and Halem (1973) found that real data leads to larger errors than simulated data. Recently, Hayden (1973) performed temperature assimilation experiments using real data over a short time period over the northern hemisphere with the Euler-backward scheme to achieve the dynamic balance. To further minimize the shock, and to increase the speed of the convergence of the dynamic balance, static balancing in the form of the geostrophic relationship was suggested. The results indicated that this method was effective in reducing the temperature errors and that the details of the surface pressure were unimportant with this particular model. Gauntlett, et al. (1974), employing the same techniques as Hayden, performed real data assimilation experiments in the southern hemisphere. They noted that variations in the assimilation frequency produced only small differences, but a two-hour assimilation frequency resulted in small but consistent improvement in subsequent forecasts. They also found that the reference level pressure at the surface is necessary to maintain the intensity of the synoptic systems. When solving the hydrostatic equation, the vertical distribution of pressure can be determined with the specification of one integration constant, the reference pressure at the reference level. Kasahara (1972) discussed the significance of this problem.

The concept of the mutual adjustment of the variables and the need to damp unwanted gravity waves is why many researchers have used the Euler-backward time-differencing scheme or a viscosity term (Shuman and Stackpole, 1969; Sadourny, 1973). These methods do not allow for variations in observational or forecast accuracy or for different physical processes, and they can require a considerable amount of simulated time to achieve the necessary implied balance.

The principle of variational optimality (Sasaki, 1970b) recognizes the existence of observational and forecast inaccuracies and through proper selection of the dynamic constraints, the quasi-geostrophic balance is achieved "instantaneously". The current research is oriented toward the development and verification of a variational model capable of assimilating remotely sensed data. Successful assimilation (dynamically matching observations and forecasts) is defined as the absence of large amplitude gravity waves in the subsequent forecast.

In the next two chapters the mathematical and numerical development of an initialization and assimilation model compatible with the shallow-water equations is presented. The shallow-water equations are used because of their simplicity and the applicability of the results to certain modes of multilayer models. The response functions for the initialization model is investigated showing that to produce dynamically consistent fields amplification of some wavelengths is necessary. The assimilation model incorporates the principal physics of the shallow-water equations and additional filters to suppress computational error. In Chapter IV, the results of a series of forecast and assimilation experiments are presented. Finally, areas for continued research effort are discussed.

CHAPTER II

FORECAST, INITIALIZATION AND ASSIMILATION MODELS

Two-dimensional barotropic motion in an inviscid, incompressible, hydrostatic fluid with a horizontal lower boundary and an upper free surface is described by the shallow-water equations. These equations when non-dimensionalized (see Appendix A) and transformed to polar-stereographic coordinates are:

$$\frac{\partial u}{\partial t} + m^2\left(u\frac{\partial u}{\partial x} + v\frac{\partial u}{\partial y}\right) + m\frac{\partial m}{\partial x}(u^2+v^2) - R_1 fv + R_1\frac{\partial \Phi}{\partial x} = 0, \qquad (1)$$

$$\frac{\partial v}{\partial t} + m^2\left(u\frac{\partial v}{\partial x} + v\frac{\partial v}{\partial y}\right) + m\frac{\partial m}{\partial y}(u^2+v^2) + R_1 fu + R_1\frac{\partial \Phi}{\partial y} = 0, \qquad (2)$$

and

$$\frac{\partial \Phi}{\partial t} + m^2\left(u\frac{\partial \Phi}{\partial x} + v\frac{\partial \Phi}{\partial y}\right) + m^2(\Phi_s + \Phi)\left(\frac{\partial u}{\partial x} + \frac{\partial v}{\partial y}\right) = 0. \qquad (3)$$

The meteorological variables are symbolized according to the convention adopted in Appendix A. This system describes not only the slow meteorological processes, Rossby waves, but the fast gravitational waves which move at a velocity that approaches the speed of sound. This system also shows considerable skill in predicting the 500 mb-geopotential configuration in extratropical regions (Gerrity and McPherson, 1969).

In continuous form Eqs.(1), (2), and (3) satisfy the conservation of total energy

$$\frac{\partial}{\partial t}\int_R \left(\Phi m^2(u^2+v^2) + R_1\Phi^2\right)\frac{dxdy}{m^2} = 0, \qquad (4)$$

provided that the net total flux of energy passing through the boundaries of the region is zero. The derivation of Eq. (4) is contained in Appendix A.

Initialization

In order to integrate Eqs. (1) - (3), initial ($t = 0$) conditions for the dependent variables must be specified. If these conditions are not properly specified, large amplitude inertial-gravity waves are excited. In middle latitudes these waves are considered to be of a scale smaller than those observable from the present upper-air network and, thus, are considered as noise to the large-scale forecast. But, due to their high phase speed, the inertial-gravity waves can contaminate the entire forecast region quite rapidly. Although it is impossible to separate different types of motion when dealing with the nonlinear equations, it is possible to minimize the gravity motions thru proper initialization (Phillips, 1960). The initialization process for this forecast model is based on variational optimization (Sasaki, 1971) in which dynamic and other subsidary conditions for the suppression of gravity waves constrain the analysis. The analysis is based upon the calculus of variations which seeks to determine functions such that a certain definite integral involving these functions and their derivatives takes on a maximum or minimum (Hildebrand, 1965). The adjustment function, J, is expressed by

$$J = \int_V \int_t L \; dV \, dt, \tag{5}$$

where L is the Lagrangian density, and V and t are the space and time domain over which the minimization is sought. The Lagrangian density is composed of a series of weighted terms representing the conditions to be satisfied. The first linear variation of J yields the Euler-Lagrange or analysis equations plus the correct number of boundary conditions such that, when it exists, a unique solution is provided (Forsythe and Wasow, 1960).

Benwell and Bretherton (1968) found that the linearized balance equation was effective in eliminating the noise from the initial data. If the wind components are not replaced by the streamfunction gradients, the resulting analysis can contain a considerable amount of divergence. Thus, the non-dimensional constraints are the linearized balance equation and horizontal non-divergence, i.e.,

$$B \equiv m^2\left[\frac{\partial^2 \Phi}{\partial x^2} + \frac{\partial^2 \Phi}{\partial y^2} - \frac{\partial(fv)}{\partial x} + \frac{\partial(fu)}{\partial y} \right], \tag{6}$$

and

$$C \equiv m^2\left[\frac{\partial u}{\partial x} + \frac{\partial v}{\partial y} \right]. \tag{7}$$

The non-dimensional adjustment functional incorporating these constraints is:

$$J = \int_R \{\tilde{\alpha}(u-\tilde{u})^2 + \tilde{\alpha}(v-\tilde{v})^2 + \tilde{\beta}(\Phi-\tilde{\Phi})^2 + \gamma(B)^2 + \Delta(C)^2\} \frac{dxdy}{m^2} \tag{8}$$

where u, v and Φ are the analyzed values sought; $\tilde{u}$, $\tilde{v}$, and $\tilde{\Phi}$ are the observed values; $\tilde{\alpha}$, $\tilde{\beta}$ are weights which are functions of the independent variables, and the first three terms are the conditions used for minimizing the variance of the difference between the analyzed and observed values. The γ and Δ terms are weak constraints which imply that the analyzed fields of geopotential and wind do not have to identically satisfy the balanced or non-divergent conditions.

The weights premultiplying the dynamic constraints are prespecified and are constant in space and time. The observational weights are prespecified but are not necessarily constant. They may be determined from the error variances of the respective observing systems, a knowledge of the reliability or accuracy of the grid point data, the degree of observational damping desired by an investigation of the response function (Wagner, 1971); they may be chosen to account for different physical effects when the analysis is performed over a wide range of latitudes.

The stationary value of the functional is found by equating the first variation to zero. A quadratic formulation of the functional insures that the stationary functions will be a minimum (Sasaki, 1970a). It is worth noting that the stationary functions do not imply that the deviations between the analyzed and observed values subject to the constraints will be a minimum everywhere in the domain or that all the deviations for each variable will be minimized, but only that the integrated sum of the deviations squared, subject to the constraints, will be a minimum. Thus, for example, it is possible to drive the geopotential deviations to zero over the domain, while causing the wind deviations to be maximized and still the functional is a minimum.

The first linear variation, assuming the solution is specified on the boundaries of the region, leads to the Euler-Lagrange or analysis equations:

$$\frac{\alpha}{m^2}(u-\tilde{u}) - \gamma f m^2\left[\frac{\partial^3\phi}{\partial y\partial x^2} + \frac{\partial^3\phi}{\partial y^2} - \frac{\partial^2(fv)}{\partial x\partial y} + \frac{\partial^2(fv)}{\partial x\partial y}\right] - \Delta m^2\left[\frac{\partial^2 u}{\partial x^2} + \frac{\partial^2 v}{\partial x\partial y}\right]$$

$$- \gamma f \frac{\partial m^2}{\partial y}\left[\frac{\partial^2 \Phi}{\partial x^2} + \frac{\partial^2 \Phi}{\partial y^2} - \frac{\partial(fv)}{\partial x} + \frac{\partial(fu)}{\partial y}\right] - \Delta \frac{\partial m^2}{\partial x}\left[\frac{\partial u}{\partial x} + \frac{\partial v}{\partial y}\right] = 0, \qquad (9)$$

$$\frac{\tilde{\alpha}}{m^2}(v-\tilde{v}) + \gamma f m^2\left[\frac{\partial^3 \Phi}{\partial x^3} + \frac{\partial^3 \Phi}{\partial x \partial y^2} - \frac{\partial^2 (fv)}{\partial x^2} + \frac{\partial (fu)}{\partial x \partial y}\right] - \Delta m^2\left[\frac{\partial^2 u}{\partial x \partial y} + \frac{\partial^2 v}{\partial y^2}\right]$$

$$+ \gamma f \frac{\partial m^2}{\partial y^2}\left[\frac{\partial^2 \Phi}{\partial x^2} + \frac{\partial^2 \Phi}{\partial y^2} - \frac{\partial(fv)}{\partial x} + \frac{\partial(fu)}{\partial y}\right] - \Delta \frac{\partial m^2}{\partial y}\left[\frac{\partial u}{\partial x} + \frac{\partial v}{\partial y}\right] = 0 \qquad (10)$$

and

$$\frac{\tilde{\beta}}{m^2}(\Phi-\tilde{\Phi}) + \gamma m^2\left[\frac{\partial^4 \Phi}{\partial x^4} + \frac{2\partial^4 \Phi}{\partial x^2 \partial y^2} + \frac{\partial^4 \Phi}{\partial y^4} + \nabla^2\left(\frac{\partial fu}{\partial y} - \frac{\partial fv}{\partial x}\right)\right]$$

$$+ \left[\frac{\partial^2 \Phi}{\partial x^2} + \frac{\partial^2 \Phi}{\partial y^2} - \frac{\partial(fv)}{\partial x} + \frac{\partial(fu)}{\partial y}\right] \gamma \nabla^2 m^2 = 0 , \qquad (11)$$

where $\nabla^2 = \left(\frac{\partial^2}{\partial x^2} + \frac{\partial^2}{\partial y^2} \right)$.

The derivation of these equations is given in Appendix B. In this form, the intimate relationships and matchings between the variables are readily apparent. In Eqs. (9) and (10) the balance constraint provides the proper relationship between geopotential and the rotational portion of the particular wind component. The divergence constraint affects only the divergent component and acts as a viscous damping term similar to that used by McPherson and Kistler (1975) in their data assimilation experiments. Since gravity modes are mainly associated with the divergent component, it is possible to reduce their effect by increasing Δ in relation to $\tilde{\alpha}$. As the ratio of $\Delta/\tilde{\alpha}$ becomes large, less of the observed divergence is transmitted to the analyzed winds. In the limit as $\Delta/\tilde{\alpha} \rightarrow \infty$, the analyzed winds are purely rotational and may be associated with a streamfunction. This is equivalent to strong constraint whereby u and v are replaced by their corresponding streamfunction gradients in the adjustment functional.

To determine the spectral modification occurring in the analysis equations, the response functions for the system of equations are examined. The image scale factor, m, and the Coriolis parameter, f, are assumed constant and equal to one. The resulting analysis equations are

$$\tilde{\alpha}(u-\tilde{u}) - \Delta\left(\frac{\partial^2 u}{\partial x^2} + \frac{\partial^2 v}{\partial x \partial y}\right) - \gamma\left(\frac{\partial^3 \Phi}{\partial y \partial x^2} + \frac{\partial^3 \Phi}{\partial y^3} - \frac{\partial^2 v}{\partial x \partial y} + \frac{\partial^2 u}{\partial y^2}\right) = 0, \quad (12)$$

$$\tilde{\alpha}(v-\tilde{v}) - \Delta\left(\frac{\partial^2 u}{\partial x \partial y} + \frac{\partial^2 v}{\partial y^2}\right) + \gamma\left(\frac{\partial^3 \Phi}{\partial x^3} + \frac{\partial^3 \Phi}{\partial x \partial y^2} - \frac{\partial^2 v}{\partial x^2} + \frac{\partial^2 u}{\partial x \partial y}\right) = 0, \quad (13)$$

and $$\tilde{\beta}(\Phi-\tilde{\Phi}) + \gamma\left(\frac{\partial^4 \Phi}{\partial x^4} + 2\frac{\partial^4 \Phi}{\partial x^2 \partial y^2} + \frac{\partial^4 \Phi}{\partial y^4} - \frac{\partial v}{\partial x^3} - \frac{\partial v}{\partial x \partial y^2} + \frac{\partial u}{\partial y \partial x^2} + \frac{\partial^3 u}{\partial y^3}\right) = 0. \quad (14)$$

The assumed continuous distributions of wind and pressure are given by

$$u = i\,U\,e^{i(kx+my)}, \qquad \tilde{u} = i\,\tilde{U}\,e^{i(kx+my)}, \quad (15)$$

$$v = i\,V\,e^{i(kx+my)}, \qquad \tilde{v} = i\,\tilde{V}\,e^{i(kx+my)}, \quad (16)$$

and $$\Phi = \underline{\Phi}\,e^{i(kx+my)}, \qquad \tilde{\Phi} = \underline{\tilde{\Phi}}\,e^{i(kx+my)}, \quad (17)$$

where U, V, and $\underline{\Phi}$ are the analyzed wave amplitudes, $i = \sqrt{-1}$, and the tildes represent the observed or initial wave amplitudes. The symbols k and m are normalized wave numbers in the x and y direction respectively, which have been made non-dimensional by 1/d, where d is the distance between grid points. The quantity x and y are distances measured along the axes divided by d. The dimensional wave numbers are given by $k^* = 2\pi/L_x$ and $m^* = 2\pi/L_y$, where L_x and L_y are the wavelengths of the wave being considered. The i premultiplying the wind components produces a

90° phase shift which is in consonance with the geostrophic wind equations.

Substitutions of Eqs. (15) - (17) into Eqs. (12) - (14) gives the following system of linear algebraic equations:

$$F\,U + H\,V + D\,\underline{\Phi} = E\,\tilde{U}\ , \tag{18}$$

$$H\,U + G\,V - C\,\underline{\Phi} = E\,\tilde{V}\ , \tag{19}$$

and

$$D\,U - C\,V + A\,\underline{\Phi} = B\,\tilde{\underline{\Phi}}\ , \tag{20}$$

where

$$A = \frac{\tilde{\beta}}{\gamma} + Z^2 \qquad E = \frac{\tilde{\alpha}}{\gamma}$$

$$B = \frac{\tilde{\beta}}{\gamma} \qquad F = \frac{\tilde{\alpha}}{\gamma} + \frac{\Delta}{\gamma}k^2 + m^2$$

$$C = kZ \qquad G = \frac{\tilde{\alpha}}{\gamma} + \frac{\Delta}{\gamma}m^2 + k^2$$

$$D = mZ \qquad H = km\left(\frac{\Delta}{\gamma} - 1\right)$$

$$Z = k^2 + m^2\ .$$

The general solution to Eqs. (18) - (20) provides little insight into the nature of the filtering due to its complexity, but some of the characteristics of the filtering may be found by considering selected choices of the weights. Seven special cases are investigated.

<u>Case 1</u>

When $\tilde{\alpha}$, $\tilde{\beta} \gg \gamma$, Δ and the wave numbers remain finite, the functional is minimized by the observed values and consequently there is no filtering.

Case 2

The other extreme is when there is no observational constraint, i.e., $\tilde{\alpha} = \tilde{\beta} = 0$. There are an infinite number of solutions which satisfy Eqs.(18) - (20).

Case 3

When $\tilde{\beta} = \gamma = 0$ and $\tilde{\alpha} = \Delta = 1$, the wind analysis is constrained by non-divergence only and equal weight is placed on the observational and dynamic constraint. For this case, Eqs. (18) - (20) reduce to

$$U = \frac{\tilde{U}(1 + m^2) - km\,\tilde{V}}{(1 + Z)} \tag{21}$$

and

$$V = \frac{\tilde{V}(1 + k^2) - km\,\tilde{U}}{(1 + Z)} \quad . \tag{22}$$

These equations show that the filtering characteristics are non-isotropic. As the wavelength in the y direction increases, i.e. $m \to 0$, the v component is not filtered, $V \to \tilde{V}$, and the filtering of the u component is a function of the wavenumber in the x direction only. As $k \to 0$, just the reverse occurs, i.e., $U \to \tilde{U}$ and $V \to \tilde{V}/(1 + m^2)$. Phase shifts and negative response values result for small values of m and k if it is assumed that $\tilde{U} = \tilde{V} = 1$. Figure 1a shows the response function for $L_y = 4381.5$ km, (m = .27318), and various wavelengths in the x-direction. The damping of the initial amplitude for the u component is large for short wavelengths and decreases as L_x increases. The damping of the initial v-component shows very little dependence on wavelength in the x direction. Figure 1b shows the response function for k = .27318 and various values of L_y. The response values are just the reverse of Fig. 1a, i.e., R(m = .27318, U) = R(k = .27318, V) where R is the functional value of Eqs. (21) and (22).

Case 4

When $\tilde{\alpha} = \tilde{\beta} = \Lambda = \gamma = 1$, which implies that equal weight is placed on the observational and dynamic constraints, Eqs. (18) - (20) reduce to

$$F\,U + D\,\underline{\Phi} = E\,\tilde{U}\,, \tag{23}$$

$$G\,V - C\,\underline{\Phi} = E\,\tilde{V}\,, \tag{24}$$

and

$$D\,U - C\,V + A\,\underline{\Phi} = B\,\tilde{\underline{\Phi}}\,. \tag{25}$$

In this case the cross derivative terms of the wind components in the u and v analysis equation identically cancel. For example, in the u analysis equation, Eq. (12), the cross derivative of v from the non-divergence constraint cancels with the cross derivative of v from the balanced constraint (H = 0). The solution of Eqs. (23) - (25) is:

$$U = \frac{\tilde{U}\,(F + Z^2 + D^2) - D\,F\,\tilde{\underline{\Phi}} - D\,C\,\tilde{V}}{F\,(F + Z^2)}\,, \tag{26}$$

$$V = \frac{\tilde{V}\,(F + Z^2 + C^2) + F\,C\,\tilde{\underline{\Phi}} - D\,C\,\tilde{U}}{F\,(F + Z^2)}\,, \tag{27}$$

and

$$\underline{\Phi} = \frac{\tilde{\underline{\Phi}}\,F + C\,\tilde{V} - D\,\tilde{U}}{F + Z^2}\,, \tag{28}$$

where F = G.

Surprisingly, these solutions show non-isotropic filtering characteristics with amplification ($R > 1$) and 180° phase shifts ($R < 0$) for certain wavelengths. As $m \to 0$, the following relationships hold:

$$U \to \frac{\tilde{U}}{(1 + k^2)}\,, \tag{29}$$

$$V \rightarrow \frac{\tilde{V}(1 + k^4) + k^3\tilde{\underline{\Phi}}}{(1 + k^2 + k^4)} , \tag{30}$$

and

$$\underline{\Phi} \rightarrow \frac{\tilde{\underline{\Phi}}(1 + k^2) + k^3\tilde{V}}{(1 + k^2 + k^4)} . \tag{31}$$

The filtering implied by Eq. (29) results only from the non-divergence constraint as shown in Case 3. In Eq. (30) the positive dependence on $\tilde{\underline{\Phi}}$ leads to amplification. For equal initial unit amplitudes of $\tilde{V}$ and $\tilde{\underline{\Phi}}$ the response for V is greater than 1 for short wavelengths and independent of wavelength for low wavenumbers. Eq. (31) acts as a very effective low pass filter and its response is similar to those derived by Wagner (1971) using first and second derivative constraints only.

At the other extreme, as $k \rightarrow 0$

$$U \rightarrow \frac{\tilde{U}(1 + m^4) - m^3\tilde{\underline{\Phi}}}{(1 + m^2 + m^4)} , \tag{32}$$

$$V \rightarrow \frac{\tilde{V}}{(1 + m^2)} , \tag{33}$$

and

$$\underline{\Phi} \rightarrow \frac{(1 + m^2)\tilde{\underline{\Phi}} - m^3\tilde{U}}{(1 + m^2 + m^4)} . \tag{34}$$

In Eq. (32), the negative dependence of $\tilde{\underline{\Phi}}$ leads to damping in all wavelengths, while Eq. (33) results entirely from non-divergence. At shorter wavelengths, Eq. (34) leads to a phase shift in the analyzed geopotential. Figs. 2a - 2c show the response function for unit initial amplitudes and various wavelengths, and confirms the above analysis.

Case 5

We consider $\gamma >> \tilde{\alpha}$ and Δ, and $\tilde{\beta} \neq \gamma$. This represents a functional composed of an observational constraint on geopotential and the balance constraint. Eqs. (18) - (20) reduce to

$$U - kV + Z\underline{\Phi} = 0 , \tag{35}$$

and

$$ZU - kZV + \left(\frac{\tilde{\beta}}{\gamma} + Z^2\right)\underline{\Phi} = \frac{\tilde{\beta}}{\gamma}\underline{\tilde{\Phi}} \tag{36}$$

which implies $\underline{\Phi} = \underline{\tilde{\Phi}}$ and U or V must be specified. If $\gamma >> \tilde{\alpha}$, $\tilde{\beta} \neq \gamma$ and $\gamma = \Delta$, the solution is the geostrophic wind equation, i.e.,

$$\begin{aligned} \underline{\Phi} &= \underline{\tilde{\Phi}} , \\ U &= -m\underline{\Phi} , \\ \text{and} \quad V &= k\,\underline{\Phi} . \end{aligned} \tag{37}$$

Thus there exists a unique solution to the analysis equations for this case only when the non-divergence constraint is included and its weight is approximately equal to γ.

Case 6

If $\gamma >> \tilde{\beta}$ and Δ, and $\tilde{\alpha} = \gamma$, the solution reduces to

$$\begin{aligned} U &= \tilde{U} , \\ V &= \tilde{V} , \\ \text{and} \quad \underline{\Phi} &= \frac{k\tilde{V} - m\tilde{U}}{Z} . \end{aligned} \tag{38}$$

The balanced constraint provides no filtering on the winds. The filtering on geopotential is anisotropic with a 180° phase shift for small wave numbers in the x direction (Fig. 3a). The general shape of the response function appears as a broad bandpass filter with the minimum damping occurring near $k = .69813$ for $m = .27318$. Figs. 3a and 3b graphically show these conditions.

Case 7

The final case to be investigated is similar to Case 6 except that $\gamma = \Delta$. Any filtering on the initial wind components results from the non-divergence constraint. Eqs. (18) - (20) reduce to

$$\left(\frac{\tilde{\alpha}}{\gamma} + Z \right) U + m Z \underline{\Phi} = \frac{\tilde{\alpha}}{\gamma} \tilde{U} \; , \tag{39}$$

$$\left(\frac{\tilde{\alpha}}{\gamma} + Z \right) V - k Z \underline{\Phi} = \frac{\tilde{\alpha}}{\gamma} \tilde{V} \; , \tag{40}$$

and
$$m U - k V + Z \underline{\Phi} = 0. \tag{41}$$

Eqs. (39) - (41) can be written as

$$U = \frac{\tilde{U} Z\left(\frac{\tilde{\alpha}}{\gamma} + m^2 \right) - m k Z \tilde{V}}{Z\left(\frac{\tilde{\alpha}}{\gamma} + Z \right)} \; , \tag{42}$$

$$V = \frac{V Z\left(\frac{\tilde{\alpha}}{\gamma} + k^2 \right) - k m Z \tilde{U}}{Z\left(\frac{\tilde{\alpha}}{\gamma} + Z \right)} \; , \tag{43}$$

and
$$\underline{\Phi} = \frac{k \tilde{V} - m \tilde{U}}{Z} \; . \tag{44}$$

As expected the response of the geopotential is unaffected by the non-divergence constraint, i.e., the geopotential is determined by the rotational portion of the wind. The filtering on the wind components is similar to that in case 3 modified by the ratio of $\tilde{\alpha} \;/\; \gamma$. Figures 4a and 4b show the response function for unit initial amplitudes and various ratios of $\tilde{\alpha} / \gamma$.

The spectral modifications-phase shifts ($R < 0$), amplification ($R > 1$) and anisotropic filtering-are a consequence of the dynamic matching of the variables. They do not occur when only a single variable is constrained by filters or simple linear equations. Physically, the modifications are expected. For example, when the vorticity or divergence fields are calculated from relatively smooth wind fields the short wavelength components are magnified. This phenomenum exists when any gradient quantity is derived. Thus, to dynamically match variables it may be necessary to amplify some wavelengths to obtain overall satisfaction of the constraints. In this discrete case, additional problems arise because of the finite representation of the differential operators and the inability to resolve components less than twice the grid spacing (which corresponds to the Nyquist frequency). This amplification can be controlled explicitly by the addition of low-pass filter constraints to the functional (Sasaki, 1970b).

Variational Assimilation Model

New data should be assimilated such that discontinuities do not result between regions where there is new data and other regions. The entire data set, forecast and observed, must reflect the physics incorporated into the forecast model in order to maintain the necessary dynamic balance. The nonlinear balance equation has been used as a strong constraint by Haltiner, et al. (1975) as an initialization and assimilation technique for a global primitive-equation model. For the forecast model presented in Chapter II, the linearized balance equation

(6) and

$$D = \frac{\partial \Phi}{\partial t} + m^2 (u \frac{\partial \Phi}{\partial x} + v \frac{\partial \Phi}{\partial y}) + m^2 \Phi_s (\frac{\partial u}{\partial x} + \frac{\partial v}{\partial y}) = 0 \tag{45}$$

do reflect the physics when used as weak constraints.

The non-dimensional adjustment functional incorporating Eqs. (6) and (45) as constraints, i.e., the variational assimilation model, is

$$J_2 = \int_t \int_R \{\tilde{\alpha}(u-\tilde{u})^2 + \tilde{\alpha}(v-\tilde{v})^2 + \beta(\Phi-\tilde{\Phi})^2 + \gamma(B)^2 + \eta(D)^2\} \frac{dxdydt}{m^2} , \tag{46}$$

where the γ term is similar to that in the initialization functional. The observations, denoted by the tildes, are either the forecast values or, where available, observed values. The weights premultiplying the observational constraints are adjusted to reflect the presence of observed data. The η term is a weak constraint similar to that used by McFarland (1975) in his assimilation of temperature. The first variation of Eq. (46) yields the assimilation equations:

$$\frac{\tilde{\alpha}}{m^2}(u-\tilde{u}) - \gamma f \frac{\partial B}{\partial y} + \eta D \frac{\partial \Phi}{\partial x} - \eta \Phi_s \frac{\partial D}{\partial x} = 0 , \tag{47}$$

$$\frac{\tilde{\alpha}}{m^2}(v-\tilde{v}) + \gamma f \frac{\partial B}{\partial x} + \eta D \frac{\partial \Phi}{\partial y} - \eta \Phi_s \frac{\partial D}{\partial y} = 0 , \tag{48}$$

and

$$\frac{\tilde{\beta}}{m^2}(\Phi-\tilde{\Phi}) + \gamma(\frac{\partial^2 B}{\partial x^2} + \frac{\partial^2 B}{\partial y^2}) - \eta(\frac{1}{m^2} \frac{\partial D}{\partial t} + \frac{\partial (uD)}{\partial x} + \frac{\partial (vD)}{\partial y}) = 0. \tag{49}$$

The integrated continuity equation (45) provides a double feedback into the wind analysis equations. These are (1) the advection effect (gradient of geopotential), and (2) the divergence effect (the last term in

Eqs. (47) and (48). To suppress temporal and spatial discontinuities (Sasaki, 1970b), and, as seen in the previous section, to control the spurious amplification of short wavelengths, additional low-pass filters are added to the functional Eq. (46). The filters are easily added to the analysis equations and have the following form

$$- \gamma_{vi} \frac{\partial^2 V}{\partial x_i^2} \tag{50}$$

for first derivative constraints, and

$$\Gamma_{vi} \frac{\partial^4 V}{\partial x_i^4} \tag{51}$$

for second derivative constraints, where γ_{vi} and Γ_{vi} are prespecified weights which can be increased in value if the solution has a tendency to diverge (Sasaki, 1970b). V represents any dependent variable, u, v, ϕ, and x_i is any independent variable.

The initialization and assimilation analysis equations are solved as boundary value problems by the numerical methods described in the next chapter. The specific finite-difference formulation for the forecast equations is also derived in Chapter III.

CHAPTER III

NUMERICAL METHODS

In order to obtain solutions to the models presented in Chapter II, it is necessary to replace the continuous partial differential equations by a system of finite-difference equations. The finite-difference approximations to the derivatives are obtained by expanding the unknown function in a convergent power series (usually a Taylor series) about an arbitrary point in the domain. The series may be truncated at any term. The order of magnitude of the truncation error is determined by the magnitude of the first term after the truncation. In general, the higher the order of the truncation error, the more accurate the finite-difference approximations (Haltiner, 1971).

The integration scheme used for Eqs. (1) - (3) is based on Grammeltvedt's scheme F (1969), the quadratic conservative advective scheme. This form of the finite-difference equations conserves total momentum in the nonlinear terms but does not conserve total energy. To derive the finite-difference equations, the following sum and difference operators are defined:

$$\alpha_x \equiv \frac{1}{\Delta} [\alpha(x_i + \frac{\Delta}{2}) - \alpha(x_i - \frac{\Delta}{2})] , \tag{52}$$

$$\bar{\alpha}^x = \frac{1}{2} [\alpha(x_i + \frac{\Delta}{2}) + \alpha(x_i + \frac{\Delta}{2})], \tag{53}$$

and

$$\bar{\alpha}^x_x = \frac{1}{2\Delta} (\alpha(x_i + \Delta) - \alpha(x_i - \Delta)] , \tag{54}$$

where α is any dependent variable, x_i is any independent variable and Δ is the horizontal grid spacing or time increment. Eq. (54) is the central-difference approximation with truncation error of the order of Δ^2. Using the definition above, Eqs. (1) - (3) are written as follows:

$$\overline{u}^t_t + m^2[(\overline{u}^x \, \overline{u}^x)_x + (\overline{v}^y \, \overline{u}^y)_y - u(\overline{u}^x_x + \overline{v}^y_y)] + K'\overline{m^2_x}^x$$

$$- R_i \, fv + R_i \, \overline{\Phi}^x_x = 0 \quad , \tag{55}$$

$$\overline{v}^t_t + m^2 \, [(\overline{u}^x \overline{v}^x)_x + (\overline{v}^y \overline{v}^y)_y - v(\overline{u}^x_x + \overline{v}^y_y)] + K' \, \overline{m^2_y}^y$$

$$+ R_i \, fv + R_i \, \overline{\Phi}^y_y = 0 \quad , \tag{56}$$

and $$\overline{\Phi}^t_t + m^2 \, [(\overline{u}^x \overline{\Phi}^x)_x + (\overline{v}^y \overline{\Phi}^y)_y] = 0 \quad , \tag{57}$$

where $K' = \left(\dfrac{u^2 + v^2}{2} \right)$.

When solving Eqs. (55) - (57) the time and space increments must be chosen such that the scheme remains computationally stable, i.e., there is no spurious amplification of any wavelengths. For a simple one-dimensional model, a sufficient condition for a stable integration scheme is $C \, \Delta t/\Delta x < 1$, where C is the largest phase speed allowed by the model (Haltiner, 1971).

Conditions for computational stability for the basic model may be found by linearizing the equations, assuming m is a constant equal to one, and assuming periodic solutions for the dependent variables. The non-dimensional linearized equations are:

$$\overline{u'_t}^{t} + U\,\overline{u'_x}^{x} + V\,\overline{u'_y}^{y} - R_1\, f\, v' + R_1\,\overline{\Phi'_x}^{x} = 0\,, \tag{58}$$

$$\overline{v'_t}^{t} + U\,\overline{v'_x}^{x} + V\,\overline{v'_y}^{y} + R_1\, f\, u' + R_1\,\overline{\Phi'_y}^{y} = 0\,, \tag{59}$$

and
$$\overline{\Phi'_t}^{t} + U\,\overline{\Phi'_x}^{x} + V\,\overline{\Phi'_y}^{y} + \Phi_s\left(\overline{u'_x}^{x} + \overline{v'_y}^{y}\right) = 0\,, \tag{60}$$

where the variables are decomposed into a basic state plus perturbations, i.e.,

$$u \rightarrow U + u'\,,$$

$$v \rightarrow V + v'\,,$$

and
$$\Phi \rightarrow \Phi_s + \Phi'\,.$$

The product of perturbation quantities (denoted by the primes) have been neglected.

Assuming the spatial distribution is represented by a trigonometric series and considering only a single harmonic of this Fourier series representation, the perturbation variables are expressed as (suppressing the primes),

$$u^n_{r,s} = u^n \exp[i(kr\Delta x + ms\Delta y) \tag{61}$$

where k and m are wave numbers in the x and y direction, respectively, r and s are grid points, Δx and Δy are grid spacing and n refers to the time step. Similar expressions hold for v^n_{rs} and Φ^n_{rs}. To eliminate the spatial dependence in Eqs. (58) - (60), the following series of identities are useful:

$$
\begin{aligned}
\left(\overline{u^{n}_{rs}}^{x}\right)_{x} &= \frac{1}{2\Delta x}\left(u^{n}_{r+1,s} - u^{n}_{r-1,s}\right) \\
&= \frac{u^{n}_{r,s}}{2\Delta x}\left(e^{-ik\Delta x} - e^{-ik\Delta x}\right) \\
&= \frac{u^{n}_{r,s}}{2\Delta x}\left(2\ i \sin\ (k\Delta x)\right) \\
&= \frac{u^{n}}{2\Delta x}\left(2\ i \sin\ (k\Delta x)\right) .
\end{aligned}
\tag{62}
$$

A similar expression is valid for the y derivatives. Thus, the resulting equations are

$$u^{n+1} = u^{n-1} + (UA + VB)u^{n} + D\ v^{n} + E\Phi^{n} = 0 , \tag{63}$$

$$v^{n+1} = v^{n-1} + (UA + VB)v^{n} - D\ u^{n} + F\Phi^{n} = 0 , \tag{64}$$

and

$$\Phi^{n+1} = \Phi^{n-1} + (UA + VB)\Phi^{n} + \Phi_{s}A\ u^{n} + \Phi_{s}Bv^{n} = 0 , \tag{65}$$

where

$$A = -2\,\frac{\Delta t}{\Delta x}\ i \sin\ (k\Delta x) ,$$

$$B = -2\,\frac{\Delta t}{\Delta y}\ i \sin\ (m\Delta y) ,$$

$$D = 2\ \Delta\ t\ R_{1}\ f ,$$

$$E = R_{1}\ A ,$$

and

$$F = R_{1}\ B .$$

Equations (63) - (64) are expressed in matrix form as:

$$\begin{bmatrix} u^{n+1} \\ v^{n+1} \\ \Phi^{n+1} \\ u^{n} \\ v^{n} \\ \Phi^{n} \end{bmatrix} = \underset{\sim}{G} \begin{bmatrix} u^{n} \\ v^{n} \\ \Phi^{n} \\ u^{n-1} \\ v^{n-1} \\ \Phi^{n-1} \end{bmatrix} \tag{66}$$

where $\underset{\sim}{G}$ is the amplification matrix

$$\underset{\sim}{G} = \begin{bmatrix} L & -D & E & 1 & 0 & 0 \\ D & L & F & 0 & 1 & 0 \\ \Phi_s A & \Phi_s B & L & 0 & 0 & 1 \\ 1 & 0 & 0 & 0 & 0 & 0 \\ 0 & 1 & 0 & 0 & 0 & 0 \\ 0 & 0 & 1 & 0 & 0 & 0 \end{bmatrix}$$

and $L = UA + VB$. The eigenvalues, λ, of the matrix $\underset{\sim}{G}$ are found from the roots of the characteristic equation

$$\det (\underset{\sim}{G} - \lambda \underset{\sim}{I}) = 0 , \tag{67}$$

where det represents the determinant and $\underset{\sim}{I}$ is the identity matrix.

The characteristic equation is

$$[\lambda(L - \lambda) + 1]^3 = \lambda^2 J^2 [1 + (L - \lambda)\lambda] , \tag{68}$$

where $J^2 = \Phi_s R_1 (A^2 + B^2) - D^2$.

The two sets of unique roots to this equation are (Irvine and Houghton, 1971)

$$\lambda = \frac{(L \pm J) \pm [(L \pm J)^2 + 4]^{\frac{1}{2}}}{2} , \tag{69}$$

and

$$\lambda = \frac{L \pm (L^2 + 4)^{\frac{1}{2}}}{2} \quad . \tag{70}$$

The von Neuman necessary condition for stability is

$$| \lambda_k | \leq 1 + 0(\Delta t) \; ,$$

where $|\lambda_k|$ is the absolute value of each of the k eigenvalues of $\underset{\sim}{G}$. The term $0(\Delta t)$ is read terms of first order in Δt and can permit exponential growth of the solution of the difference equation, when legitimate, in accordance with the original differential equation (Haltiner, 1971). Eq. (69) is more restrictive than Eq. (70) and is used to derive conditions for λ_k. If $(L \pm J) > \sqrt{-4}$, then $|\lambda| \geq 1$ for all k and m. Expanding $(L \pm J)$ gives

$$UA + VB \pm (R \; \Phi_s (A^2 + B^2) - D^2)^{\frac{1}{2}} \leq \sqrt{-4} \quad . \tag{71}$$

Substituting for the maximum value of the sine and further algebraic manipulation results in

$$\frac{\Delta t}{\Delta x} \left[U + V \pm \sqrt{\Phi_s} \sqrt{2R_1 + \left(\frac{R_1 f \Delta x}{\Phi_s}\right)^2} \;\right] \leq 1 \; , \tag{72}$$

where $\Delta x = \Delta y$. Once Δx and Φ_s are specified and upper bound estimates for U and V are made, this equation can be solved for Δt. Since the above analysis is valid only for the linear case, a smaller Δt is normally used for the nonlinear equaions.

Another formulation of the finite-difference equations which involves considerable nonlinear smoothing is the semi-momentum form of Shuman (1962). The scheme is written as:

$$\overline{u}^{t}_{t} + \overline{[\overline{m^2}^{xy}(\overline{u}^{xy}\,\overline{u_x}^{y} + \overline{v}^{xy}\,\overline{u_y}^{x}) + R_1\overline{\Phi_x}^{y} - R_1\overline{f}^{xy}\,\overline{v}^{xy} + \overline{K'}^{xy}\,\overline{m^2}^{y}]}^{xy} = 0 \ , \qquad (73)$$

$$\overline{v}^{t}_{t} + \overline{[\overline{m^2}^{xy}(\overline{u}^{xy}\,\overline{v_x}^{y} + \overline{v}^{xy}\,\overline{v_y}^{x}) + R_1\overline{\Phi_x}^{y} + R_1\overline{f}^{xy}\,\overline{u}^{xy} + \overline{K'}^{xy}\,\overline{m^2}^{x}]}^{xy} = 0 \ , \qquad (74)$$

and

$$\overline{\Phi}^{t}_{t} + \overline{[\overline{m^2}^{xy}(\overline{u}^{xy}\,\overline{\Phi_x}^{y} + \overline{v}^{xy}\,\overline{\Phi}^{x}(\overline{u_x}^{y} + \overline{v_y}^{x})]}^{xy} = 0 \ . \qquad (75)$$

These equations result from repeated applications of Eqs. (52) and (53). This complex averaging process may be reduced to a series of simple procedures. The upper most overbars are simple averages and are communative, i.e.,

$$\overline{A + B}^{xy} = \overline{A}^{xy} + \overline{B}^{xy} \ ,$$

where A and B are any averaged or differenced quantities.

Referring to Fig. 5, $\overline{A_5}^{xy} = \frac{1}{4}(A_{10} + A_{11} + A_{12} + A_{13})$. To determine the value of A_{10}, for example, the following formulas are necessary:

$$\overline{A_{10}}^{xy} = \tfrac{1}{4}(A_1 + A_2 + A_3 + A_4) \ ,$$

$$\overline{(A_{10})_y}^{x} = \frac{1}{2\Delta y}(A_5 + A_2 - A_1 - A_4) \ ,$$

and

$$\overline{(A_{10})_x}^{y} = \frac{1}{2\Delta y}(A_5 + A_4 - A_1 - A_2) \ .$$

Similar expression exists for A_{11}, A_{12}, and A_{13}.

Through proper initialization, the integration of the forecast equation is begun with only low frequencies in the advecting velocity, but the nonlinear centered-difference equations will eventually develop large-amplitude, temporal high-frequency computational modes thru nonlinear interactions. Robert, *et al.* (1970) investigated this phenomena for a one-dimensional problem. They developed a technique whereby the high frequencies were suppressed resulting in a stable integration. Polger (1971) extended the theory to two dimensions. The device to control the high frequencies is to average the advective coefficients of the nonlinear terms. It is called the "star" operator and is defined as $(\ )^* \equiv \frac{1}{2}[(\ )^{n-1} + (\ )^n]$, which simply averages the present and immediate past time steps for a given function. Thus, in Eqs. (73) and (74) $\overline{u}^{xy}$ and $\overline{v}^{xy}$ are replaced by $\overline{u^*}^{xy}$ and $\overline{v^*}^{xy}$.

Neither forecast scheme conserves total energy although the continuous system does as seen in Eq. (4). Recently, Sasaki (1975) developed from a variational approach a simple method to force the finite-difference equations to conserve total energy and total mass. The finite-difference analogue to the energy conservation equation is

$$TE \equiv \Delta x \Delta y \,\Sigma[\{\Phi_{ij}^{n} \frac{m_{ij}^2}{2}((u_{ij}^{n+1})^2 + (v_{ij}^{n+1})^2) + \frac{R_1}{2}(\Phi_{ij}^{n+1})^2\} \frac{1}{m_{ij}^2}] - T^o = 0\ , \tag{76}$$

where T^o is the value initially, i.e., $n = -1$. At subsequent time steps $(n \geq 0)$ the forecast values are adjusted (modified) so that Eq. (76) is always satisfied. The development of the adjustment equations is given in Appendix C.

The conservation of total mass is insured by calculating the total mass at each forecast time step, determining the difference between this value and the initial value of mass, normalizing this difference by the total area and adjusting each grid point by the normalized difference, i.e.,

$$h^{n+1} = \tilde{h}^{n+1} - \frac{\left(\sum_{ij}\left(\frac{\tilde{h}^{n+1}}{m^2}\right) - \sum_{ij} \frac{\tilde{h}^{o}}{m^2}\right)}{\sum \frac{1}{m^2}} \quad . \tag{77}$$

In solving the initialization equations (9) - (11) or the assimilation analysis equations (47) - (49) as boundary value problems the continuous differential operators are replaced by centered finite-difference operators as defined in Appendix D. Thus Eqs. (47) - (49) are written as

$$-A_1\nabla_{xx}u - A_2\nabla_{yy}u - A_3\nabla_{tt}u + A_4\, u - A_5\nabla_y u - A_6\nabla_x u + A_7 = 0 \ , \tag{78}$$

$$-B_1\nabla_{xx}v - B_2\nabla_{yy}v - B_3\nabla_{tt}v + B_4 v - B_5\nabla_x v - B_6\nabla_y v + B_7 = 0 \ , \tag{79}$$

and

$$\begin{aligned}(C_1\nabla_{xxxx} + C_2\nabla_{xxyy} + C_3\nabla_{yyyy})\Phi + C_4(\nabla_{xxx} + \nabla_{xyy})\Phi + C_5(\nabla_{yxx}+\nabla_{yyy})\Phi \\ - C_6\,\nabla_{tt}\Phi + C_7\nabla_{xx}\Phi + C_8\nabla_{yy}\Phi - C_9(u\,\nabla_{xt} + v\,\nabla_{yt})\Phi - C_{10}\nabla_{xy}\Phi \\ - C_{11}\,\nabla_x\Phi - C_{12}\nabla_y\Phi - C_{13}\nabla_t\Phi + C_{14}\Phi + C_{15} = 0 \ ,\end{aligned} \tag{80}$$

where $A_1 = \eta\, \Phi_s^{\,2}\, m^2 + \gamma_{us}$,

$A_2 = \gamma\, f^2\, m^2 + \gamma_{us}$,

$A_3 = \gamma_{ut}$,

$$A_4 = \Big(\frac{\tilde{\alpha}}{m^2} - \gamma\, f\, m^2\nabla_{yy}f - \gamma f\,\nabla_y f\,\nabla_y m^2 + \eta\, m^2(\nabla_x\Phi)^2 - \eta\,\Phi_s m^2\nabla_{xx}\Phi$$
$$- \eta\,\Phi_s\,\nabla_x\,\Phi\,\nabla_x\, m^2\Big) \ ,$$

$$h^{n+1} = \tilde{h}^{n+1} - \frac{\left(\sum\limits_{ij}\left(\frac{\tilde{h}^{n+1}}{m^2}\right) - \sum\limits_{ij}\frac{\tilde{h}^{o}}{m^2}\right)}{\sum \frac{1}{m^2}} \quad . \tag{77}$$

In solving the initialization equations (9) - (11) or the assimilation analysis equations (47) - (49) as boundary value problems the continuous differential operators are replaced by centered finite-difference operators as defined in Appendix D. Thus Eqs. (47) - (49) are written as

$$-A_1\nabla_{xx}u - A_2\nabla_{yy}u - A_3\nabla_{tt}u + A_4\, u - A_5\nabla_y u - A_6\nabla_x u + A_7 = 0 \ , \tag{78}$$

$$-B_1\nabla_{xx}v - B_2\nabla_{yy}v - B_3\nabla_{tt}v + B_4 v - B_5\nabla_x v - B_6\nabla_y v + B_7 = 0 \ , \tag{79}$$

and

$$\begin{aligned}(C_1\nabla_{xxxx} + C_2\nabla_{xxyy} + C_3\nabla_{yyyy})\Phi + C_4(\nabla_{xxx} + \nabla_{xyy})\Phi + C_5(\nabla_{yxx} + \nabla_{yyy})\Phi \\ - C_6\,\nabla_{tt}\Phi + C_7\nabla_{xx}\Phi + C_8\nabla_{yy}\Phi - C_9(u\,\nabla_{xt} + v\,\nabla_{yt})\Phi - C_{10}\nabla_{xy}\Phi \\ - C_{11}\,\nabla_x\Phi - C_{12}\nabla_y\Phi - C_{13}\nabla_t\Phi + C_{14}\Phi + C_{15} = 0 \ ,\end{aligned} \tag{80}$$

where $A_1 = \eta\,\Phi_s^{\,2}\,m^2 + \gamma_{us}$,

$A_2 = \gamma\, f^2\, m^2 + \gamma_{us}$,

$A_3 = \gamma_{ut}$,

$$A_4 = \left(\frac{\tilde{\alpha}}{m^2} - \gamma\, f\, m^2\nabla_{yy}f - \gamma f\,\nabla_y f\,\nabla_y m^2 + \eta\, m^2(\nabla_x\Phi)^2 - \eta\,\Phi_s m^2\nabla_{xx}\Phi - \eta\,\Phi_s\,\nabla_x\,\Phi\,\nabla_x\, m^2\right) ,$$

$$A_5 = \gamma\, f(2\, m^2\, \nabla_y f + f\, \nabla_y\, m^2)\ ,$$

$$A_6 = \eta\, \Phi_s^{\,2}\, \nabla_x\, m^2\ ,$$

$$A_7 = (-\frac{\tilde{\alpha}}{m^2}\, \tilde{u} - \gamma f m^2[\nabla_{xxy}\Phi + \nabla_{yyy}\Phi - \nabla_y f\, \nabla_x v - f\nabla_{xy} v - \nabla_y v\, \nabla_x f - v\nabla_{xy} f]$$

$$- \gamma f\, \nabla_y m^2[\nabla_{xx}\Phi + \nabla_{yy}\Phi - f\, \nabla_x v - v\, \nabla_x f]$$

$$+ \eta\, \nabla_x\Phi[\nabla_t\Phi + m^2\, v\, \nabla_y\Phi + m^2\, \Phi_s\, \nabla_y v]$$

$$- \eta\Phi_s[\nabla_{xt}\Phi + m^2 v\, \nabla_{xy}\Phi + m^2\nabla_y\Phi\, \nabla_x v + v\, \nabla_y\Phi\, \nabla_x m^2 + m^2\Phi_s\nabla_{xy} v + \Phi_s\nabla_y v\nabla_x m^2])\ ,$$

$$B_1 = \gamma\, f^2 m^2 + \gamma_{vs}\ ,$$

$$B_2 = \eta\, \Phi_s^{\,2}\, m^2 + \gamma_{vs}\ ,$$

$$B_3 = \gamma_{vt}\ ,$$

$$B_4 = (\frac{\tilde{\alpha}}{m^2} - \gamma\, f\, m^2\nabla_{xx} f - \gamma f\nabla_x f\, \nabla_x m^2 + \eta m^2(\nabla_y\Phi)^2 - \eta\Phi_s m^2\nabla_{yy}\Phi - \eta\Phi_s\nabla_y\Phi\nabla_y m^2)\ ,$$

$$B_5 = \gamma f(2m^2\, \nabla_x f + f\, \nabla_x\, m^2)\ ,$$

$$B_6 = \eta\, \Phi_s^{\,2}\, \nabla_y\, m^2\ ,$$

$$B_7 = (-\frac{\tilde{\alpha}}{m^2}\, \tilde{v} + \gamma f m^2[\nabla_{xxx}\Phi + \nabla_{xyy}\Phi + \nabla_x f\nabla_y u + f\nabla_{xy} u + \nabla_x u\nabla_y f + u\nabla_{xy} f]$$

$$+ \gamma f\nabla_x m^2[\nabla_{xx}\Phi + \nabla_{yy}\Phi + f\nabla_y u + u\, \nabla_y f]$$

$$+ \eta \nabla_y \Phi[\nabla_t \Phi + m^2 u \nabla_x \Phi + m^2 \Phi_s \nabla_x u]$$

$$- \eta \Phi_s [\nabla_{yt} \Phi + m^2 u \nabla_{xy} \Phi + m^2 \nabla_x \Phi \nabla_y u + m^2 \Phi_s \nabla_{xy} u + \Phi_s \nabla_y m^2 \nabla_x u]) \quad ,$$

$$C_1 = \gamma m^2 + \Gamma_s \quad ,$$

$$C_2 = 2 \gamma m^2 \; ,$$

$$C_3 = \gamma m^2 + \Gamma_s \, ,$$

$$C_4 = 2 \gamma \nabla_x m^2 \, ,$$

$$C_5 = 2 \gamma \nabla_y m^2 \, ,$$

$$C_6 = \frac{\eta}{m^2} + \gamma_{\Phi t} \quad ,$$

$$C_7 = (\gamma[\nabla_{xx} m^2 + \nabla_{yy} m^2] - \eta m^2 u^2) \; ,$$

$$C_8 = (\gamma[\nabla_{xx} m^2 + \nabla_{yy} m^2] - \eta m^2 v^2) \; ,$$

$$C_9 = 2 \eta \quad ,$$

$$C_{10} = 2 \eta m^2 u v \, ,$$

$$C_{11} = \eta[\nabla_t u + m^2 (u \nabla_x u + v \nabla_y u) + u^2 \nabla_x m^2 + uv \nabla_y m^2 + m^2 u (\nabla_x u + \nabla_y v)] \, ,$$

$$C_{12} = \eta[\nabla_t v + m^2 (u \nabla_x v + v \nabla_y v) + v^2 \nabla_y m^2 + uv \nabla_x m^2 + m^2 v (\nabla_x u + \nabla_y v)] \, ,$$

$$C_{13} = \eta(\nabla_x u + \nabla_y v) \, ,$$

$$C_{14} = \frac{\tilde{\beta}}{m^2} \ ,$$

$$C_{15} = \gamma[f\{m^2(-\nabla_{yyx}v + \nabla_{yyy}u - \nabla_{xxx}v + \nabla_{xxy}u) + Q(\nabla_x u - \nabla_x v)$$

$$+ 2\nabla_x m^2(\nabla_{xy}u - \nabla_{xx}v) + 2\nabla_y m^2(\nabla_{yy}u - \nabla_{xy}v)\}$$

$$+ \nabla_x f\{m^2(-\nabla_{yy}v - 3\nabla_{xx}v + 2\nabla_{xy}u) - Qv - 2\nabla_x m^2(2\nabla_x v - \nabla_y u)$$

$$- 2\ \nabla_y\ m^2\ \nabla_y\ v\}$$

$$+ \nabla_y f\{m^2(-2\nabla_{xy}v + 3\nabla_{yy}u + \nabla_{xx}u) + Qu + 2\nabla_y m^2(2\nabla_y u - \nabla_x v)$$

$$+ 2\ \nabla_x\ m^2\ \nabla_x\ u\}$$

$$+ m^2\ \nabla_{xx}f\{-\ 3\ \nabla_x v + \nabla_y u - 2v\}$$

$$+ m^2\ \nabla_{yy}f\{-\ \nabla_x v + 3\nabla_y u + 2u\}$$

$$+ m^2\{u(\nabla_{xxy}f + \nabla_{yyy}f) - v(\nabla_{xxx}f + \nabla_{yyx}f)\}$$

$$+ 2\ m^2\nabla_{xy}f\{-\ \nabla_y v + \nabla_x u + u\nabla_x m^2 - v\nabla_y m^2\}$$

$$- \eta\ \Phi_s\{\nabla_{xt}u + \nabla_{yt}v + um^2(\nabla_{xx}u + \nabla_{xy}v) + vm^2(\nabla_{xy}u + \nabla_{yy}v)$$

$$+(\nabla_x u + \nabla_y v)(u\nabla_x m^2 + v\nabla_y m^2) + m^2(\nabla_x u + \nabla_y u)^2\}]$$

$$- \frac{\tilde{\beta}}{m^2}\tilde{\Phi} \ ,$$

and $$Q = \nabla_{xx}m^2 + \nabla_{yy}\ m^2 \ .$$

These equations cannot be applied to the outer two grid points because of the fourth-order finite-difference algorithm. Therefore, these points are held to the original value. Also, the outermost points must remain unadjusted because these are boundary value problems and the natural boundary conditions are applied.

The solution of this coupled system is obtained through the use of a cyclic relaxation method. Let $u^{(1)}$, $v^{(1)}$ and $\Phi^{(1)}$ be a first (guessed) approximation to the solution. These approximations are then substituted in Eq. (78). $v^{(1)}$ and $\Phi^{(1)}$ are considered known solutions with respect to Eq. (78) which is solved by Liebmann overrelaxation for $u^{(2)}$. Eq. (79) is solved in the same manner for $v^{(2)}$ using $v^{(1)}$, $u^{(2)}$ and $\Phi^{(1)}$. The second approximation for Φ yield $\Phi^{(2)}$ when Eq. (80) is solved. In functional form this process is

$$\begin{aligned} & H_1\ (u^P, v^P, \Phi^P, \tilde{u}) \rightarrow u^{P+1}\ , \\ & H_2\ (u^{P+1}, v^P, \Phi^P, \tilde{v}) \rightarrow v^{P+1}\ , \\ \text{and} \qquad & H_3\ (u^{P+1}, v^{P+1}, \Phi^P, \tilde{\Phi}) \rightarrow \Phi^{P+1}\ , \end{aligned} \tag{81}$$

where the appropriate values of u, v and Φ are substituted into A_i, B_i, C_i. This cyclic process is repeated a specified number of times or until a predetermined tolerance criteria is met. Each equation is solved by Liebmann overrelaxation (Haltiner, 1971). Consider, for example, Eq. (78),

$$(-A_1\nabla_{xx}-A_2\nabla_{yy} - A_3\nabla_{tt} + A_4^P - A_5\nabla_y - A_6\nabla_x)u^{P,\nu} + A_7^P = R_u^{P,\nu}, \tag{82}$$

where the first superscript refers to the cycle and the second superscript refers to the stage in the relaxation process. $R_u^{P,\nu}$ represents the non-satisfaction of Eq. (78). The corrections at the $(\nu+1)$st stage are calculated so that $R_u^{P,\nu+1}$ is identically zero. This is accomplished by modifying the central grid point value only. Substituting $u_{i,j,k}^{P,\nu+1}$ into Eq. (82) yields

$$(-A_1\nabla_{xx} - A_2\nabla_{yy} - A_3\nabla_{tt} + A_4^P - A_5\nabla_y - A_6\nabla_x)u_{i,j,k}^{P,\nu+1} + A_7^P = 0. \quad (83)$$

Subtracting Eq. (82) from Eq. (83) gives the desired reduction formulae

$$u_{i,j,k}^{P,\nu+1} = u_{i,j,k}^{P,\nu} - \frac{\omega R_u^{P,\nu}}{\alpha_u^{\nu}} , \quad (84)$$

where $$\alpha_u^{\nu} = 2\left(\frac{A_1}{\Delta x^2} + \frac{A_2}{\Delta y^2} + \frac{A_3}{\Delta t^2} \right) + A_4 ,$$

and ω is the overrelaxation parameter. ω must be between one and two to insure convergence of the relaxation process (Haltiner, 1971).

Each grid point is modified in succession until the maximum residual, $R_u^{P,\nu}$, over the entire grid, is less than a pre-selected tolerance criteria.

The reduction of the residuals for v and Φ during the relaxation process is achieved by:

$$v^{P,\nu+1} = v^{P,\nu} - \omega \frac{R_v^{P,\nu}}{\alpha_v^{\nu}} , \quad (85)$$

and $$\Phi^{P,\nu+1} = \Phi^{P,\nu} - \omega \frac{R_\Phi^{P,\nu}}{\alpha_\Phi^{\nu}} , \quad (86)$$

where $$\alpha_v^{\nu} = 2\left(\frac{B_1}{\Delta x^2} + \frac{B_2}{\Delta y^2} + \frac{B_3}{\Delta t^2} \right) + B_4^P ,$$

and $$\alpha_{\Phi}^{\nu} = \frac{6C_1}{\Delta x^4} + \frac{4C_2}{\Delta x^2 \Delta y^2} + \frac{6C_3}{\Delta y^4} + \frac{2C_6}{\Delta t^2} - \frac{2C_7}{\Delta x^2} - \frac{2C_8}{\Delta y^2} + C_{14} .$$

CHAPTER IV

SIMULATION AND RESULTS

For the simulations, the model is initialized by first prescribing the geopotential, Φ, using the relationship:

$$\Phi(x,y) = \Phi_s + \Phi' \tanh\left[\frac{x' - b\cos\frac{2\pi}{L_y}y'}{d}\right], \tag{87}$$

where Φ_s is the basic state geopotential,

Φ' is the perturbation geopotential,

$x' = x - x_o$, x_o is the half width of the channel,

$y' = y - y_o$, y_o is the half length of the channel,

b is the north-south amplitude of the geopotential field,

d is a parameter which determines the width of the jet,

and L_y is the basic east-west wavelength.

Values used are:

$\Phi_s = 54605.6\ m^2\ sec^{-2}$ (500-mb standard atmospheric geopotential),

$\Phi' = 980\ m^2\ sec^{-2}$,

$b = 2\Delta s$,

$d = 3\Delta s$,

$L_y = 23\Delta s$,

and $\Delta s = \Delta x = \Delta y = 190500$ m.

The Coriolis parameter is evaluated from a beta plane centered at 43.29° N. The image scale factor is a constant, equal to one. The flow is periodic in the east-west direction, while the normal component on the north-south boundaries is essentially zero (the maximum value is .02 m sec^{-1}). The analysis and forecast grid is 15 x 24 grid points; the grid spacing is 190.5 km horizontally. Figure 6 shows the grid orientation with respect to the cartesian axes. Also identified are particular points and cross-sections used in subsequent discussions. The initial wind components are calculated from the geostrophic wind equations. These fields are then dynamically adjusted via the initialization model described in Chapter II, with the weak constraint non-dimensional weights set equal. Figure 7 shows the resulting balanced non-dimensional geopotential field. The maximum gradient is in the center of the channel varying as a cosine wave in the east-west direction. Away from the center the gradient is very weak. The corresponding v-component, Fig. 8, follows the geopotential pattern and represents an east-west jet with a maximum fluid velocity of approximately 14.5 m sec^{-1}. The u component, Fig. 9, reaches its maximum velocity at the inflection points in the geopotential field. Both components become essentially zero at the north-south boundaries. The divergence field associated with the components is of the order of magnitude of 10^{-7} sec^{-1}.

Figure 10 shows the number of relaxation iterations the u and v components required per cycle. The increase on the second cycle indicates a strong initial adjustment and is characteristic of this type of functional (Sasaki, 1970b; Sasaki and Lewis, 1970). After that the number of iterations per cycle monotonically decreases until cycle number 21, where each increases one iteration then continue to decrease. A measure of the overall convergence of the cyclic relaxation method to produce a solution is given by the maximum residual of the first relaxation iteration. This indicates the degree to which the previous values satisfy the analysis equation. As shown in Fig. 11, the maximum adjustment for the wind components occurs in the first 12 cycles and then adjust very slowly thereafter. The oscillation in the residual of the u component occurs because its value is very close to the pre-specified tolerance criteria and any slight change in the value of the other variables causes a drastic change in this residual. The decrease of the geopotential residual is slow after the third cycle indicating that the balanced portion of the winds and geopotential are dynamically adjusted quite rapidly and that the further adjustment in the winds is due primarily to the non-divergence requirement. This is expected since the components for the simulations are initially derived using the geostrophic equations.

These dynamically compatible fields are the initial conditions for the forecast model. Before integrating the equations, Δt is selected so that the linear computational stability requirement of Eq. (72) is satisfied. Substitution of the specified values for Φ_s, Δs, and the estimated maximum velocity of 100 m sec^{-1} into Eq. (72) yields a non-dimensional $\Delta t = .00526$. Since the forecast equations are nonlinear, Δt is specified as .003 (300 sec). The eastward translation of the synoptic wave is governed by phase speed formulae for Rossby waves (Haltiner, 1971). The north-south distribution of the translational velocity (zonal average of the v component) is shown in Fig. 12. Substitution of the maximum value into the phase speed formulae gives a net eastward translation of 5.0 m sec^{-1}. Thus, during the six-hour forecast period, the displacement of the principal wave is approximately .6 of a grid interval.

The north-south boundary value of the variables are held constant during the forecast period. To suppress the two grid interval waves which may arise, a "diffusive" operator is used at the first row of grid points on the region encompassing the interior of the boundary. The forecast equations become (Polger, 1971):

$$u^{n+1} = \bar{u}^{n} - \Delta t\, F_u^{\,n} ,$$

$$v^{n+1} = \bar{v}^{n} - \Delta t\, F_v^{\,n} ,$$

$$\text{and} \qquad \Phi^{n+1} = \bar{\Phi}^{n} - \Delta t\, F_\Phi^{\,n} ,$$

where the bar indicates the average of the immediately adjacent points. $F_u^{\,n}$, $F_v^{\,n}$, $F_\Phi^{\,n}$ are the tendencies of u, v, and Φ respectively for time level n. These tendencies are calculated from either forecast scheme. This diffusive operator is actually the first step of the Lax-Wendroff method (Richtmeyer, 1962). Figure 13 shows the six-hour time trace of the forecast variables for the Scheme F formulation at point A in Fig. 6. The traces are essentially constant reflecting a) the suitability of the initialization scheme (no large amplitude gravity waves), and b) the stationarity of the Rossby wave. The forecast using the Shuman formulation was similar and differed only in the third significant digit. Both forecast schemes conserved total energy and mass quite well during the six hours and consequently did not require any energy or mass adjustment. To determine the sensitivity of the forecast models to imbalances, a 102 m height perturbation is added to the corresponding initialized value at point A. Figure 14 shows the time reaction of the perturbation geopotential at point A for Scheme F. Initially, a large amplitude gravity wave is created. As the energy is dispersed over the region, the amplitude of the gravity wave at this point decreases. This is predicted by the simple geostrophic adjustment theory in which the direction of the adjustment is dependent on the Rossby radius of defomation λ. For this model $\lambda = (\Phi_s / f^2)^{\frac{1}{2}} = 2.34 \times 10^6$ m. Thus, for perturbation wavelengths less than λ, the final field is determined from the wind field, i.e., the wind field changes very little and the mass field conforms to the wind field.

To verify that this imbalance excites gravity waves, the geopotential time trace for point B, 1278 km from point A, is shown in Fig. 15. The field begins to oscillate at approximately 90 minutes into the forecast. This requires a phase speed of 237 m sec^{-1}. For the linearized system, the phase speed of gravity waves is $C_g = |V| \pm 234$ m sec^{-1} (Haltiner, 1971). The amplitude at point B is smaller showing that the energy contained in the imbalance is dispersed over the entire region. Figure 16 shows the response of the Shuman model. The addition of the time filter damps the amplitude of the gravity wave and the phase angle is displaced 15 min compared to Scheme F. Towards the end of the six-hour forecast both schemes have approximately the same amplitude.

To produce "observed" data for the assimilation experiments the initial values and the values from the first four time steps of the forecast model are saved. The actual values of the variables did not change during this 10 minute period because of the suitability of the initialization scheme. Refer to Fig. 13 for an example of the stationarity of the values. The forecast geopotential is modified over a subset of the region because, for the linear system of shallow-water equations, the perturbation geopotential can be associated with a temperature perturbation (Phillips, 1971) and temperatures are the most common parameter derived from remote sensed data. The total set, forecast values plus the modified values, are the "observed" data set. The weight on the modified geopotential was specified as ten times the weight on the forecast geopotential values except in experiment 2. The modifications represent two situations. The first modification (I) simulates the situation where the forecast phase speed is correct but subsequent observations reveal that the magnitude of the synoptic scale wave is considerably different from the forecast. This is achieved by doubling Φ' in Eq. (87). The outer four rows on the north and south boundaries are not modified. This creates an extremely large discontinuity in time and space. Fig. 17a shows the modified geopotential height field. Figs. 17b-d are cross sectional views of the modified field. The forecast values at t = 10 minutes are also shown for comparison.

The second modification (II) represents the situation where the forecast amplitude is correct but the forecast phase speed is slow compared to the observations. The resulting geopotential is shown in Figs. 18a-d. The discontinuities in space and time are much smaller in this case.

Before beginning the assimilation experiments it is necessary to determine the relative magnitude of the various terms in the coefficients in Eqs. (78) - (80) including the constant space and time increments and their powers. This is necessary to insure that in the actual numerical experiment certain terms do not dominate the analysis and lead to total rejection of any new observed data. A simple example can clarify this effect. Consider the analysis equation which results from an observational constraint and a first derivative time constraint. The analysis equation is

$$\epsilon \nabla_t^2 Q - \tilde{\alpha} (Q - \tilde{Q}) = 0 , \qquad (88)$$

where all terms are non-dimensional. Assuming that the characteristic time scale is 10^5 sec and that the particular Δt used is 300 sec (5 min), then Eq. (88) is written as

$$1.1 \times 10^5 \epsilon \Delta_t^2 Q - (Q - \tilde{Q}) = 0 , \qquad (89)$$

where $\Delta_t^2 Q = Q(t+1) + Q(t-1) + 2Q(t)$ and $\tilde{\alpha} = 1$.

Furthermore, all observations $\tilde{Q}$ are assumed equal except one. If the observation number of time levels used in the analysis is small, the filter weight, ϵ, must be chosen much less than one or the first term will dominate the second term. Consequently the odd observation will be rejected even if it is true. If the number of time levels is large, the analysis equation can accommodate this observation more easily by adjusting the values on either side so that "curvature" is very small. For this example, a new weight can be defined, i.e., $\epsilon' = 1.1 \times 10^5 \epsilon$. This new weight just changes the foundation or basis for determing the direction of the adjustment (towards the observations or dynamics). For the analysis equations (78) - (80) the dominant terms resulted from the variation of the integrated continuity equation because the non-dimensional time step, necessary to satisfy the linear computational stability criterion, is approximately 10^{-2} - 10^{-3}. Thus, the largest coefficient associated with the temporal derivatives are 10^2 - 10^3 times larger than any other dynamic coefficient. Consequently, the weak constraint weight, η, is reduced so that the resulting coefficients are approximately the same order of magnitude as those resulting from the balance constraint. This reduces somewhat the time coupling but does allow new observations to be assimilated instead of rejected.

A series of experiments using modification I and the weights listed in Table 1 shows a wide range of assimilation effects. In the first experiment the observational weights are

$$\tilde{\alpha} = 10^6 \quad \text{and} \quad \tilde{\beta} = 10^{11} .$$

This insures that the dynamic constraints are overridden and this experiment is similar to the sensitivity analysis performed on the forecast models. Due to the nature of the discontinuities in the observed data set, the gravity waves are large and more extensive. Figure 19 shows the time trace of the variables at point B. The temporal discontinuity in the geopotential is very dramatic. The trace preceeding the discontinuity are the values from the original forecast. During the assimilation, the magnitude of the variables at t = 5 min was dynamically adjusted but its value is not shown on the trace. The initial amplitude of the gravity wave is nearly 50 percent the amplitude of the synoptic scale wave. Both the wind components show a small amplitude oscillation. Point B is located at the edge of the geopotential discontinuity and, the variables reflect some non-adjustment. At point A, which is in the center of the channel, the amplitude of the gravity wave is much smaller initially reflecting only a slight imbalance between the wind and the geopotential. At later times, the amplitude increases as there is multiple interaction of the gravity waves (Fig. 20). The wind time traces, in the center of the channel, are similar to those of Fig. 19. Figs. 21a, b, c show the forecast field at t = 3 hrs. The presence of high-frequency gravity waves is easily seen in the erratic nature of the contours.

In all experiments, the constraints of conservation of total energy and mass are imposed using the original initial values. The assimilated fields, in this experiment, increased the non-dimensional energy by 286 units (1.5%) and the non-dimensional mass by 13 units (.06%). The mass adjustment, performed first, decreased the total mass to the initial value. This has the effect of lowering the basic state geopotential. For the linear system of forecast equations this would reduce the phase speed of the gravity waves but for the nonlinear system, this causes the phase speeds to remain essentially constant. The required energy adjustment is very small. The maximum value for λ_E is 2×10^{-4} justifying the linearization technique used in the development of the iterative scheme(Appendix C). The adjusted total energy is essentially constant during the forecast because the constraint is considered satisfied if the adjusted energy is within 5 units of the initial value. The adjusted kinetic energy (K.E.) and potential energy (P.E.) oscillate (Fig. 22) due to the energy transformations taking place during the forecast through nonlinear interactions, and to the nonidentical satisfaction of the constraint. The energy adjustment does effect the total mass but generally by less than one unit. This represents a .005% change with respect to the total change.

In all experiments, a single forward time step was used initially and after the assimilation to start the forecast. After the assimilation, a centered-time step procedure was tested but a computational mode

(Haltiner, 1971) was present. This resulted from the decreased weight on the integrated continuity equation. The fields were dynamically matched in space but not as well in time. Thus, alternate time levels were coupled and maintained their integrity. The restart method, a forward time step, is an effective method to prevent the computational mode (Kurihara, 1965).

In experiment 2 the observational weights were decreased so that the dynamical adjustments could take place. The effect of the dynamics is seen in Figs. 23a and b. The observed values are plotted for comparison. The analysis model has eliminated the sharp discontinuity and provided a smooth transition from the boundary to the interior where the analysis nearly matches the observed data. The original discontinuity has most of its power in the 2-4Δs waves but the balance constraint effectively reduces the amplitude of these waves (Fig. 2a). The transition is better where the discontinuity is symmetric with respect to the channel. This is seen by comparing Figs. 23a and 23b. In Fig. 23a, the original discontinuity near the northern border is larger than that in Fig. 23b. Consequently, the analysis has more curvature at this point. The wind components respond to the analyzed geopotential. The increase in the v component (Figs. 24a and b) reflects the increased gradient of geopotential. Also, there is the expected amplification of the shorter wavelengths from the balanced constraint (Fig. 2a). This is seen in the 4Δs wave in the v component near the northern and southern borders (Fig. 24b). The effects of the divergence constraint are seen in Fig. 25. The divergence constraint on u acts primarily in the x direction. The analyzed u component is smooth and contains no small scale information.

The forecast from these assimilated data still showed the existence of gravity waves but there is a 60% reduction in the amplitude over experiment 1. Fig. 26 shows the geopotential at points B and A respectively. There appears to be only one low amplitude gravity wave in comparison to the many that appear in Figs. 19 and 20.

In the third experiment, the weight on the geopotential observations was .5 the weight in experiment 2. The dynamic weight, η, was increased to .001. As with all the experiments the magnitude of the maximum first residual decreased as the number of cycles increased. For this experiment this residual decreased one to two orders of magnitude for each variable by the 12th cycle. At this point the assimilation process was stopped. The results at time t = 10 min are shown in Figs. 27a-29. The analyzed values show less of the effect of the discontinuity and are more in line with the original forecast, i.e., the dynamic effect is stronger. The results of the forecast from this set are shown in Fig. 30. At point B, the amplitude of the gravity wave is only 18% of the amplitude of experiment 1. The three-hour forecast, Fig. 31c, has much less noise than Fig. 21c, indicating the dimenished amplitude of the gravity waves. Their effect is more noticeable near the original discontinuity. In the center of the channel only the synoptic wave is detectable. The u component shows the synoptic pattern except near the northern and southern boundaries (compare Fig. 31a and Fig. 21a).

In the last experiment with modification I the weight on the observed geopotential was specified as 500. In this case the modified geopotential was rejected and, in fact, the analysis at t = 10 min corresponded to the original forecast values and thus, the 3-hour forecasts are nearly identical.

In the final experiment, modification II is used to generate the observed field. The weight on the modified geopotential is increased to 5000 while all other weights remain the same as in the previous experiment. The Shuman scheme is the forecast model. As shown in Fig. 18, the discontinuities are generally less severe than the other experiments. The dynamic adjustment is better in this case; although the Shuman scheme does smooth, only a small amplitude wave as seen in Fig. 32. The wind components are in balance with the geopotential. The 3-hour forecast is shown in Fig. 33. The northern and southern boundary effects are clearly seen. In Figs. 33b and 33c the axis of the trough curves to match the boundary values. In the center of the channel the axis of the geopotential trough (Fig. 33c) is where the modified values placed it but it gradually deviates from the observed as the boundaries are approached. This effect is also seen in the wind components. In the SW and NE corner of Fig. 33c there is a short wavelength perturbation ($4\Delta s$). These areas correspond to areas of maximum discontinuity in the observed field and the greatest imbalance between the analyzed fields.

CHAPTER V

CONCLUSIONS AND REMARKS

The initialization and assimilation models are developed within the frame work of variational calculus. The technique incorporates the principal physics of the forecast model, as well as observations, into the total system of analysis equations. These equations are solved as boundary value problems in which the observed data set, including forecast and observed values,are dynamically adjusted or matched. Investigation of the spectral modifications necessary to satisfy the dynamical constraints shows that significant modifications may be necessary depending on the wavelengths and amplitudes contained in the observed field. The modifications include amplification, filtering, and phase shifting of certain wavelengths, both long and short. The relative weighting on the observations significantly affects the shape and value of response curves.

The modified geopotential, used in the assimilation experiments, is a severe departure from the forecast fields. These departures exposed the strengths and limitations of the assimilations model. The model is capable of handling extreme differences and producing dynamically sound fields in which there is a large reduction in the amplitude of the gravity waves. The dynamic matching may lead to the amplification of certain wavelengths in the wind components. This phenomenon, analytically investigated for the initialization functional, is observed in the results of the assimilation functional. It seems to be the most plausible effect in the adjustment process because dynamic constraints support these wavelengths rather than the increased damping of shorter wavelengths for all variables.

The limitations of the assimilation model involve the spatial and temporal extent of the asynoptic data (modified geopotential for the simulations) and their relationship to the total space-time domain considered. The asynoptic data must cover an area large enough to adequately redefine part of the large-scale wave, or else, the assimilation model will significantly dampen or eliminate the data by the strong damping of short wavelengths in the geopotential field by the balance constraint. The boundaries of the region must be far enough removed from the area of the asynoptic data to allow the natural dynamic adjustment, or else, sharp gradients and non-matched fields will result near the boundaries. This in turn leads to gravity waves. If the boundaries cannot be removed from the asynoptic data, the subsequent forecast variables can be returned to the assimilation model for further dynamic adjustment and minimization of the amplitude of the gravity waves. The observed weights must be modified and the forecast period should be such that the boundary values are not affected by the gravity waves. With time invariant or cyclic boundaries this presents no problem, but with time varying boundaries it can since they determine the homogeneous solution to the analysis equations.

The constraint of conservation of total energy and mass in the finite-difference formulation of the forecast equations is simple and effective. The approach can be applied to other conservative quantities.

It can also be applied to the case where there are sources or sinks, or a non-zero net flux of energy thru the boundaries providing their time dependence can be specified.

Several promising areas for continued research result from this investigation. Research should continue on the spectral modification occurring in the dynamic adjustment process and the specific role of the observational and dynamic weights. This can be accomplished using very simple dynamical constraints, for example, the continuity equation and the geostrophic wind equations or a much more detailed investigation of the simple initialization model presented. The resulting modifications hold promise in the study and clarification of the energetics of the atmosphere from a variational approach since the functional does represent a minimization of error energies.

The cyclic relaxation process is very time consuming. The direct solver method (Rosmond and Faulkner, 1975) with its large reduction in solution time and more accurate solutions could make this assimilation method operationally attractive, at least over a limited area.

The final recommendation for continued research involves the balance equation which is an effective means of suppressing the noise in the P.E. forecast. The assimilation model should be extended to include the full nonlinear balance equations because for large-scale flow the nonlinear terms are approximately the same order of magnitude as the advection of the Coriolis parameter. As the horizontal length scale decreases, but still in the synoptic range, the nonlinear terms can not be arbitrarily neglected. As a first step, the nonlinear terms could be determined from the observations. They would not take part in the variations and would only enter the forcing function. They could be recalculated after each cyclic as suggested by Lewis (1972). This would allow for some nonlinear effects in the resulting analysis.

BIBLIOGRAPHY

Achtemeier, G. L., 1972: Variational initialization of atmospheric fields—a quasi-geostrophic diagonistic model. Ph.D. Dissertation, Florida State University, Tallahassee, Florida, 216 pp.

Alaka, M. A., and R. C. Elvander, 1972: Optimum interpolation from observations of mixed quality. Monthly Weather Review, 100, 612-624.

Barnes, S. L., 1973: Mesoscale objective map analysis using weighted time-series observations. NOAA Technical Memo ERL-NSSL-62, 60 pp.

Bengtsson, L., 1975: 4-dimensional assimilation of meteorological observations. GARP Publication Series No. 15, WMO-ICSU Joint Organizing Committee, 76 pp.

Benwell, G. R., and F. P. Bretherton, 1968: A pressure oscillation in a 10-level atmospheric model. Quarterly Journal of the Royal Meteorological Society, 94, 400, 123-131.

Blumen, W., 1967: On nonlinear geostrophic adjustment. Journal of the Atmospheric Sciences, 24, 325-332.

Bolin, B., 1953: The adjustment of a non-balance velocity field towards geostrophic equilibrium in a stratified fluid. Tellus, 5, 373-385.

Carnahan, B., H. Luther, and J. Wilkes, 1969: Applied Numerical Methods. John Wiley and Sons, New York, 604 pp.

Charney, J. G., 1955: The use of the primitive equations of motion in numerical prediction. Tellus, 7, 22-26.

________, M. Halem, and R. Jastrow, 1969: Use of incomplete historical data to infer the present state of the atmosphere. Journal of the Atmospheric Sciences, 26, 1160-1163.

Forsythe, G. E., and W. R. Wasow, 1960: Finite-difference Methods for Partial Differential Equations. John Wiley & Sons, New York, 444 pp.

Gandin, L. S., 1965: Objective Analysis of Meteorological Fields. Israeli Program for Scientific Translations, Jerusalem, 242 pp.

Gauntlett, D. J., and R. Seaman, 1974: Four-dimensional data assimilation experiments in the Southern Hemisphere. Journal of Applied Meteorology, 13, 845-853.

Gerrity, J., and R. McPherson, 1969: Development of a fine-mesh limited-area prediction model. Monthly Weather Review, 97, 665-669.

Gordon, C. T., L. Umscheid, and K. Miyakoda, 1972: Simulation experiments for determining wind data requirements in the tropics. Journal of the Atmospheric Sciences, 29, 1064-1075.

Grammeltvedt, A., 1969: A survey of finite-difference schemes for the primitive equations for a barotropic fluid. Monthly Weather Review, 97, 384-404.

Haltiner, G. J., 1971: Numerical Weather Prediction. John Wiley & Sons, New York, 317 pp.

________, E. Barker, and Y. K. Sasaki, 1975: An initialization technique for primitive models using a balance-equation constraint. Presented at the JOC Study Group Conference on Four-Dimensional Data Assimilation, Paris, 17-21 November, 1975.

Hayden, C., 1973: Experiments in the four-dimensional assimilation of Nimbus 4 SIRS data. Journal of Applied Meteorology, 12, 425-435.

Hess, S. L., 1959: Introduction to Theoretical Meteorology. Henry Holt Company, New York, 362 pp.

Hildebrand, F. B., 1965: Methods of Applied Mathematics. Prentice Hall Inc., Englewood-Cliffs, N. J., 362 pp.

Holl, M. M., and B. R. Mendenhall, 1971: Fields by information blending, sea-level pressure version, Final report, Project M-167, Contract No. N-66314-70-C-5226, Meteorology International Incorporated, Monterey, California, 66 pp.

Houghton, D., A. Kasahara, and W. Washington, 1966: Long-term integration of the barotropic equations by the Lax-Wendroff method. Monthly Weather Review, 94, 141-150.

Inman, R. L., 1970: Papers on operational objective analysis schemes at the National Severe Storms Forecast Center. NOAA Technical Memo ERLTM-NSSL 51, 91 pp.

Jastrow, R., and M. Halem, 1970: Simulated studies related to GARP. Bulletin of the American Meteorological Society, 51, 490-513.

________, and M. Halem, 1973: Simulation studies and the design of the first GARP global experiment. Bulletin of the American Meteorological Society, 54, 13-21.

Kaplin, M., and D. Paine, 1973: A 32-km moist primitive equation model providing for scale interaction. Journal of the Atmospheric Sciences, 30, 213-222.

________, and D. Paine, 1974: The linking of multi-scaled energy sources leading to atmospheric development. Part II. A severe tornado-producing convective squall-line system. Scientific Report No. 2, Contract No. GA-35250, National Science Foundation, Washington, D.C., 54 pp.

Kasahara, A., 1972: Simulation experiments for meteorological observing systems for GARP. Bulletin of the American Meteorological Society, 53, 252-264.

Kluge, J., 1970: Uber die Verwendung variabler gewichtefunktionen bei der anpassung meteorologischer nach Sasaki. Gerlands Beitrage zur Geophysik, 80, 375-382.

Kurihara, Y., 1965: On the use of the implicit and iterative methods for the time integration of the wave equation. Monthly Weather Review, 93, 33-46.

Lewis, J. M., 1971: Variational subsynoptic analysis with application to severe local storms. Monthly Weather Review, 99, 786-795.

________, 1972: An operational upper air analysis using the variational method. Tellus, 24, 514-530.

________, and T. H. Grayson, 1972: The adjustment of surface wind and pressure by Sasaki's variational matching technique. Journal of Applied Meteorology, 11, 586-597.

Magata, M., and K. Nishida, 1971: On the computational errors in the numerical experiments. Journal of the Meteorological Society of Japan, 49, 774-783.

McFarland, M. J., 1975: Variational optimization analysis of temperature and moisture advection in a severe storm environment. Ph.D. Dissertation, University of Oklahoma, Norman, Oklahoma, 79 pp.

McPherson, R., and R. Kistler, 1975: Theoretical and experimental comparison of selected time integration methods applied to four-dimensional assimilation. NOAA Technical Memo NWS NMC-56, 62 pp.

Morel, P., G. Lefevre, and G. Rabreau, 1971: On initialization and non-synoptic data assimilation. Tellus, 23, 197-206.

Nitta, T., and J. B. Hovermale, 1969: A technique of objective analysis and initialization for the primitive forecast equations. Monthly Weather Review, 97, 652-658.

Nitta, T., 1971: Response of a dynamical model to partially produced imbalance in meteorological fields. Journal of the Meteorological Society of Japan, 49, 628-637.

Økland, H., 1970: On the adjustment towards imbalance in primitive equation weather prediction models. Monthly Weather Review, 98, 271-279.

________, 1972: On the balance, initialization and data assimilation in primitive equation prediction models. Journal of the Atmospheric Sciences, 29, 641-648.

Phillips, N. A., 1960: On the problem of initial data for the primitive equations. Tellus, 12, 121-126.

________, 1971: Ability of the Tadjbakhsh method to assimilate temperature data in a meteorological system. Journal of the Atmospheric Sciences, 28, 1325-1328.

Polger, P., 1971: A study of non-linear computational instability for a two-dimensional model. NOAA Technical Memo NWS NMC-49, 22 pp.

Richardson, L. F., 1911: The approximate arithmetical solution by finite differences of physical problems involving differential equations, with an application to the stress in a masonary dam. Philosophical Transactions of the Royal Society of London, Ser. A, 210, 307-357.

Robert, A., F. Shuman, and J. Gerrity, 1970: On partial difference equations in mathematical physics. Monthly Weather Review, 98, 1-6.

Rosmond, T., and F. Faulkner, 1975: Direct solution of elliptic equations by block cyclic reduction and factoralization. Environmental Prediction Research Facility Technical Note No. 20, 34 pp.

Ross, S. L., 1964: Differential Equations. Blaisdell Publishing Co., Waltham, Mass., 594 pp.

Rossby, C. G., 1938: On the mutual adjustment of pressure and velocity distribution in certain simple current systems. Journal of Marine Research, 1, 239-263.

Rutherford, I., and R. Asselin, 1972: Adjustment of the wind field to geopotential data in a primitive equation model. Journal of the Atmospheric Sciences, 29, 1059-1063.

Sadourny, R., 1973: Forced geostrophic adjustment in large scale flows. Unpublished manuscript, Laboratoire de Meteorologie Dynamique du DNRS, 92--Meudon-Bellevue, France.

Sasaki, Y. K., 1969: Proposed inclusion of time variation terms, observational and theoretical, in numerical variational objective analysis. Journal of the Meteorological Society of Japan, 47, 115-124.

Sasaki, Y. K., 1970a: Some basic formalisms in numerical variational analysis. Monthly Weather Review, 98, 875-883.

________, 1970b: Numerical variational analysis formulated under the constraints as determined by long wave equations and a low-pass filter. Monthly Weather Review, 98, 884-898.

________, 1971: Low pass and band pass filters in numerical variational optimization. Journal of the Meteorological Society of Japan, 49, 766-773.

________, 1975: Variational design of finite difference scheme for initial value problem of conservative system. Submitted to Journal of Computational Physics.

________, and J. M. Lewis, 1970: Numerical variational objective analysis of the planetary boundary layer in conjunction with squall line formation. Journal of the Meteorological Society of Japan, 48, 381-388.

Shuman, F. G., 1962: Numerical experiments with the primitive equations. Proceedings of the International Symposium on Numerical Weather Prediction in Tokyo, Nov. 7-13, 1960, Meteorological Society of Japan, 85-107.

________, and J. Stackpole, 1969: The currently operational NMC model, and results of a recent numerical experiment. Proceedings WMO/IUGG Symposium of Numerical Weather Prediction, Tokyo, Japan, November 26-December 4, 1968, II-85, 98, Japan Meteorological Agency, Tokyo.

Shumbera, A. L., 1970: AFGWC macro-scale upper air analysis model. AFGWC Technical Memo 70-2, 24 pp.

Sweet, R., 1973: A generalized cyclic reduction algorithm. Unpublished National Center for Atmospheric Research Manuscript, Boulder, Colorado.

Talagrand, O., 1972: A note on the damping of inertia-gravity waves in four-dimensional assimilation of meteorological data. Journal of the Atmospheric Sciences, 29, 1571-1574.

Temperton, C., 1973: Some experiments in dynamic initialization for a simple primitive equation model. Quarterly Journal of the Royal Meteorological Society, 99, 303-319.

Wagner, K. K., 1971: Variational analysis using observational and low-pass filtering constraints. Master's Thesis, University of Oklahoma, 39 pp.

Washington, W. M., 1964: A note on the adjustment towards geostrophic equilibrium in a simple fluid system. Tellus, 16, 530-534.

Williamson, D., and R. Dickinson, 1972: Periodic updating of meteorological variables. Journal of the Atmospheric Sciences, 29, 190-193.

________, and A. Kasahara, 1971: Adaption of meteorological variables forced by updating. Journal of the Atmospheric Sciences, 28, 1313-1324.

APPENDIX A

THE SHALLOW WATER AND TOTAL ENERGY EQUATIONS

The primitive equations for barotropic-divergent flow, developed in terms of coordinates on the polar sterographic projection to facilitate the handling of meteorological data, have the following form:

$$\frac{\partial u}{\partial t} + m^2(u \frac{\partial u}{\partial x} + v \frac{\partial u}{\partial y}) + m \frac{\partial m}{\partial x} (u^2 + v^2) - fv + \frac{\partial \Phi}{\partial x} = 0 \text{ ,} \quad \text{(A-1)}$$

$$\frac{\partial v}{\partial t} + m^2(u \frac{\partial v}{\partial x} + v \frac{\partial v}{\partial y}) + m \frac{\partial m}{\partial y} (u^2 + v^2) + fu + \frac{\partial \Phi}{\partial y} = 0 \text{ ,} \quad \text{(A-2)}$$

and

$$\frac{\partial \Phi}{\partial t} + m^2 (\frac{\partial(\Phi u)}{\partial x} + \frac{\partial(\Phi v)}{\partial y}) = 0 \text{ .} \quad \text{(A-3)}$$

The symbols used are:

x,y	=	horizontal cartesian coordinates on polar stereographic projection,
t	=	time,
m	=	image scale factor,
		$m = \frac{1 + \sin \theta_o}{1 + \sin \theta}$, θ_o is the reference latitude (60^oN) and θ is any latitude,
u	=	scaled x-component of velocity (horizontal velocity, earth distance per unit time, divided by the image scale factor),
v	=	scaled y-component of velocity,
f	=	Coriolis parameter, $2 \Omega \sin Q$, where Ω is the angular velocity of rotation of the earth,
and Φ	=	the geopotential height of an isobaric surface, gz, where g is the acceleration due to gravity and z is the geometric height above mean sea level.

The equations can be transformed to a dimensionless form (starred variables) by replacement of all variables, dependent and independent, by their scaled counterparts. Thus,

$$u = V\,u^*, \qquad t = \tau\,t^*,$$
$$v = V\,v^*, \qquad f = F\,f^*,$$
$$\Phi = \bar{\Phi}\,\Phi^*, \qquad x = L\,x^*,$$

and

$$y = L\,y^*,$$

where

$$V = 10 \text{ m sec}^{-1},$$
$$F = 10^{-4} \text{ sec}^{-1},$$
$$L = 10^{6} \text{ m},$$
$$\bar{\Phi} = FVL = 10^{3} \text{ m}^2 \text{ sec}^{-2},$$

and

$$\tau = L/V = 10^{5} \text{ sec}.$$

The characteristic parameters are representative of the large-scale flow patterns in middle latitude. The intent of the non-dimensionalization has not been to determine the relative magnitude of each term, necessarily, but to facilitate the computations and the selection of the weights. Substituting these into Eqs. (A-1) - (A-3), dropping the star notation, and rearranging yields

$$\frac{\partial u}{\partial t} + m^2\left(u\frac{\partial u}{\partial x} + v\frac{\partial u}{\partial y}\right) + m\frac{\partial m}{\partial x}(u^2 + v^2) - R_1 fv + R_1\frac{\partial \Phi}{\partial x} = 0, \quad \text{(A-4)}$$

$$\frac{\partial v}{\partial t} + m^2\left(u\frac{\partial v}{\partial x} + v\frac{\partial v}{\partial y}\right) + m\frac{\partial m}{\partial y}(u^2 + v^2) + R_1 fu + R_1\frac{\partial \Phi}{\partial y} = 0, \quad \text{(A-5)}$$

and

$$\frac{\partial \Phi}{\partial t} + m^2\left(\frac{\partial(\Phi u)}{\partial x} + \frac{\partial(\Phi v)}{\partial y}\right) = 0, \quad \text{(A-6)}$$

where $R_1 (= \frac{FL}{V} = 10)$ is the inverse of the Rossby number. Expanding Eq. (A-6) yields

$$\frac{\partial \Phi}{\partial t} + m^2 (u \frac{\partial \Phi}{\partial x} + v \frac{\partial \Phi}{\partial y}) + m^2 \Phi (\frac{\partial u}{\partial x} + \frac{\partial v}{\partial y}) = 0 . \qquad \text{(A-7)}$$

The non-dimensional geopotential, Φ, is composed of a basic state Φ_s, independent of time and space, plus perturbations upon the basic state. The scaling factor for geopotential is such that the non-dimensional perturbations are of the order of unity. Consequently, the basic state Φ_s is of the order of $10^1 - 10^2$. For example, $\Phi_s = 54.6056$ using the 500-mb standard atmospheric value. Since large-scale divergence is normally an order of magnitude smaller than the scaling factor (V/L), all terms in Eq. (A-7) are of the order of unity.

The total energy equation may be derived by multiplying Eq. (A-4) by $m^2 u \Phi$, Eq. (A-5) by $m^2 v \Phi$, and adding the equations. This gives

$$m^2 \Phi \frac{\partial K}{\partial t} + m^2 (m^2 u \Phi \frac{\partial K}{\partial x} + m^2 v \Phi \frac{\partial K}{\partial y}) + R_1 m^2 u \frac{\partial}{\partial x} (\frac{\Phi^2}{2}) + R_1 m^2 v \frac{\partial}{\partial y} (\frac{\Phi^2}{2})$$

$$+ m^2 \Phi K (\frac{\partial m^2}{\partial x} + \frac{\partial m^2}{\partial y}) = 0 , \qquad \text{(A-8)}$$

where $K = \frac{u^2 + v^2}{2}$.

Equation (A-8) can be further manipulated by recognizing that

$$m^2 u \Phi \frac{\partial K}{\partial x} = \frac{\partial (m^2 u \Phi K)}{\partial x} - u \Phi K \frac{\partial m^2}{\partial x} - m^2 u K \frac{\partial \Phi}{\partial x} - m^2 K \Phi \frac{\partial u}{\partial x} , \qquad \text{(A-9)}$$

and similarly for the y and t derivatives. Thus, Eq. (A-8) becomes

$$\frac{\partial(\Phi K')}{\partial t} + m^2\left(\frac{\partial(u\Phi K')}{\partial x} + \frac{\partial(v\Phi K')}{\partial y}\right) - m^2K'\left(u\frac{\partial\Phi}{\partial x} + v\frac{\partial\Phi}{\partial y}\right) - m^2K'\Phi\left(\frac{\partial u}{\partial x}+\frac{\partial v}{\partial y}\right)$$

$$+ R_1m^2 \left(u \frac{\partial}{\partial x}\left(\frac{\Phi^2}{2}\right) + v \frac{\partial}{\partial y}\left(\frac{\Phi^2}{2}\right)\right) - K' \frac{\partial\Phi}{\partial t} = 0 , \qquad \text{(A-10)}$$

where $K' = K \times m^2$.

Multiplication of Eq. (A-7) by K' and addition to Eq. (A-10) gives

$$\frac{\partial(\Phi K')}{\partial t} + m^2\left(\frac{\partial(u\Phi K')}{\partial x} + \frac{\partial(v\Phi K')}{\partial y}\right) + R_1 m^2\left(u \frac{\partial}{\partial x}\left(\frac{\Phi^2}{2}\right) + v \frac{\partial}{\partial y}\left(\frac{\Phi^2}{2}\right)\right)= 0. \qquad \text{(A-11)}$$

Multiplying Eq. (A-7) by $R_1\Phi$ and adding to Eq. (A-11) results in

$$\frac{\partial E}{\partial t} + m^2\left(\frac{\partial(u\Phi K')}{\partial x} + \frac{\partial(v\Phi K')}{\partial y}\right) + m^2\left(\frac{\partial}{\partial x}\left(uR_1\frac{\Phi^2}{2}\right)+ \frac{\partial}{\partial y}\left(vR_1\frac{\Phi^2}{2}\right)\right)$$

$$+ m^2R_1\frac{\Phi^2}{2}\left(\frac{\partial u}{\partial x} + \frac{\partial v}{\partial y}\right) + m^2R_1\left(u\frac{\partial}{\partial x}\left(\frac{\Phi^2}{2}\right) + v\frac{\partial}{\partial y}\left(\frac{\Phi^2}{2}\right)\right) = 0 \qquad \text{(A-12)}$$

where $E = \Phi K' + \dfrac{R_1\Phi^2}{2}$.

Combining the last four terms of Eq. (A-12) gives

$$\frac{\partial E}{\partial t} + m^2\left(\frac{\partial(uT)}{\partial x} + \frac{\partial(vT)}{\partial y}\right) = 0 , \qquad \text{(A-13)}$$

where $T = \Phi(K' + R_1\Phi)$.

If Eq. (A-13) is integrated over a region for which the flux of energy across the boundaries is zero, Eq. (4) results.

APPENDIX B

DERIVATION OF THE ANALYSIS EQUATIONS

In taking the first variation, only the unknown dependent functions are varied. These include u, v and Φ and their derivatives. The independent variables x, y, and t, the weak constraint weights, and the observed values are known and are not varied. As shown in Hildebrand (1965), the variational operator acts in much the same way as the partial differential operators. The laws of variation of sums, products, ratios, and powers are completely analogous to the corresponding laws of differentiation.

The first variation of Eq. 8 is

$$\delta J = 0 = \int_R \{2\tilde{\alpha}(u-\tilde{u})\delta u + 2\tilde{\alpha}(v-\tilde{v})\delta v + 2\tilde{\beta}(\Phi-\tilde{\Phi})\delta\Phi + 2\gamma B\ \delta B$$

$$+ 2\gamma C\ \delta C\} \frac{dxdy}{m^2}\ , \qquad \text{(B-1)}$$

where $\delta B \equiv m^2\{ \frac{\partial^2 \delta\Phi}{\partial x^2} + \frac{\partial^2 \delta\Phi}{\partial y^2} - \frac{\partial f}{\partial x}\delta v - f\frac{\partial \delta v}{\partial x} + \frac{\partial f}{\partial y}\delta u + f\frac{\partial \delta u}{\partial y}\}$,

$$\delta C \equiv m^2 \left(\frac{\partial \delta u}{\partial x} + \frac{\partial \delta v}{\partial y} \right) ,$$

and δu is the variation of the function u, etc.

Substitution of δB and δC in Eq. (B-1) and repeated integration by parts leads to

$$\delta J = 0 = \int_R \{\delta u[\alpha(u-u) - \Delta \frac{\partial C}{\partial x} + \gamma B \frac{\partial f}{\partial y} - \gamma \frac{\partial (fB)}{\partial y}]$$

$$+ \delta v[\tilde{\alpha}(v-\tilde{v}) - \Delta \frac{\partial C}{\partial y} - \gamma B \frac{\partial f}{\partial x} + \gamma \frac{\partial (fB)}{\partial x}] \qquad \text{(B-2)}$$

$$+ \delta\Phi[\tilde{\beta}(\Phi-\tilde{\Phi}) + \gamma (\frac{\partial^2 B}{\partial x^2} + \frac{\partial^2 B}{\partial y^2})]\} \, dxdy + [\text{Boundary Conditions}] \; .$$

For satisfying the extremum condition, $\delta J = 0$, for arbitrary and independent variations of δu, δv, and $\delta\Phi$, their respective coefficients must each vanish identically in the domain. This leads to Eqs. (9) - (11). The boundary conditions are satisfied by specifying u, v and Φ on the boundaries and thus, δu, δv, and $\delta\Phi$ are zero there. In practice, the observed values are specified as boundary values and since these are not dynamically matched and may contain noise (short wavelength components), the boundary values are filtered (Sasaki, 1970b). Also, specifying these values determines the solution, once the weights have been selected. Consequently, the boundaries of the domain should be placed such that the objectively analyzed values adequately represent the solution.

Although the operations have been carried out for the continuous form, the same variational properties hold for the finite-difference analogues (Sasaki, 1969, 1970b).

APPENDIX C

CONSERVATION OF TOTAL ENERGY IN THE FORECAST MODEL

It is required that the forecast values of the variables continually satisfy Eq. (76). Sasaki's approach is based on the fundamental hypothesis that the solution $u_{i,j}^{n+1}$, $v_{i,j}^{n+1}$, and $\Phi_{i,j}^{n+1}$ that satisfies Eq. (76) is also a stationary value that minimizes a weighted sum of the variances of $(u_{i,j}^{n+1} - \tilde{u}_{i,j}^{n+1})$, $(v_{i,j}^{n+1} - \tilde{v}_{i,j}^{n+1})$, and $(\Phi_{i,j}^{n+1} - \tilde{\Phi}_{i,j}^{n+1})$ integrated over the entire domain, where the tilde terms are the predicted values from the finite-difference forecast equations. Based on this hypothesis, the variational functional is written as:

$$J_E = \Delta x \Delta y \; \Sigma\{[\tilde{\alpha}(u^{n+1} - \tilde{u}^{n+1})^2 + \tilde{\alpha}(v^{n+1} - \tilde{v}^{n+1})^2 + \tilde{\beta}(\Phi^{n+1} - \tilde{\Phi}^{n+1})^2] \frac{1}{m^2}\}$$

$$+ \lambda_E\{\Delta x \Delta y \; \Sigma[\{\Phi^{n+1} \frac{m^2}{2}((u^{n+1})^2 + (v^{n+1})^2) + \frac{R_1}{2}(\Phi^{n+1})^2] \frac{1}{m^2}\}, \qquad \text{(C-1)}$$

where the subscripts i,j are suppressed, and λ_E is a Lagrange multiplier which is constant in space but may vary in time. This formulation requires that the constraint (term multiplying λ_E) is exactly satisfied. The first variation of Eq. (C-1) should vanish ($\delta J_E = 0$). The procedure for taking the first variation of J_E with respect to u^{n+1}, v^{n+1}, Φ^{n+1}, and λ_E in the discrete form are identical to those of the continuous form listed in Appendix B. Since the variations are arbitrary on the interior, the resulting Euler-Lagrange equations are:

$$2\tilde{\alpha}(u^{n+1} - \tilde{u}^{n+1}) + \lambda_E m^2 \Phi^{n+1} u^{n+1} = 0 , \qquad (C-2)$$

$$2\tilde{\alpha}(v^{n+1} - \tilde{v}^{n+1}) + \lambda_E m^2 \Phi^{n+1} v^{n+1} = 0 , \qquad (C-3)$$

$$2\tilde{\beta}(\Phi^{n+1} - \tilde{\Phi}^{n+1}) + \lambda_E m^2 \left(\frac{(u^{n+1})^2 + (v^{n+1})^2}{2}\right) + \lambda_E R_1 \Phi^{n+1} = 0, \qquad (C-4)$$

and $$\Delta x \Delta y \, \Sigma\left[\left\{\Phi^{n+1} \frac{m^2}{2}((u^{n+1})^2 + (v^{n+1})^2) + R_1 (\Phi^{n+1})^2\right\} \frac{1}{m^2}\right] - T^o = 0 . \qquad (C-5)$$

In order to obtain solutions for Eqs. (C-2) - (C-5), the following assumptions are made:

a) λ_E is small,

b) m^2 is constant and equal to 1,

c) in Eqs. (C-2) and (C-4), $\Phi_s \gg \Phi'$, which implies $\Phi^{n+1} \sim \Phi_s$,

and d) in Eq. (C-4) $R_1 \Phi^{n+1} \gg [(u^{n+1})^2 + (v^{n+1})^2] / 2$.

Therefore, the solutions are approximated by:

$$u^{n+1} = \frac{2\tilde{\alpha}}{2\tilde{\alpha} + \lambda_E \Phi_s} \tilde{u}^{n+1} = \left[1 - \frac{\lambda_E \Phi_s}{2\tilde{\alpha}} + 0(\lambda_E^2 \Phi_s^2)\right] \tilde{u}^{n+1} , \qquad (C-6)$$

$$v^{n+1} = \frac{2\tilde{\alpha}}{2\tilde{\alpha} + \lambda_E \Phi_s} \tilde{v}^{n+1} = \left[1 - \frac{\lambda_E \Phi_s}{2\tilde{\alpha}} + 0(\lambda_E^2 \Phi_s^2)\right] \tilde{v}^{n+1} , \qquad (C-7)$$

and $$\Phi^{n+1} = \frac{2\tilde{\beta}}{2\tilde{\beta} + \lambda_E R_1} \tilde{\Phi}^{n+1} = \left[1 - \frac{\lambda_E R_1}{2\tilde{\beta}} + 0(\lambda_E^2 R_1^2)\right] \tilde{\Phi}^{n+1} , \qquad (C-8)$$

where 0( ) is the order of magnitude. Since the finite-difference equations have the same spatial and temporal truncation error, it is further assumed that the fractional adjustment is the same for u^{n+1}, v^{n+1}, and

Φ^{n+1}. Thus, for $\tilde{\alpha} = 1$ and $\tilde{\beta} = \frac{R_1}{\Phi_s}$, Eqs. (C-6) - (C-8) are written as:

$$u^{n+1} = (1 - \lambda^*) \tilde{u}^{n+1} , \tag{C-9}$$

$$v^{n+1} = (1 - \lambda^*) \tilde{v}^{n+1} , \tag{C-10}$$

and

$$\Phi^{n+1} = (1 - \lambda^*) \tilde{\Phi}^{n+1} , \tag{C-11}$$

where $\lambda^* = \frac{\lambda_E \Phi_s}{2}$. Substitution of Eqs. (C-9) - (C-11) into Eq. (C-5) yields, after rearrangement,

$$R \lambda^{*3} - S \lambda^{*2} + Q \lambda^* + P = 0 , \tag{C-12}$$

where $R = \Phi_s^{\,3} \widetilde{KE}$,

$$S = (2\Phi_s^{\,3} + \Phi_s^{\,2}) (\widetilde{KE}) + \Phi_s^{\,2} \widetilde{PE} ,$$

$$Q = 3\Phi_s \widetilde{KE} + 2\Phi_s \widetilde{PE} ,$$

$$P = T_o - \widetilde{KE} + \widetilde{PE} ,$$

$$\widetilde{KE} = \frac{\Delta x \Delta y}{2} \sum_{i,j} \tilde{\Phi}^{n+1} ((\tilde{u}^{n+1})^2 + (\tilde{v}^{n+1})^2) ,$$

and

$$\widetilde{PE} = \frac{R_1 \Delta x \Delta y}{2} \sum_{i,j} (\tilde{\Phi}^{n+1})^2 .$$

A modified Newton method for finding the zeros of a polynomial is used to solve Eq. (C-12) (Carnahan, Luther, and Wilkes, 1969). Let $\lambda^{*\nu}$ be the ν-th approximation to the solution of Eq. (C-12). Substitution into Eq. (C-12) results in a residual r^ν, i.e.,

$$R(\lambda^{*\nu})^3 - S(\lambda^{*\nu})^2 + Q \lambda^{*\nu} + P = r^\nu . \tag{C-13}$$

The $(\nu+1)$st guess is

$$\lambda^{*\nu+1} = \lambda^{*\nu} - \frac{r^{\nu}}{FD} , \tag{C-14}$$

where FD is the first derivative of Eq. (C-12)

$$FD \equiv 3 R \lambda^{*2} - 2 S \lambda^{*} + Q .$$

This $(\nu+1)$st guess of λ^* is used to correct or modify the forecast fields by Eqs. (C-9) - (C-11). The corrected values become the new observed values and the terms in Eqs. (C-12) - (C-14) are recalculated. This process is repeated until P is less than or equal to some prespecified tolerance.

APPENDIX D

CENTERED FINITE-DIFFERENCE OPERATORS

The following finite-difference operators are defined in order to solve the analysis equations numerically. Let Q represent any dependent variable; i, j, k are the grid indicies along x, y and t axes, respectively. The grid spacing in the horizontal plane is represented by Δs and in time by Δt. For derivative evaluation at i, j or k, only those subscripts different from i, j or k are identified. The operators are:

$$\nabla_x Q]_{ijk} = \frac{1}{2\Delta s}[Q(i + 1) - Q(i - 1)], \tag{D-1}$$

$$\nabla_y Q]_{ijk} = \frac{1}{2\Delta s}[Q(j + 1) - Q(j - 1)], \tag{D-2}$$

$$\nabla_{xx} Q]_{ijk} = \frac{1}{\Delta s^2}[Q(i + 1) + Q(i - 1) - 2 Q], \tag{D-3}$$

$$\nabla_{yy} Q]_{ijk} = \frac{1}{\Delta s^2}[Q(j + 1) + Q(j - 1) - 2 Q], \tag{D-4}$$

$$\nabla_{tt} Q]_{ijk} = \frac{1}{\Delta t^2}[Q(k + 1) + Q(k - 1) - 2 Q], \tag{D-5}$$

$$\nabla_{xy} Q]_{ijk} = \frac{1}{4\Delta s^2}[Q(i+1,j+1) - Q(i-1,j+1) - Q(i+1,j-1) + Q(i-1,j-1)], \tag{D-6}$$

$$\nabla_{xt} Q]_{ijk} = \frac{1}{4\Delta t\Delta s}[Q(i+1,k+1) - Q(i-1,k+1) - Q(i+1,k-1) + Q(i-1,k-1)], \tag{D-7}$$

$$\nabla_{yt}Q]_{ijk} = \frac{1}{4\Delta t\Delta s}[Q(j+1,k+1)-Q(j-1,k+1)-Q(j+1,k-1)+Q(j-1,k-1)], \qquad \text{(D-8)}$$

$$\nabla_{xxx}Q]_{ijk} = \frac{1}{2\Delta s^3}[Q(i+2) - Q(i-2) - 2(Q(i+1) - Q(i-1))] , \qquad \text{(D-9)}$$

$$\nabla_{yyy}Q]_{ijk} = \frac{1}{2\Delta s^3}[Q(j+2) - Q(j-2) - 2(Q(j+1) - Q(j-1))], \qquad \text{(D-10)}$$

$$\nabla_{xyy}Q]_{ijk} = \frac{1}{2\Delta s^3}[Q(i+1,j+1) - Q(i-1,j+1) - Q(i-1,j-1) + Q(i+1,j-1)$$

$$+ 2(Q(i-1,j) - Q(i+1,j))], \qquad \text{(D-11)}$$

$$\nabla_{yxx}Q]_{ijk} = \frac{1}{2\Delta s^3}[Q(i+1,j+1) + Q(i-1,j+1) - Q(i+1,j-1) - Q(i-1,j-1)$$

$$+ 2(Q(i,j-1) - Q(i,j+1))], \qquad \text{(D-12)}$$

$$\nabla_{xxxx}Q]_{ijk} = \frac{1}{\Delta x^4}[Q(i+2) + Q(i-2) - 4(Q(i+1) + Q(i-1)) + 6Q], \qquad \text{(D-13)}$$

$$\nabla_{yyyy}Q]_{ijk} = \frac{1}{\Delta s^4}[Q(j+2) + Q(j-2) - 4(Q(j+1) + Q(j-1)) + 6Q], \qquad \text{(D-14)}$$

and

$$\nabla_{xxyy}Q]_{ijk} = \frac{1}{\Delta s^4}[Q(i+1,j+1) + Q(i-1,j+1) + Q(i-1,j-1) + Q(i+1,j-1)$$

$$- 2(Q(i+1,j) + Q(i-1,j) + Q(i,j+1) + Q(i,j-1)) + 4Q]. \qquad \text{(D-15)}$$

TABLE 1

Weights

Experiment Number	$\tilde{\alpha}$	$\tilde{\beta}_o$	$\tilde{\beta}_F$	γ	η	γ_{vs}	$\gamma_{vt}=\gamma_{\Phi s}=\gamma_{\Phi t}$	Forecast Scheme
1	10^6	10^{11}	10^{10}	1.	.001	.1	.0001	Scheme F
2	10	5000	1000	1.	.0003	.1	.0001	Scheme F
3	1	2500	250	1.	.001	.1	.0001	Scheme F
4	1	500	50	1.	.001	.1	.0001	Scheme F
5	1	5000	500	1.	.001	.1	.0001	Semi-Momentum Shuman

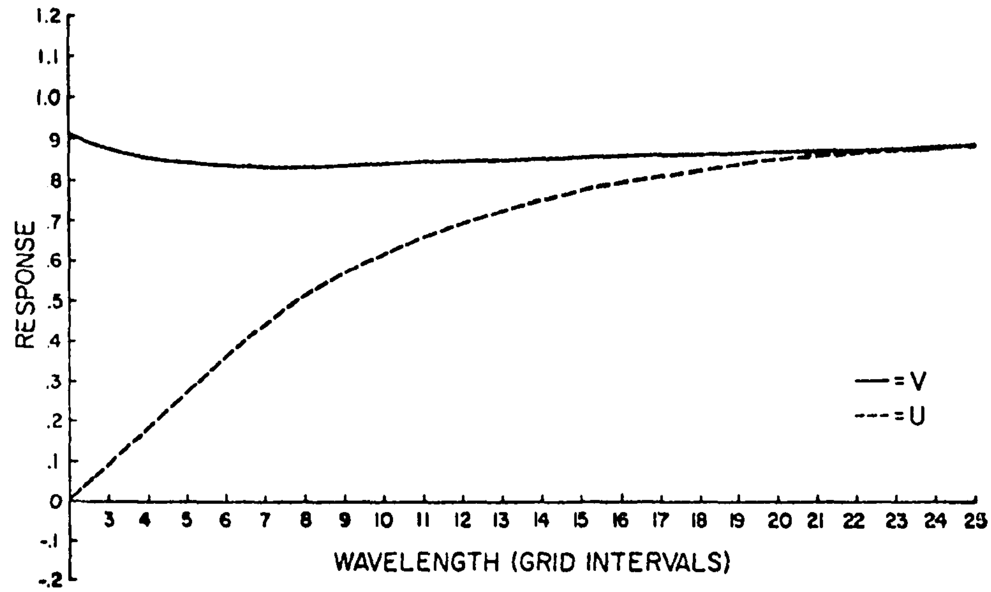

Figure 1a. Response function for u and v as a function of wavelength in the x-direction, expressed as multiples of the grid interval, for L_y = 4381.5 km, $\tilde{\beta} = \gamma = 0$, and $\tilde{\alpha} = \Delta = 1$.

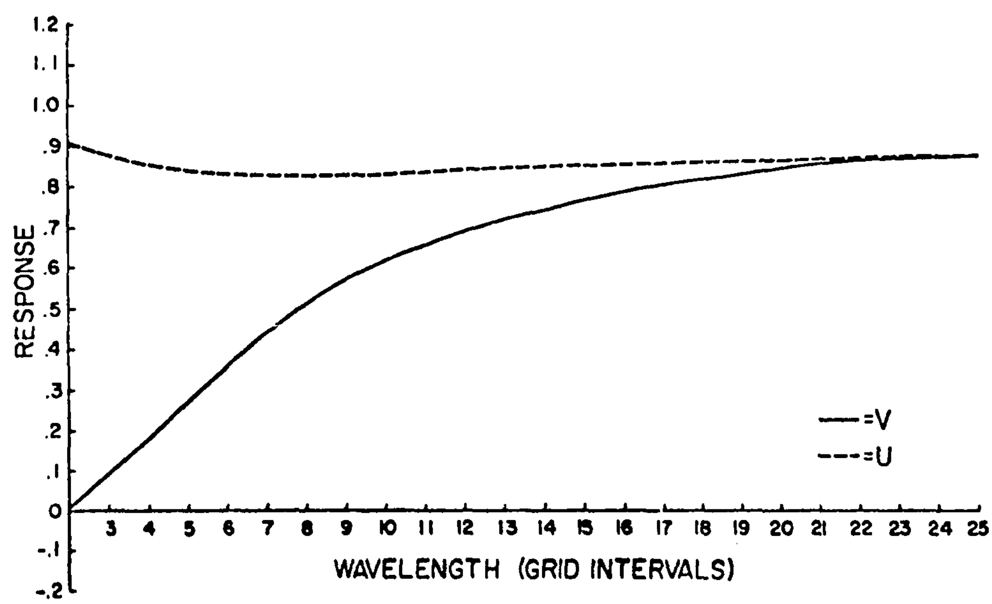

Figure 1b. Same as Fig. 1a except it is a function of wavelength in the y-direction for L_x = 4381.5 km.

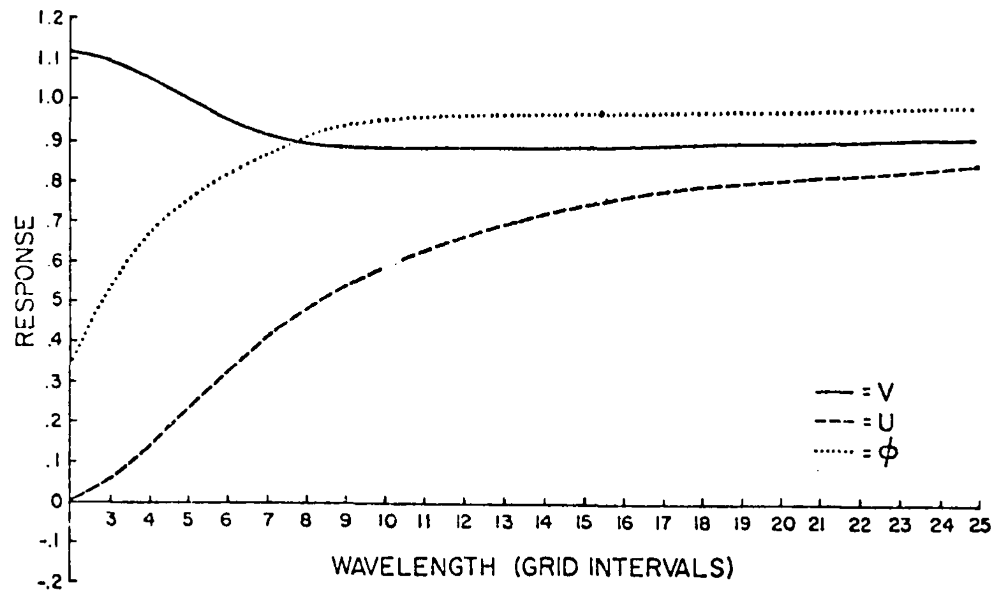

Figure 2a. Response function for u, v and Φ as a function of wavelength in the x-direction, expressed as multiples of the grid interval, for L_y = 4381.5 km, and $\tilde{\alpha} = \tilde{\beta} = \Delta = \gamma = 1$.

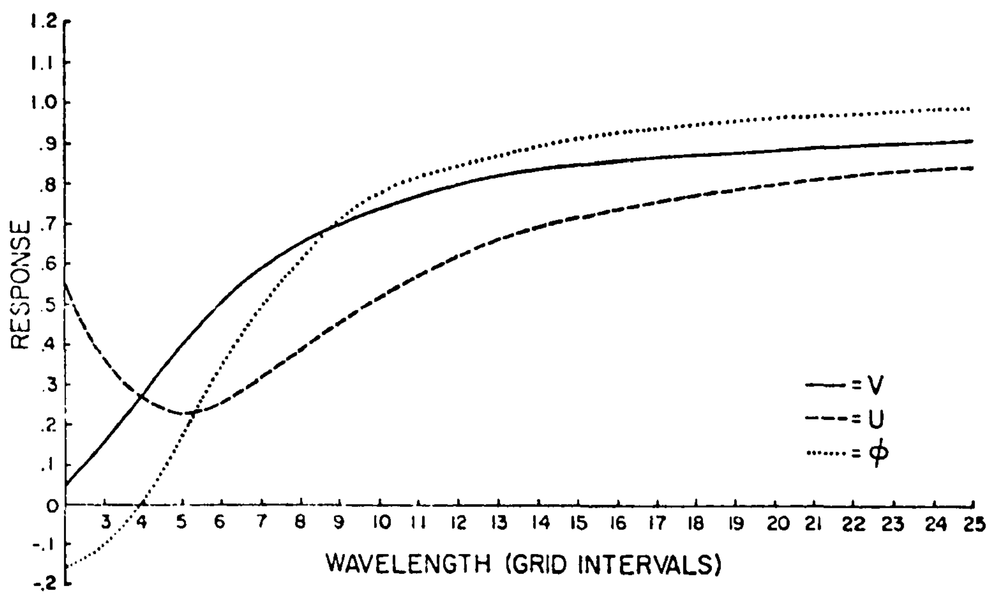

Figure 2b. Same as Fig. 2a except it is a function of wavelength in the y-direction for L_x = 4381.5 km.

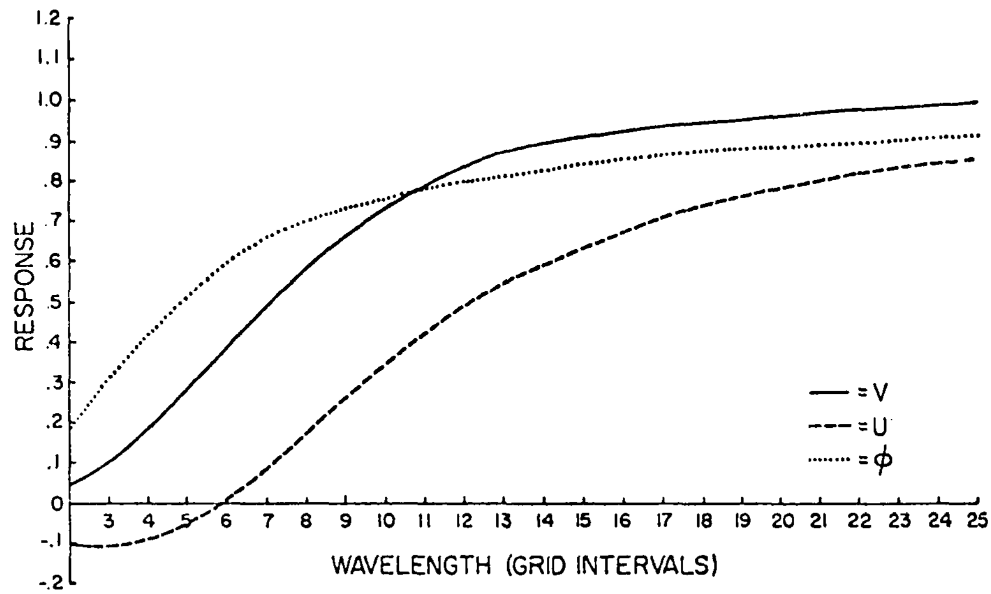

Figure 2c. Same as Fig. 2a except it is a function of wavelength for $L_x = L_y$.

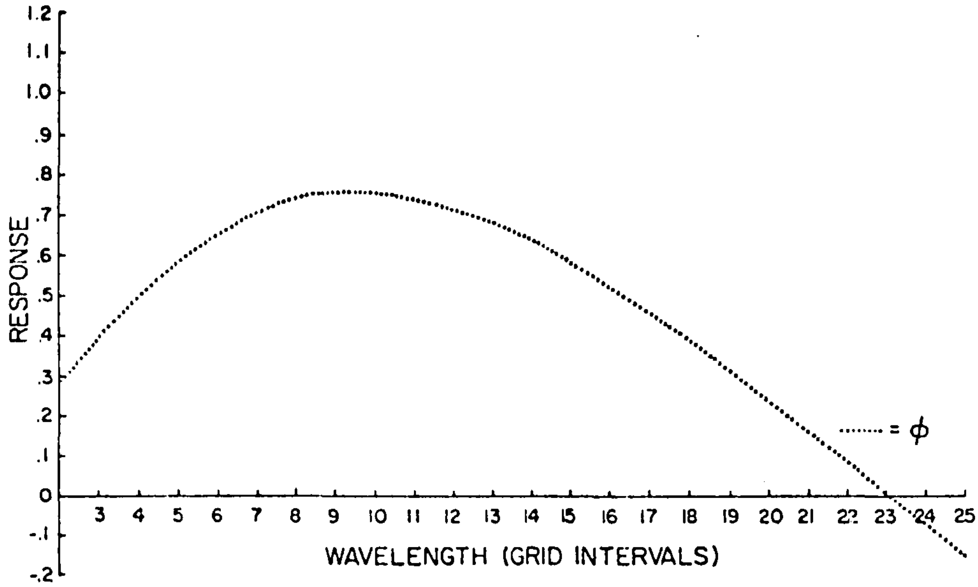

Figure 3a. Response function for Φ as a function of wavelength in the x-direction, expressed as multiples of the grid interval, for L_y = 4381.5 km, $\tilde{\alpha} = \gamma$, and $\gamma \gg \tilde{\beta}$ and Δ.

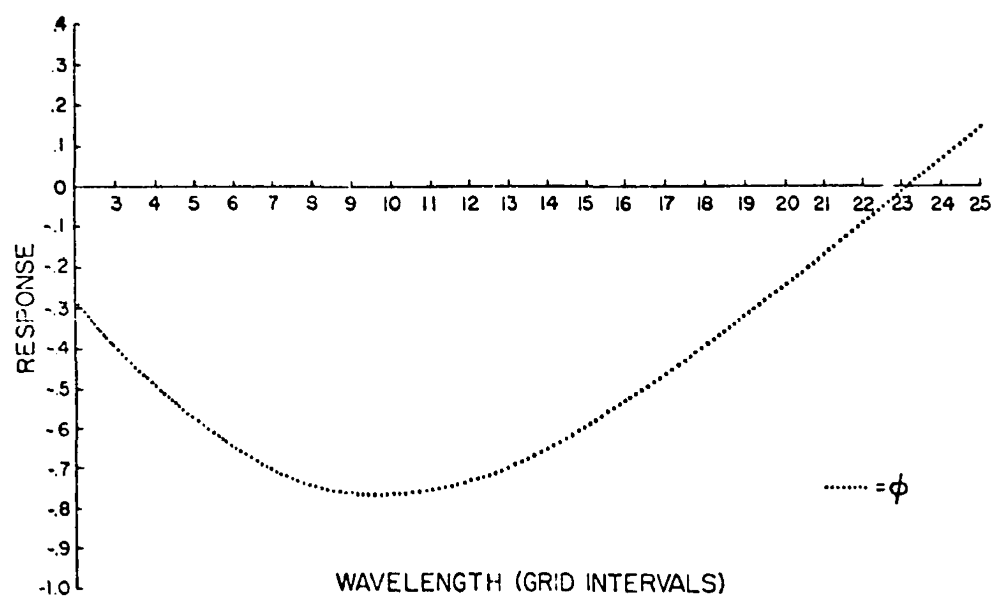

Figure 3b. Same as Fig. 3a except it is a function of wavelength in the y-direction for L_x = 4381.5 km.

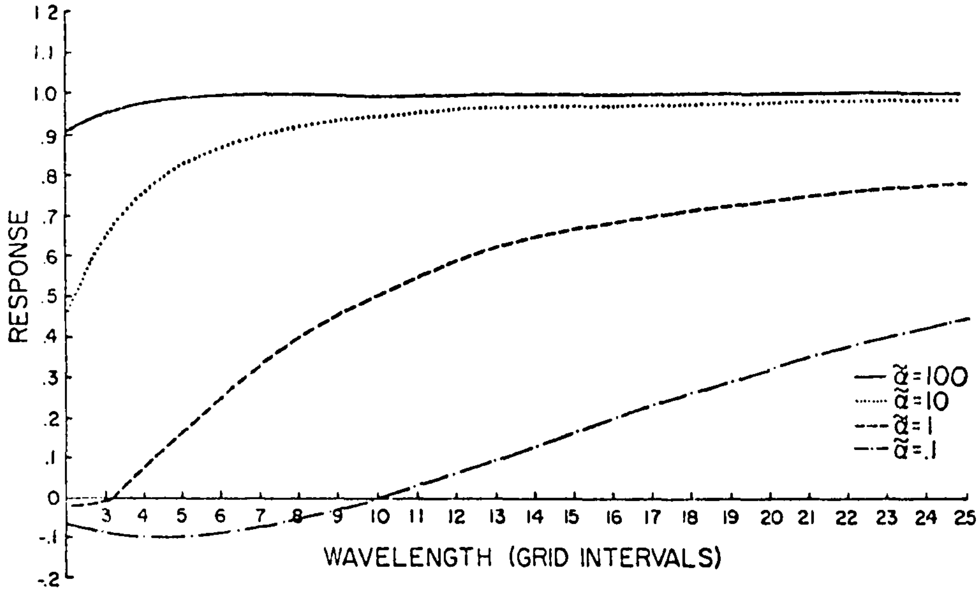

Figure 4a. Response function for u as a function of wavelength in the x-direction, expressed as multiples of the grid interval for L_y = 4381.5 km, $\tilde{\beta}$ = 0, $\gamma = \Delta = 1$ and various observational weights, $\tilde{\alpha}$.

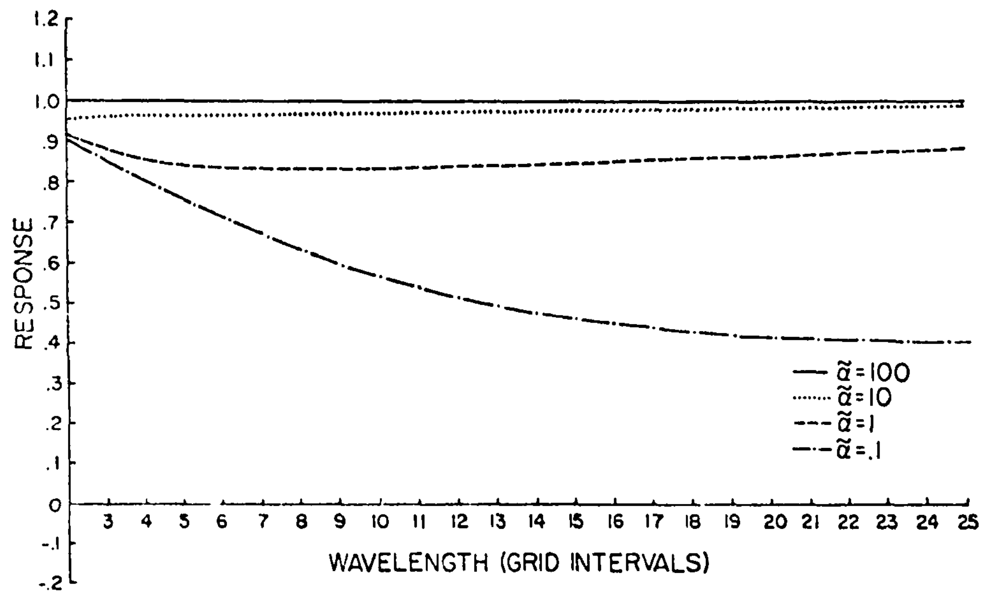

Figure 4b. Same as Fig. 4a except it is for v.

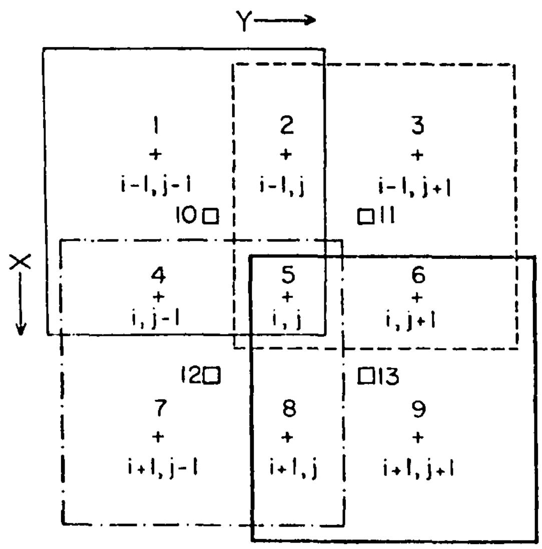

Figure 5. Grid lattice for constructing Shuman's semi-momentum finite-difference operators.

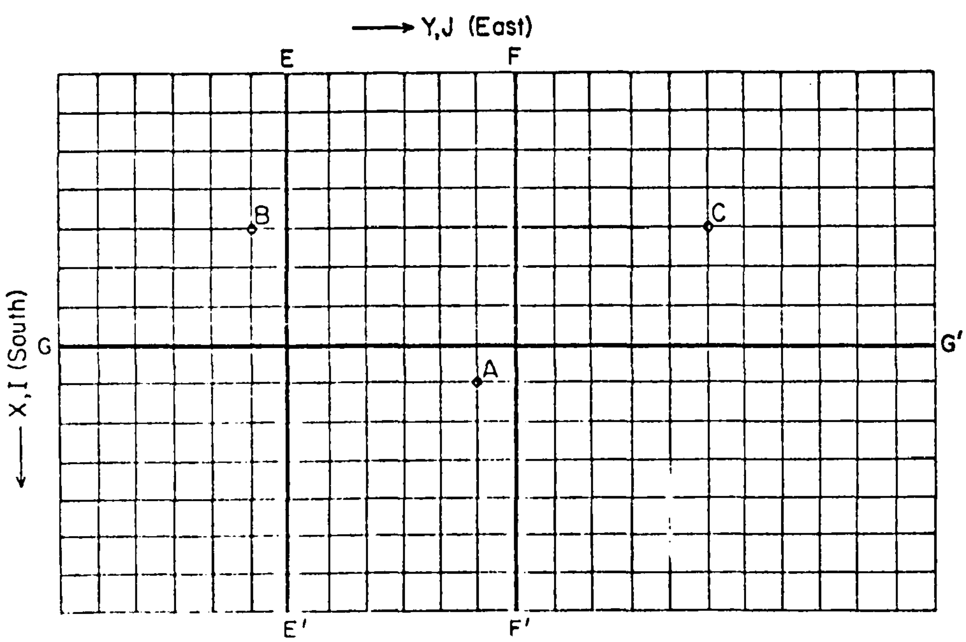

Figure 6. Grid orientation with respect to a cartesian coordinate system, and points and cross-sections used in subsequent figures.

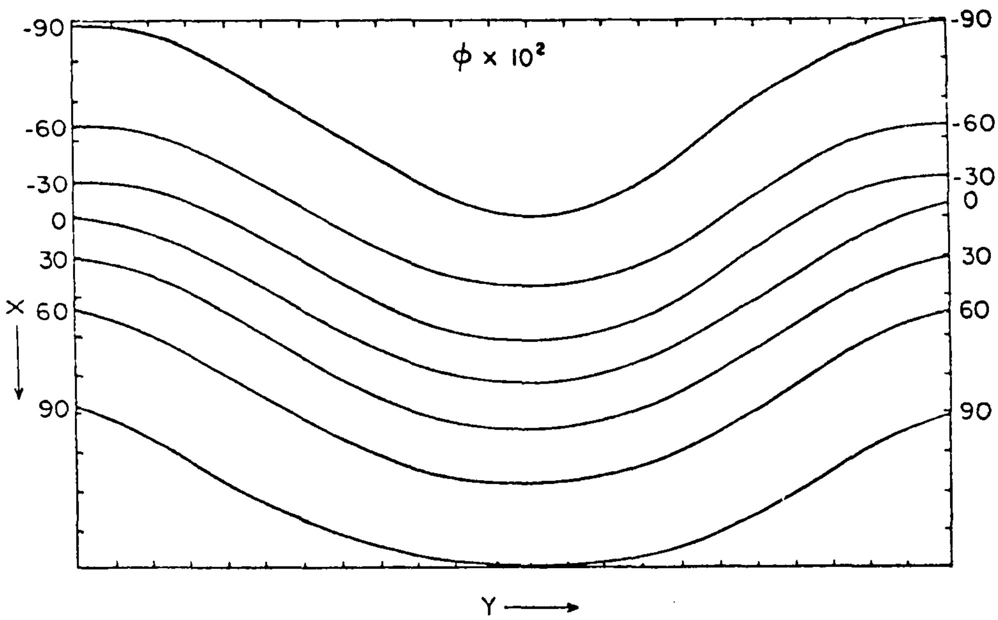

Figure 7. Initial (t = 0) non-dimensional geopotential after dynamic adjustment.

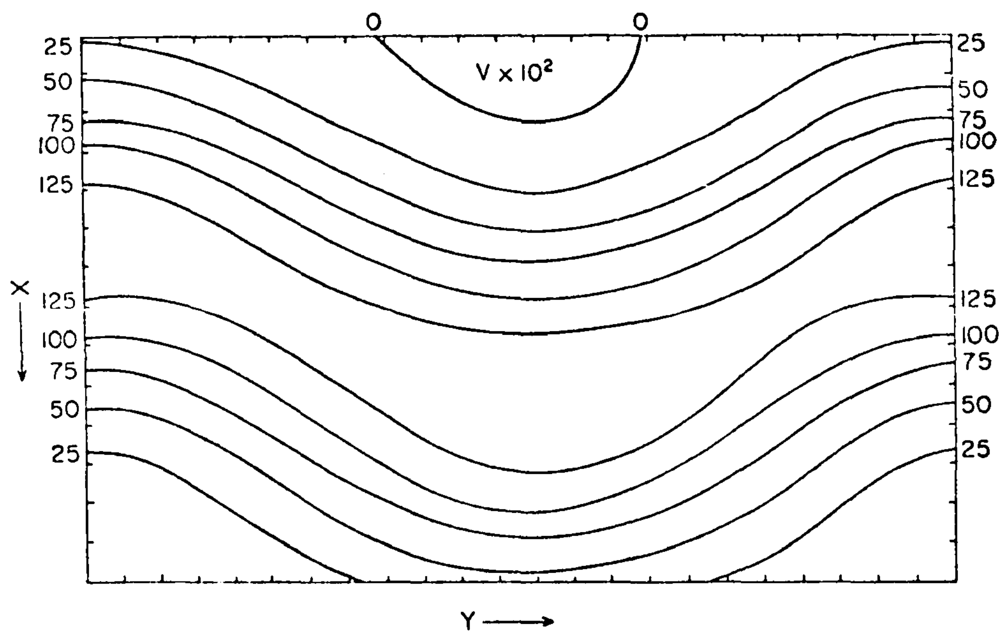

Figure 8. Initial (t = 0) non-dimensional v component after dynamic adjustment.

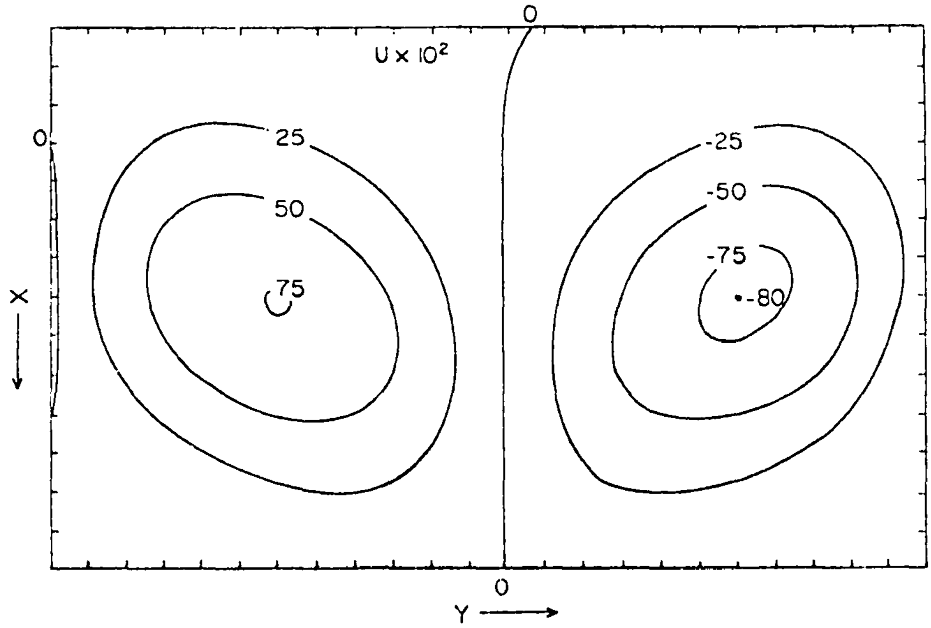

Figure 9. Initial (t = 0) non-dimensional u component after dynamic adjustment.

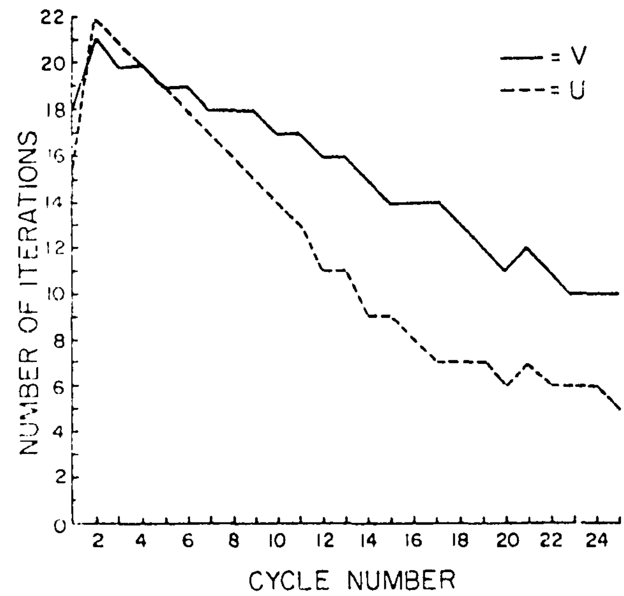

Figure 10. Number of relaxation iterations per cycle for the u and v components during the initialization process.

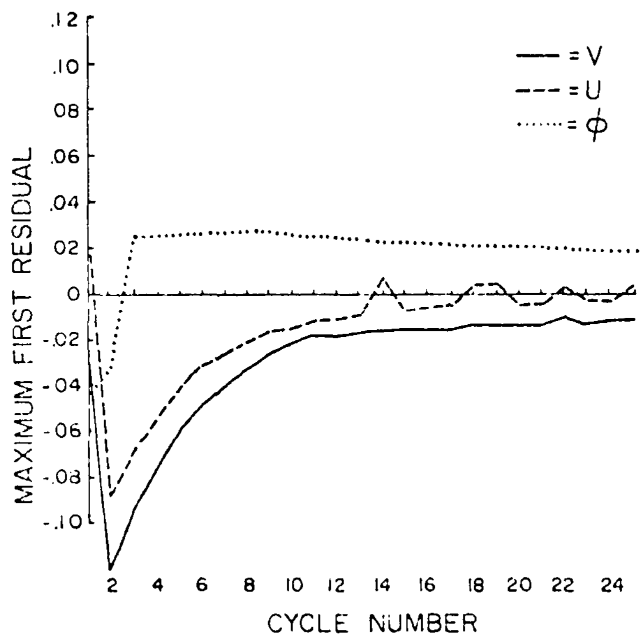

Figure 11. Maximum residual of the first relaxation iteration per cycle for u, v and Φ during the initialization process.

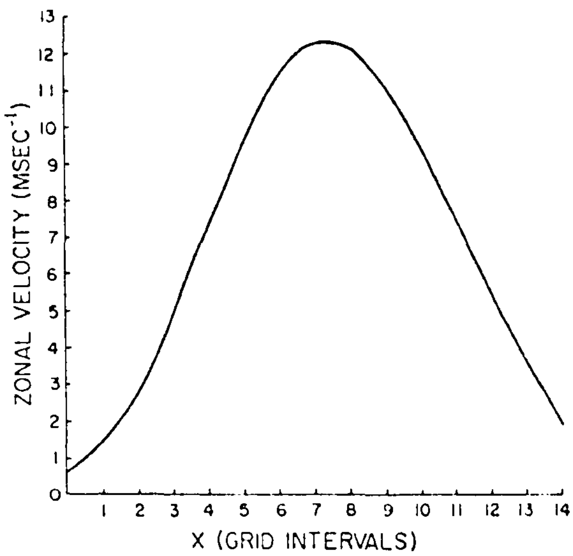

Figure 12. Zonally averaged velocity distribution for the initial conditions; the abscissa is distance, in grid intervals, from the northern boundary.

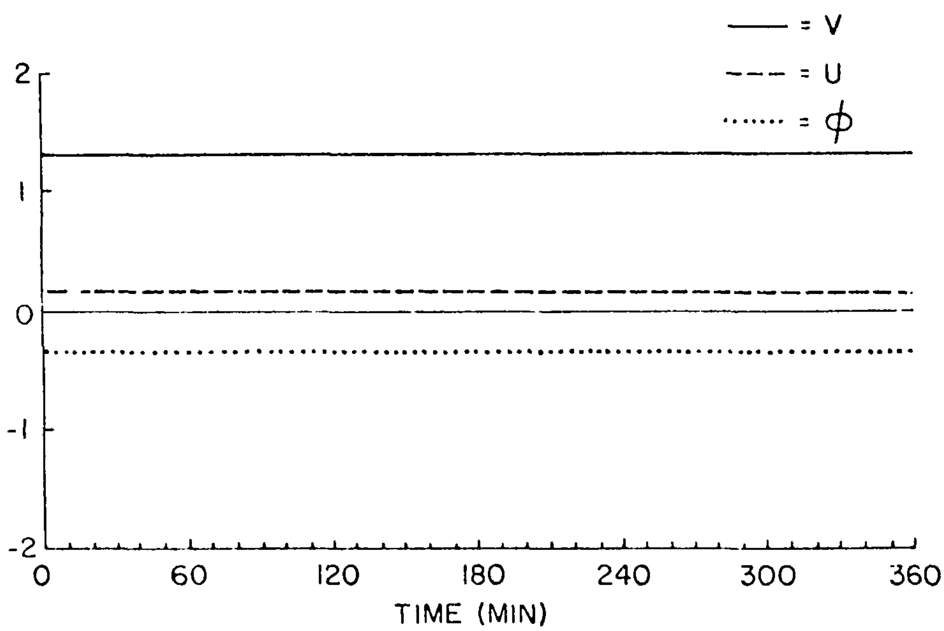

Figure 13. Time trace of the non-dimensional forecast variables, u, v, and Φ, from Grammeltvedt's Scheme F at Point A.

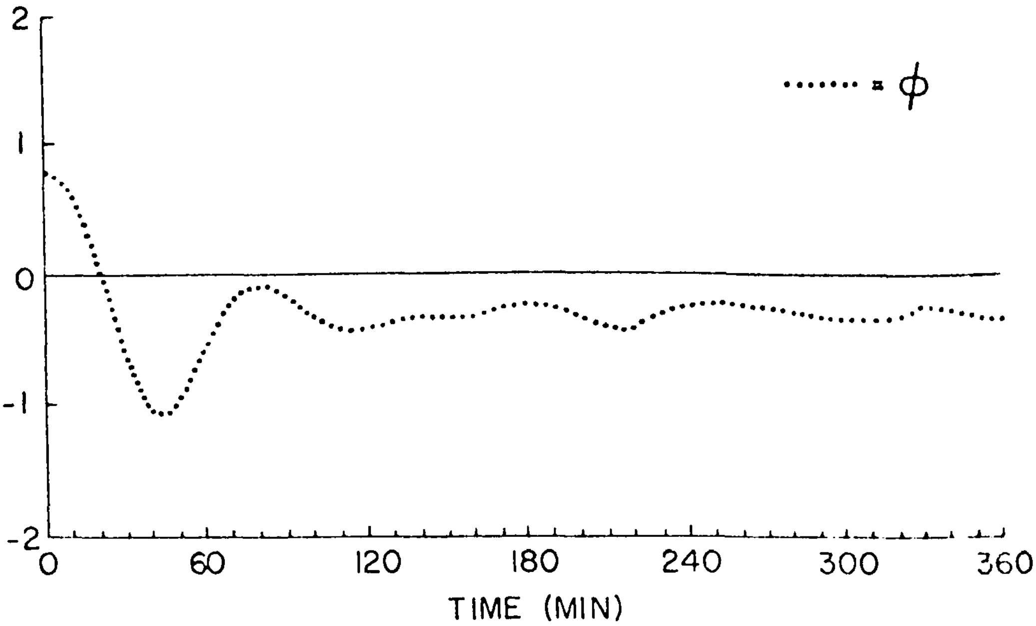

Figure 14. Time trace of the non-dimensional geopotential perturbation at point A from the Scheme F formulation.

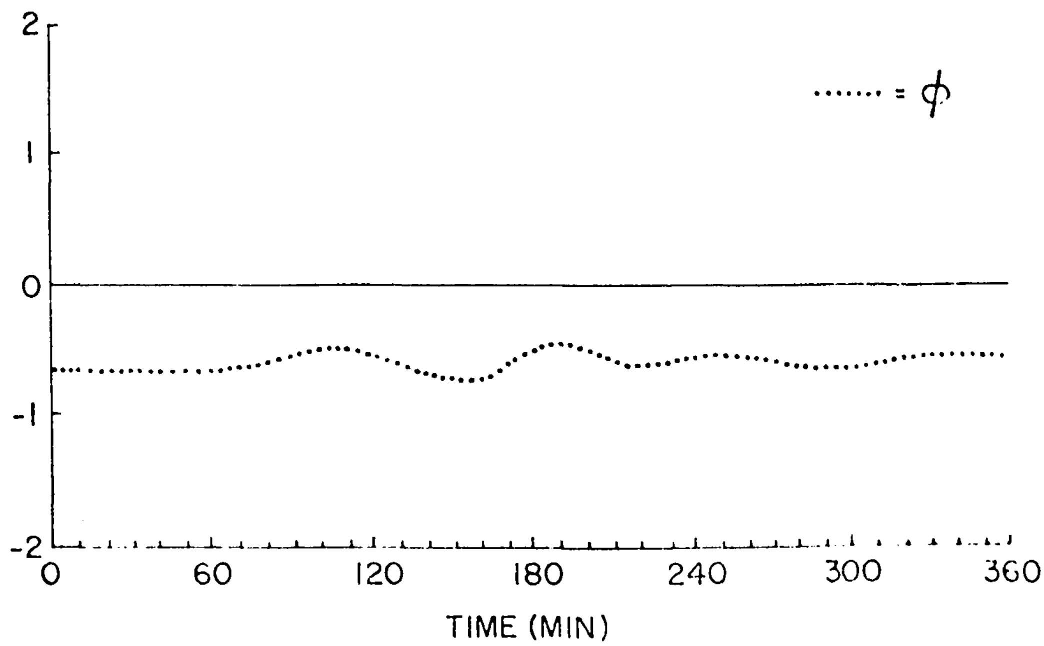

Figure 15. Same as Fig. 14 except it is at point B.

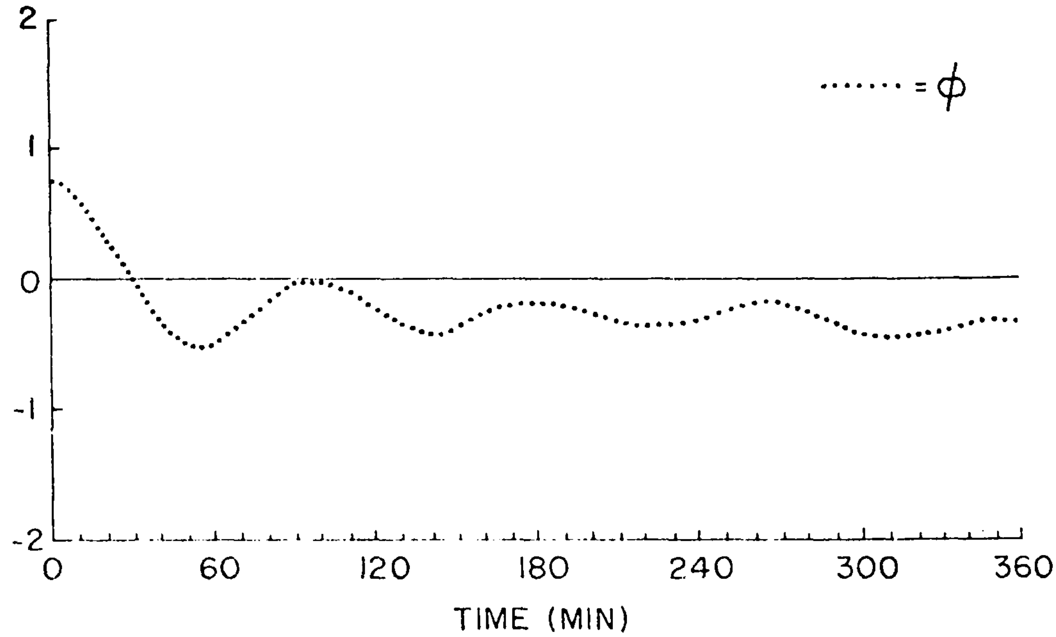

Figure 16. Same as Fig. 15 except it is from Shuman's semi-momentum formulation.

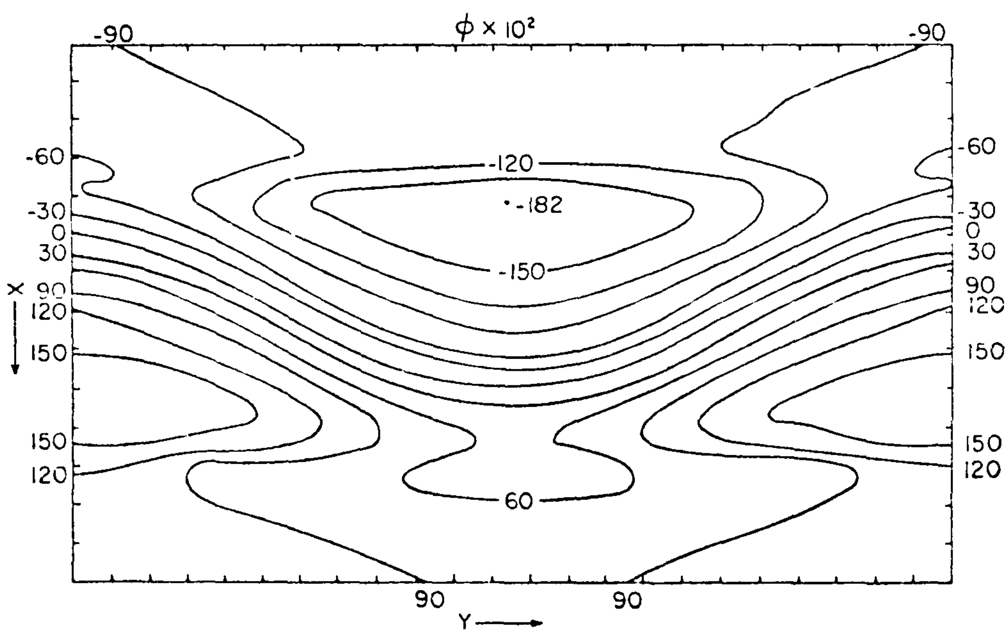

Figure 17a. Non-dimensional geopotential perturbation resulting from modification I at t = 10 minutes; this field is the simulated observed data.

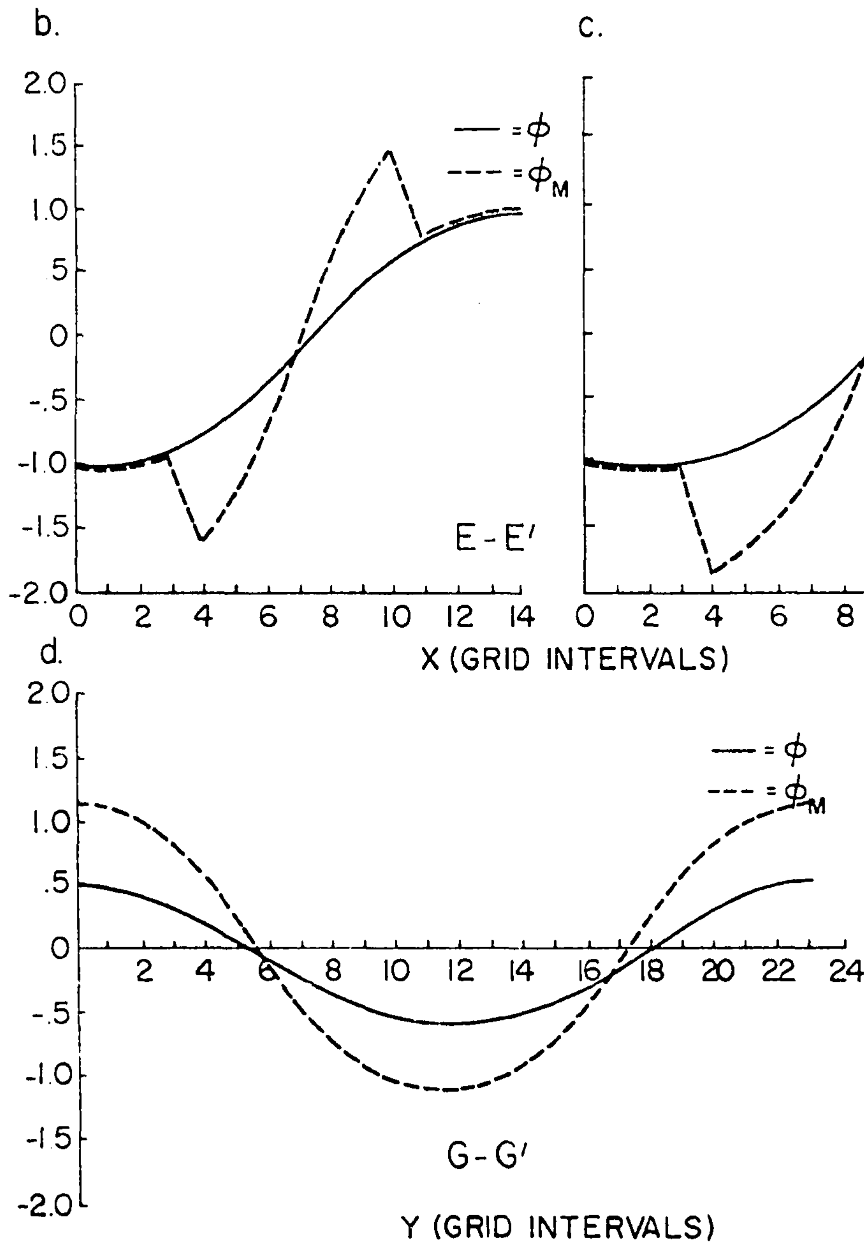

Figures 17b - d. Cross-sectional views of the modified geopotential Φ_m in Fig. 17a. The forecast geopotential, Φ, at $t = 10$ minutes is plotted for comparison.

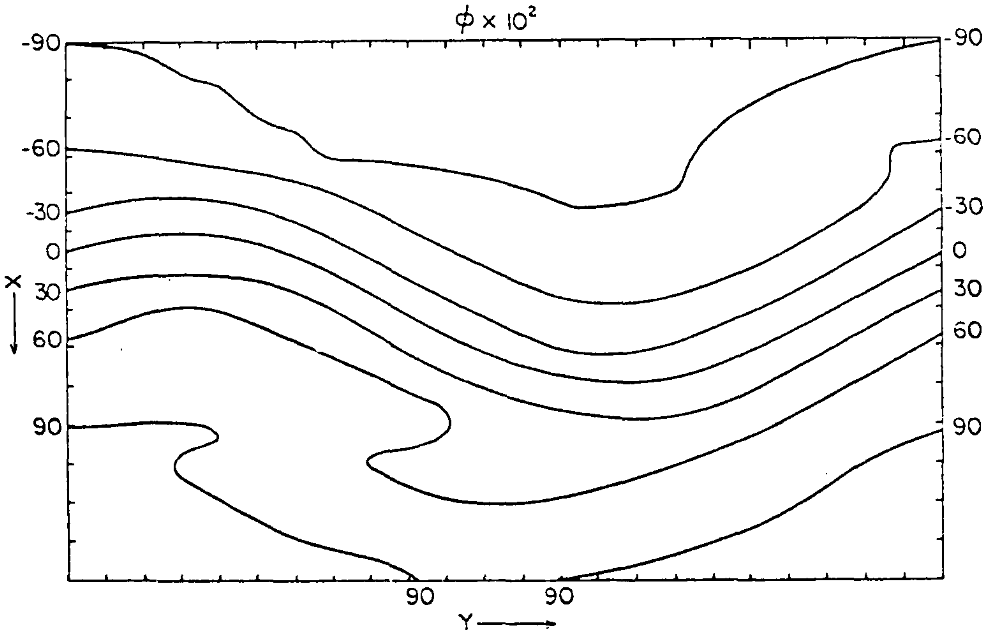

Figure 18a. Same as Fig. 17a except it results from modification II.

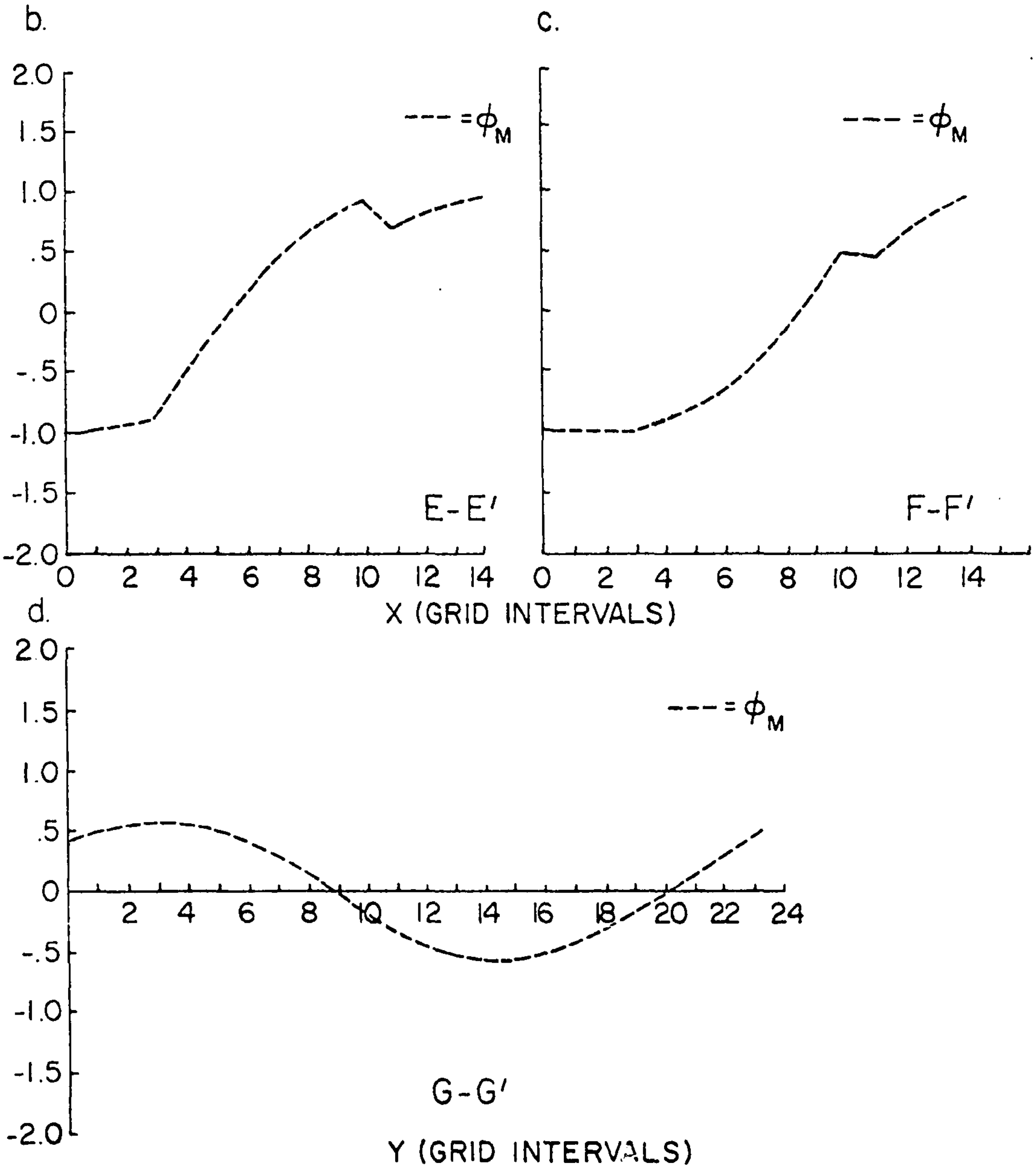

Figures 18b - d. Cross-sectional views of the modified geopotential in Fig. 18a.

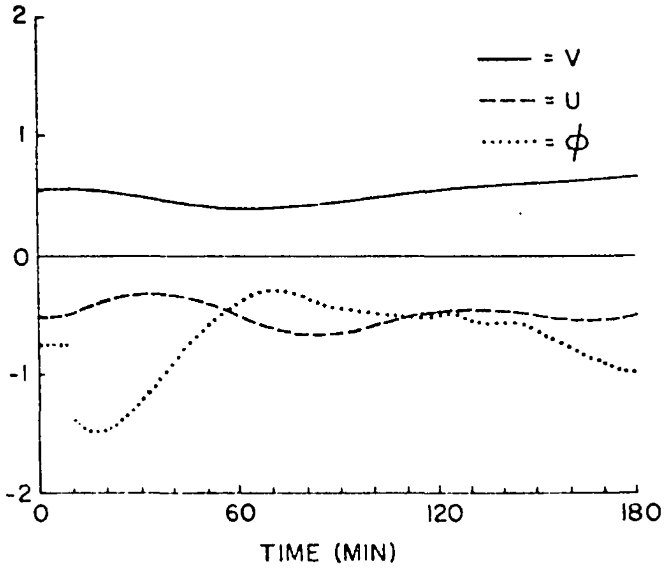

Figure 19. Time trace of the non-dimensional forecast variables at point B for experiment 1.

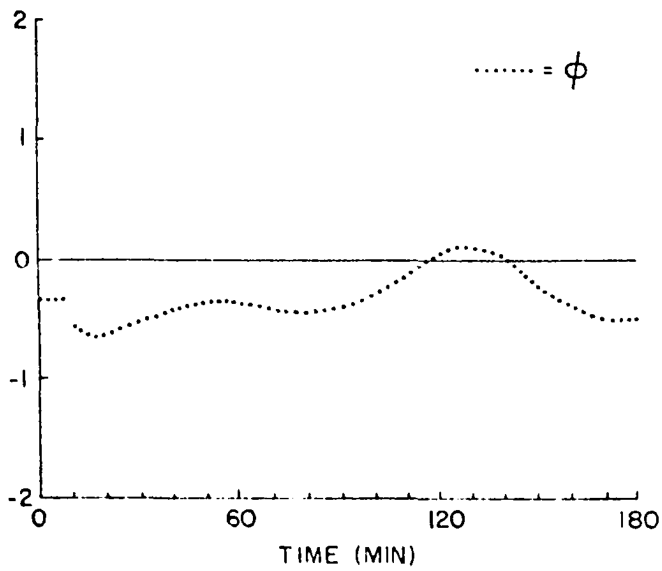

Figure 20. Time trace of the non-dimensional geopotential perturbation at point A for experiment 1.

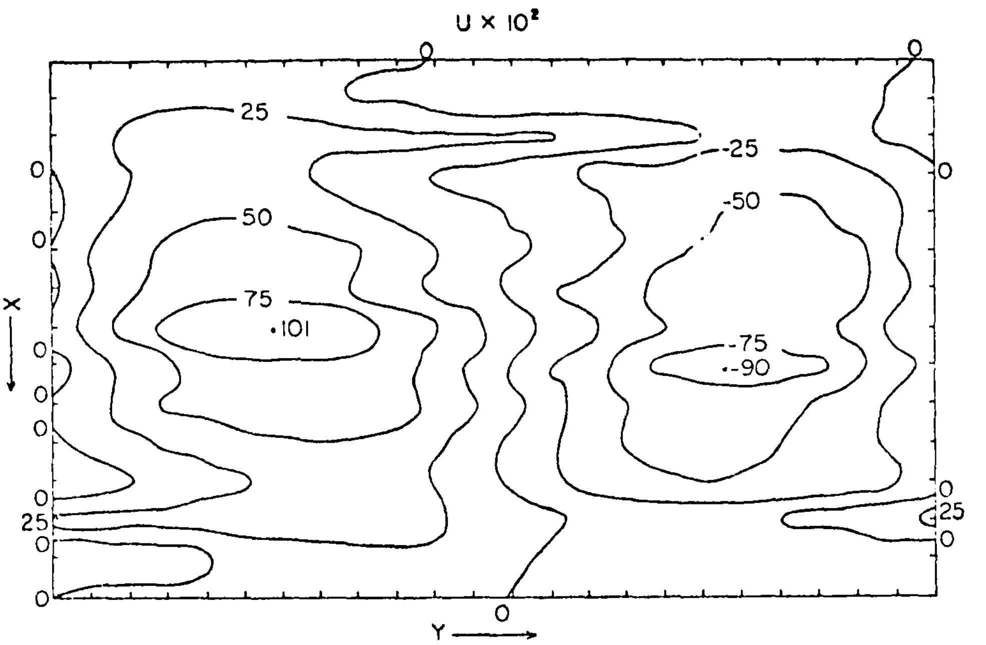

Figure 21a. Three-hour forecast of the non-dimensional u component for experiment 1.

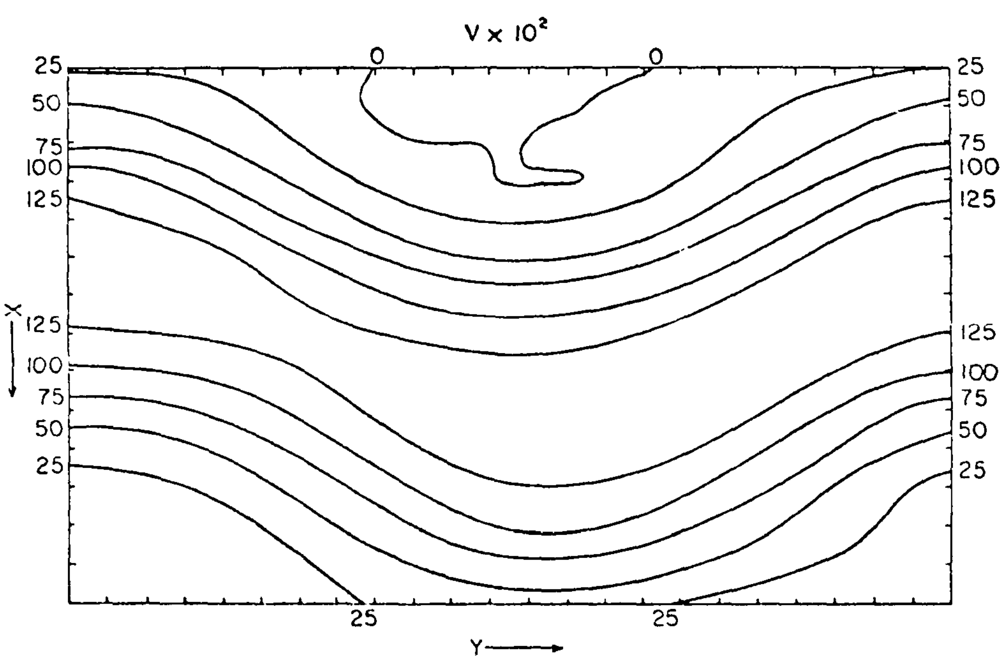

Figure 21b. Three-hour forecast of the non-dimensional v component for experiment 1.

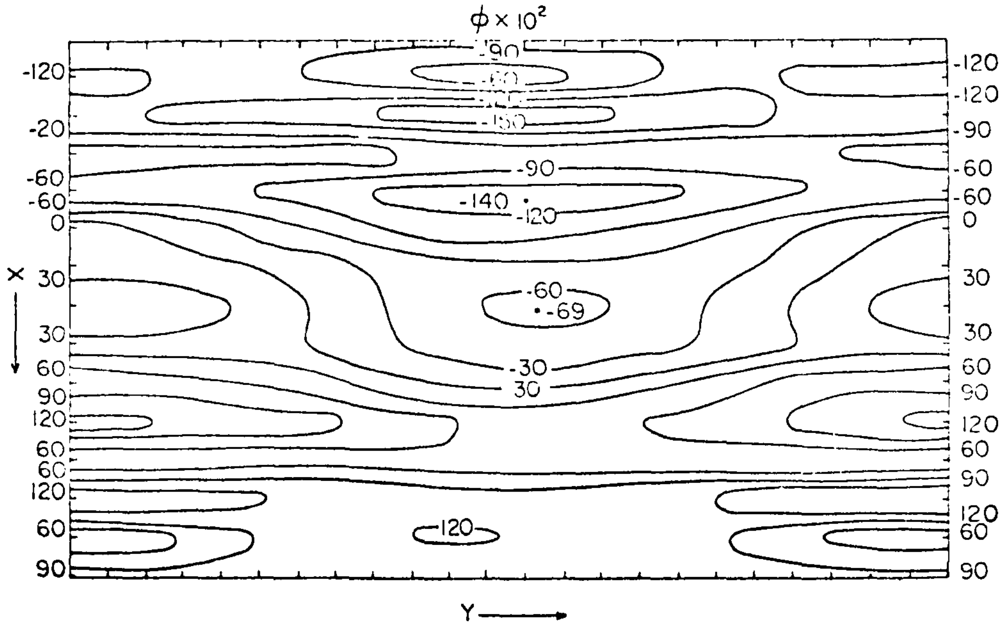

Figure 21c. Three-hour forecast of the non-dimensional geopotential perturbation for experiment 1.

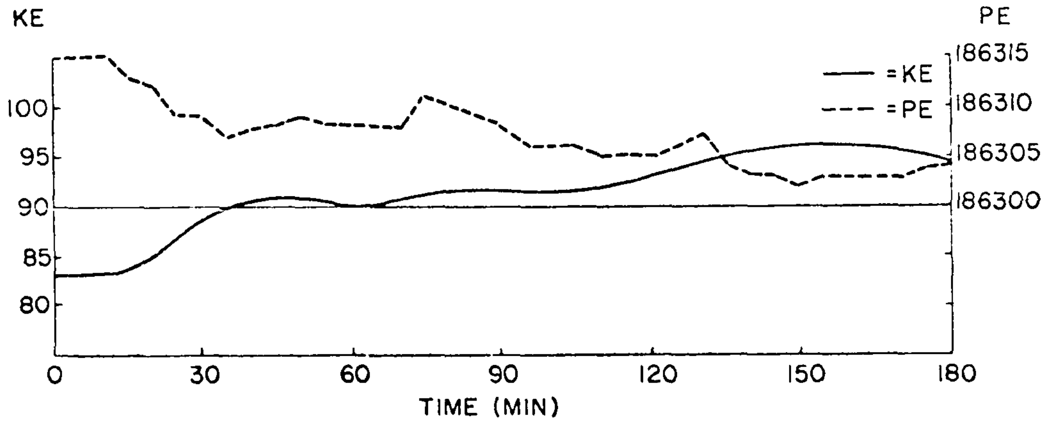

Figure 22. Non-dimensional adjusted kinetic energy (KE) and potential energy (PE) for experiment 1.

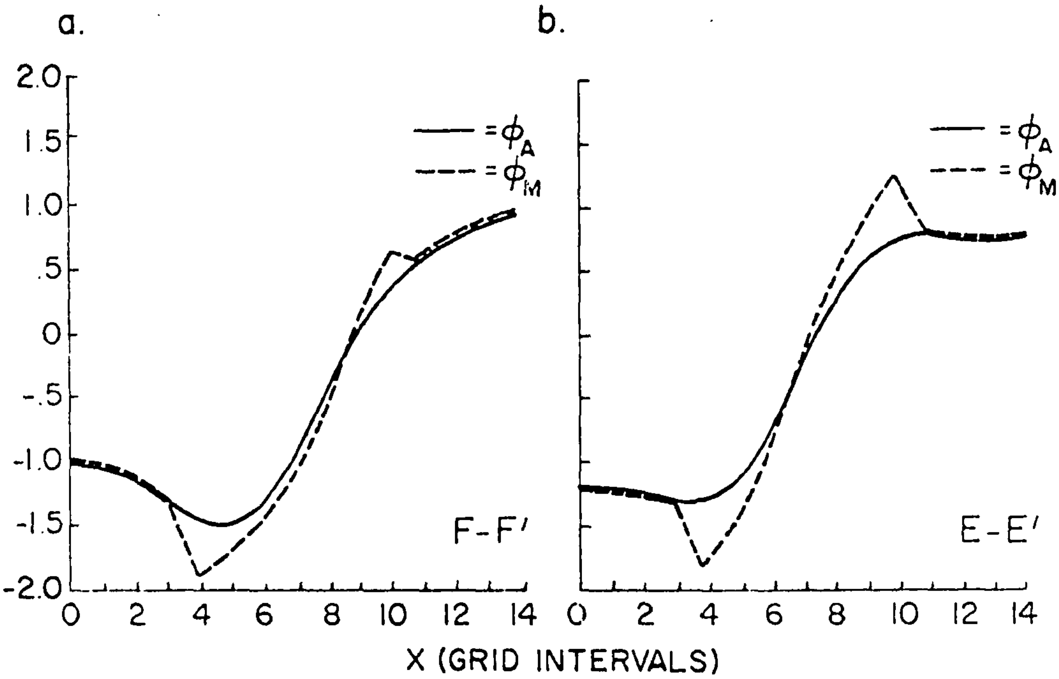

Figures 23a and b. Cross-sectional views of the non-dimensional geopotential after assimilation, Φ_A, for experiment 2; the modified geopotential Φ_M is plotted for comparison.

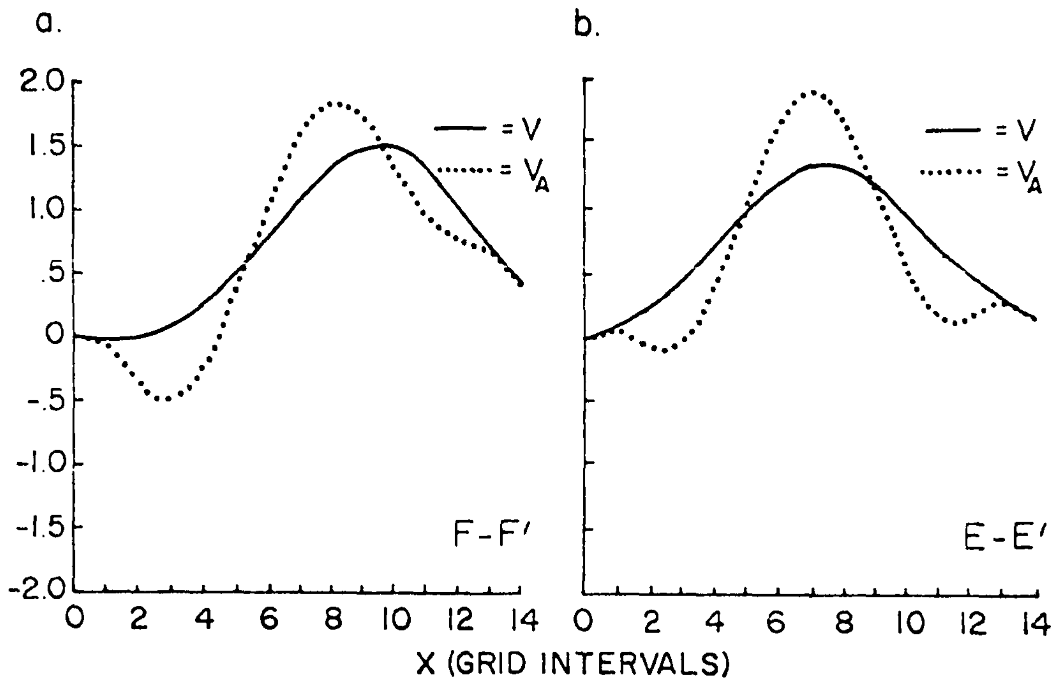

Figures 24a and b. Same as Figs. 23a and b except it is for the non-dimensional v component.

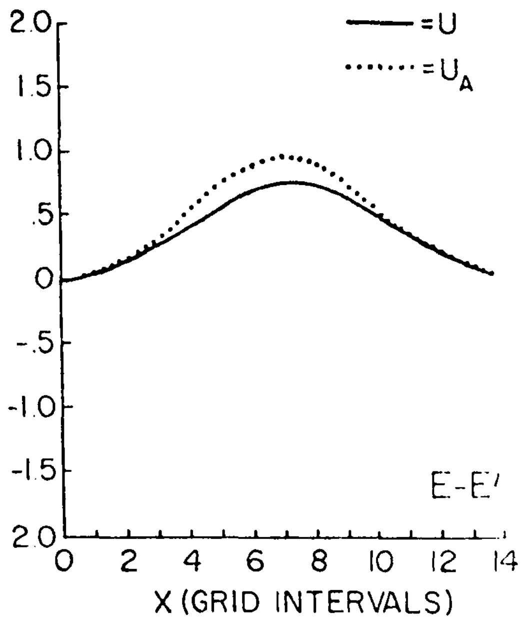

Figure 25. Same as Fig. 23b except it is for the non-dimensional u component.

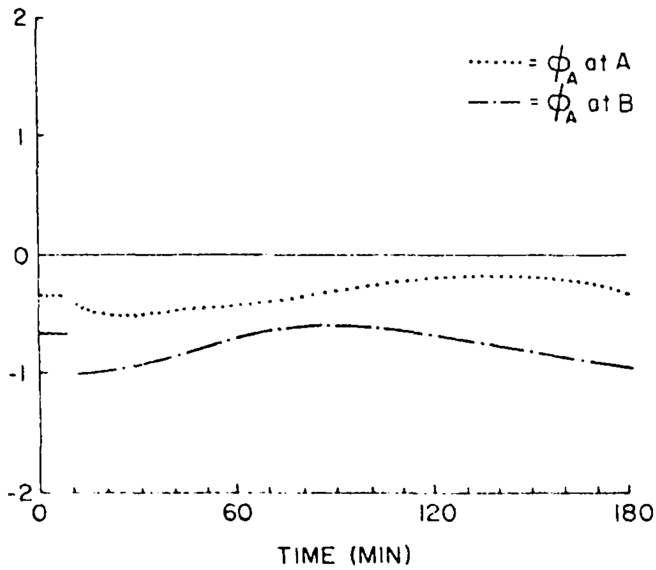

Figure 26. Time trace of the assimilated non-dimensional geopotential perturbation at points A and B for experiment 2.

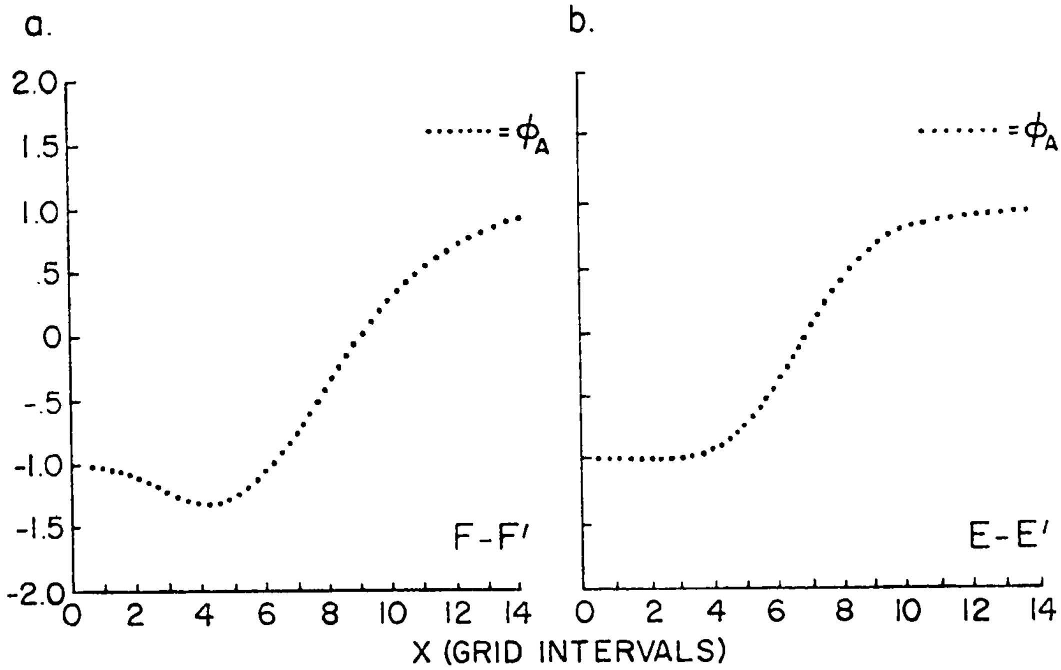

Figures 27a and b. Cross-sectional views of the assimilated non-dimensional geopotential perturbation at t = 10 minutes for experiment 3.

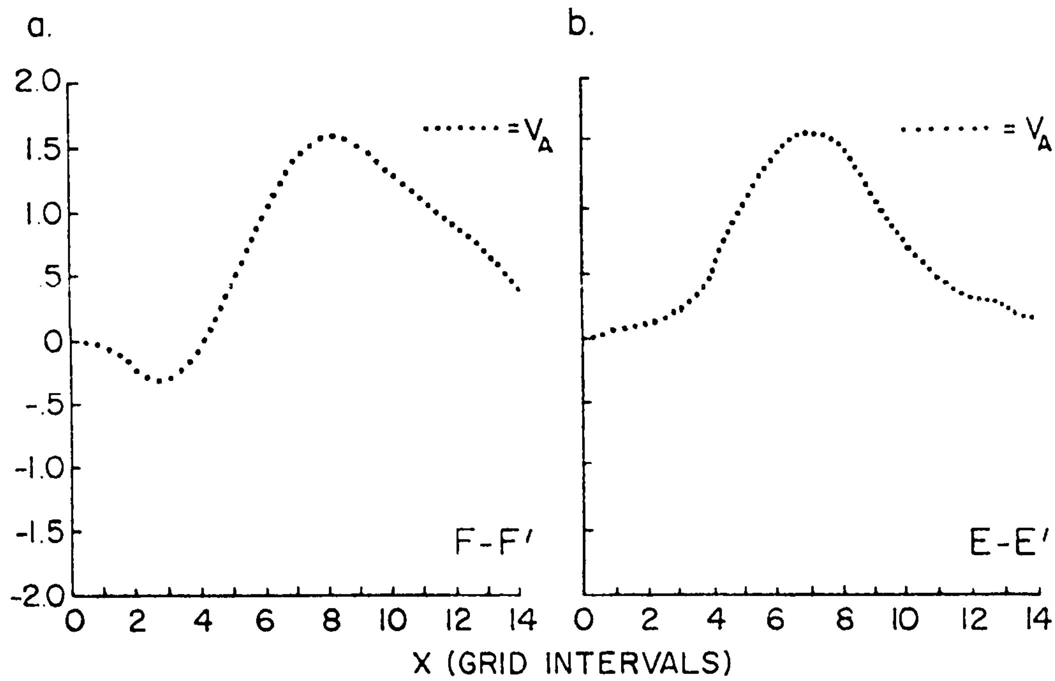

Figures 28a and b. Same as Figs. 27a and b except it is for the assimilated non-dimensional v component.

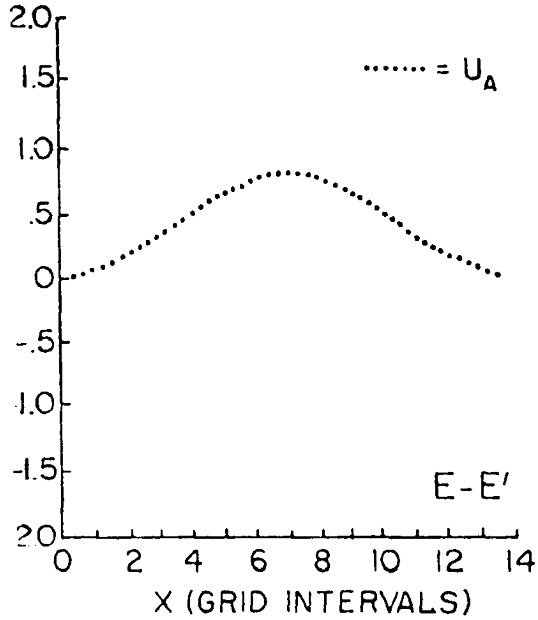

Figure 29. Same as Fig. 27b except it is for the assimilated non-dimensional u component.

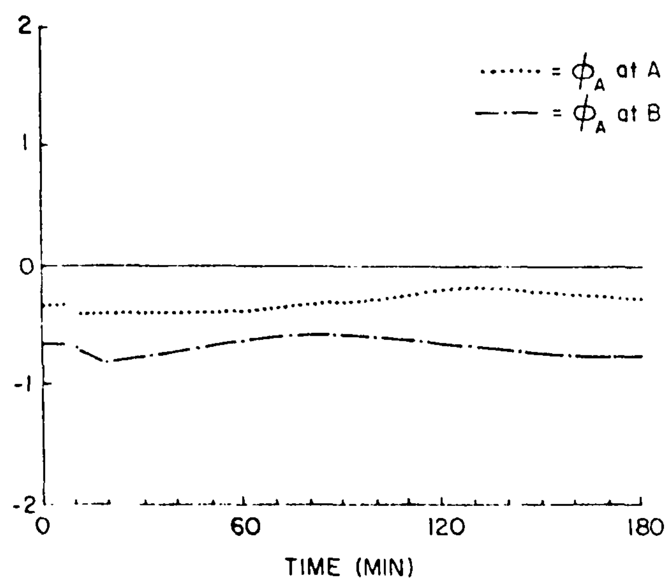

Figure 30. Time trace of the assimilated non-dimensional geopotential perturbation at points A and B for experiment 3.

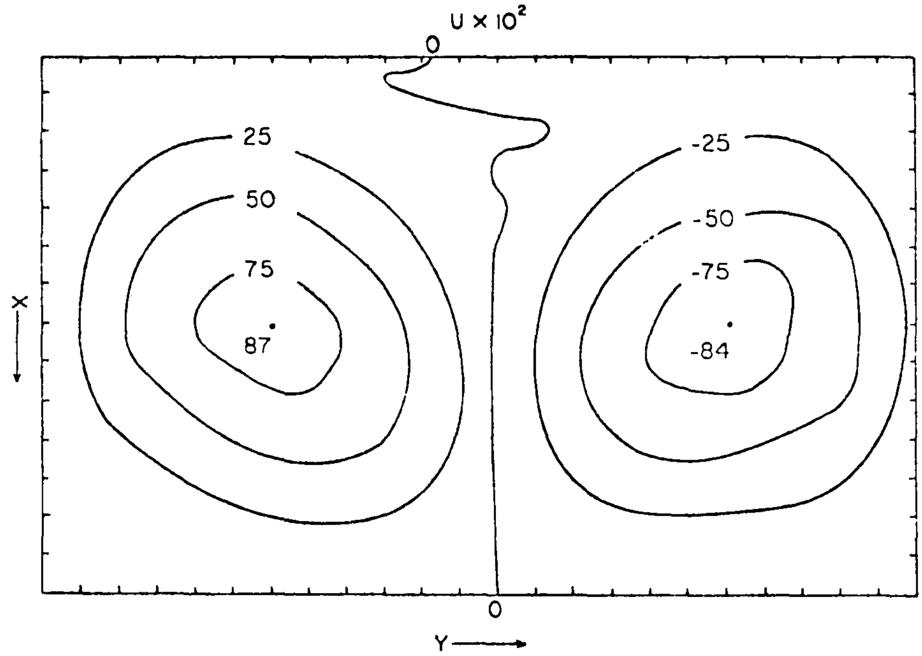

Figure 31a. Three hour forecast of the non-dimensional u component for experiment 3.

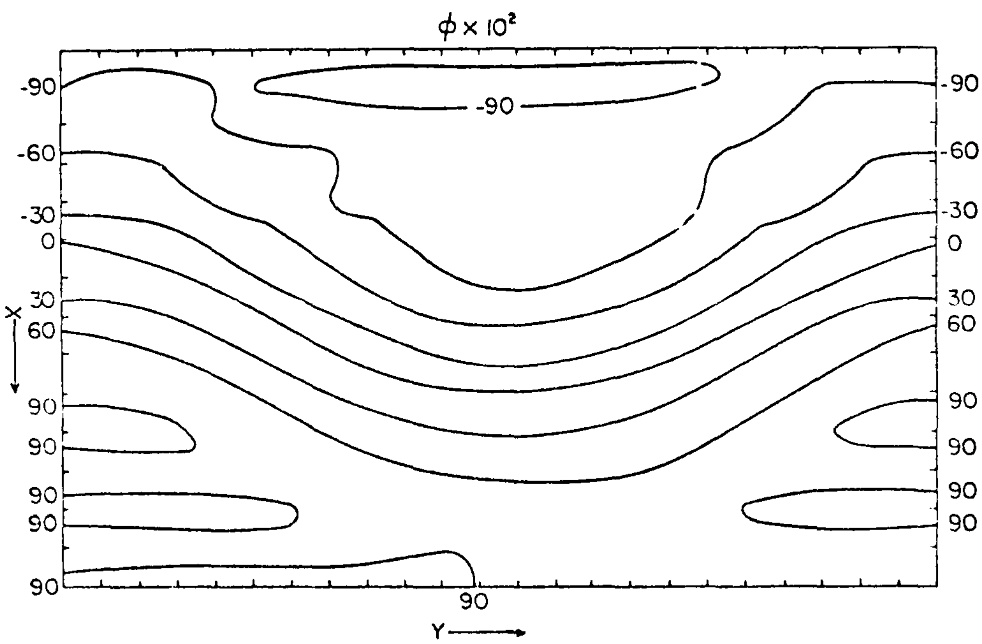

Figure 31b. Three hour forecast of the non-dimensional geo-potential perturbation for experiment 3.

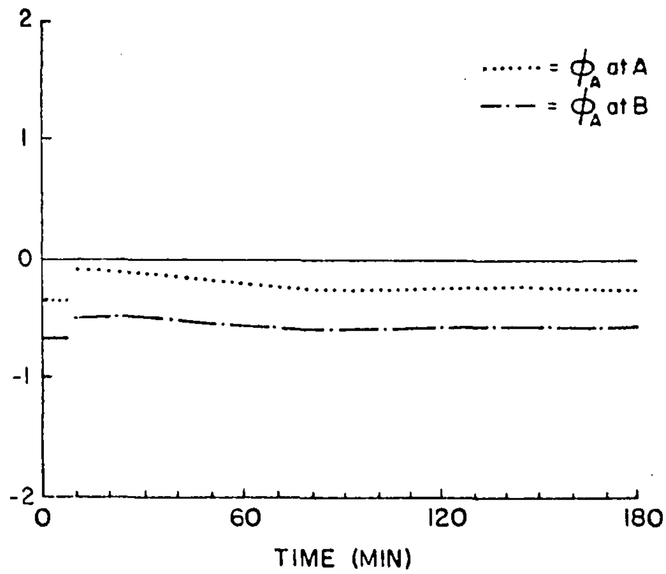

Figure 32. Time trace of the assimilated non-dimensional geopotential at points A and B for experiment 5.

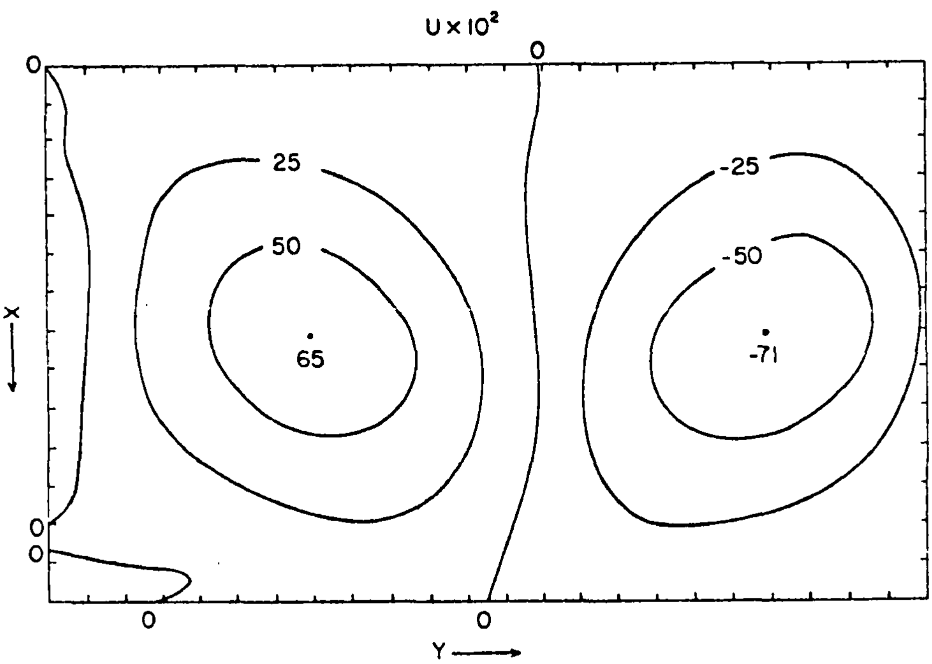

Figure 33a. Three hour forecast of the non-dimensional u component for experiment 5.

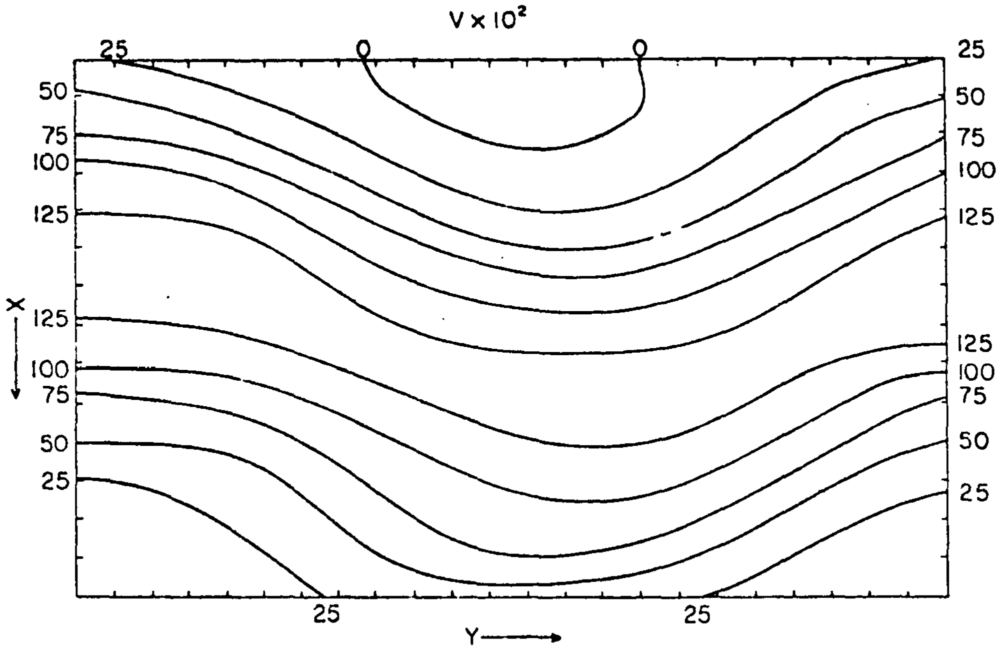

Figure 33b. Three hour forecast of the non-dimensional v component for experiment 5.

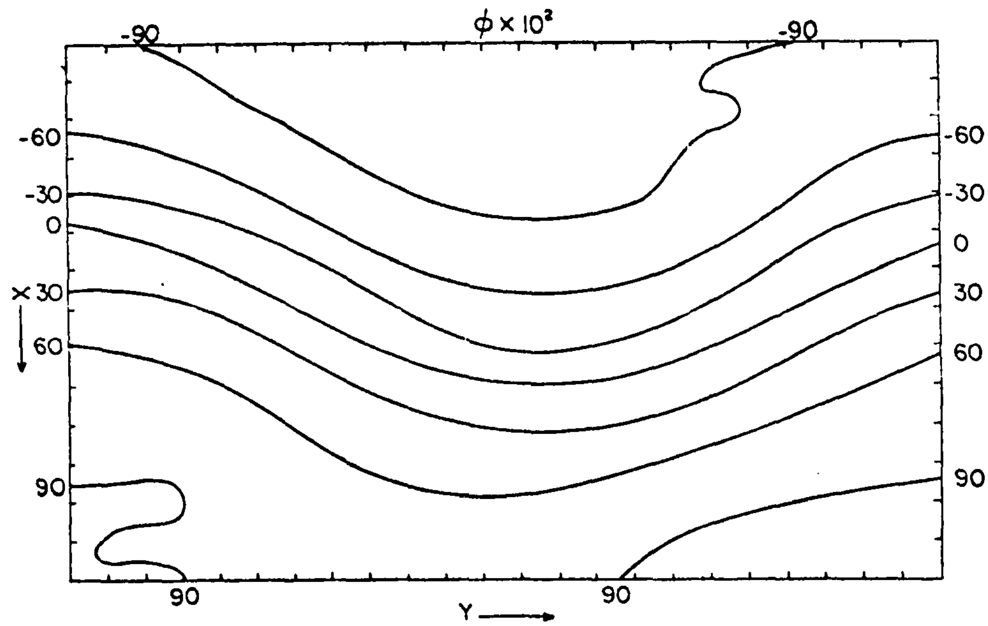

Figure 33c. Three hour forecast of the non-dimensional geo-potential perturbation for experiment 5.